

Induction of functional human macrophages in humanized mice

**Dissertation with the aim of achieving a doctoral degree at the Faculty
of Mathematics, Informatics and Natural Sciences**

Department of Biology of the University of Hamburg

Submitted by Jan Engelhardt

Hamburg, 2016

Date of oral defense: November 4th, 2016

The following evaluators recommend the admission of the dissertation:

Prof. Dr. med. Klaus Pantel

Prof. Dr. Julia Kehr

I hereby declare, on oath, that I have written the present dissertation by my own and have not used other than the acknowledged resources and aids.

Munich, 09.11.2016

Signature

Table of contents

1.	Summary	3
2.	Introduction	5
3.	Materials	15
4.	Methods	21
5.	Results	36
5.1.	Characterization of CD34-enriched fetal liver cells.....	36
5.2.	Characterization of lymphoid organs in HIS BRG mice	38
5.2.1.	Peripheral blood	38
5.2.2.	Bone marrow	40
5.2.3.	Thymus	42
5.2.4.	Lymph nodes	46
5.2.5.	Spleen	47
5.3.	Cross reactivity of mouse CSF-1 on human CSF-1 receptor.....	49
5.4.	Biological activity of mouse CSF-1 on human CSF-1R.....	52
5.5.	Induction of supraphysiological mouse CSF-1 levels in HIS BRG mice.....	54
5.6.	Induction of human monocytes and macrophages in HIS BRG mice.....	56
5.7.	Inhibition of human myelopoiesis in HB2 mice	60
5.8.	Functionality of human macrophages in HB2 mice <i>in vivo</i>	62
5.9.	Growth of human xenograft tumor cells in HIS BRG and HB2 mice	62
5.10.	Human macrophages mediate graft versus host disease in HB2 mice.....	66
6.	Discussion	69
7.	Supplementary figures	81
8.	Table of figures	85
9.	Abbreviation index	85
10.	References	86

1. Summary

Cancer still represents one of the most deadly diseases worldwide and efficient therapies to combat cancer are urgently required. The concept of cancer immunotherapy is based on the idea to redirect the body's own immune system against cancer cells and using its potency to inhibit tumor growth, which has been demonstrated previously in several clinical trials. The need for evaluating human specific, immunological targets and mechanisms in preclinical settings pushed the development of advanced mouse models. In this context, human immune system (HIS) mice generated by transplantation of human hematopoietic stem cells into immunodeficient mice were described to mimic major parts of human hematopoiesis preferentially for B and T cell development. Although different HIS mice models have been established, a poor reconstitution of human innate immune cells still limits the use of HIS mice as preclinical model for cancer therapies. Incomplete development of innate human immune cells in HIS mice has been attributed to insufficient or lack of cytokine cross reactivity. Several reports have highlighted that the underrepresentation of human monocytes and macrophages in HIS mice is caused by a lack of cross reactivity of the mouse macrophage colony stimulating factor (CSF-1) to the human CSF-1 receptor (CSF-1R). Recently published affinity data however suggest, that mouse CSF-1 can indeed bind to human CSF-1R with ultra-low affinity. This indicates that physiological concentrations of mouse CSF-1 in conventional HIS mice are simply too low to promote human monocyte and macrophage development. To test this hypothesis, BALB/c-RAG (2)^{-/-}IL2rg^{-/-} mice (BRG mice) were injected with human hematopoietic stem cells and the developing human immune system was characterized. Primary and secondary lymphoid organs were found to be repopulated with high numbers of human lymphoid cells while human myeloid cell types were clearly underrepresented. Biacore binding assay confirmed that the binding affinity of mouse CSF-1 to human CSF-1R was 12,000-fold lower compared to its cognate receptor. *In vitro* characterization revealed that mouse CSF-1 exhibited biological activity on human CSF-1R at supraphysiological concentrations, which was demonstrated by activation of the CSF-1R signaling pathway and subsequent differentiation of human monocytes into macrophages. In HIS BRG mice, supraphysiological mouse CSF-1 levels were induced by antibody-mediated blockade of the mouse CSF-1R *in vivo* (HB2 mice). Blockade of CSF-1R did not only significantly decrease mouse monocytes and macrophages, but also resulted in increased frequencies of human monocytes in peripheral blood and *de novo* infiltration of human macrophages in all tissues analyzed. Human macrophages were inducible by anti-mouse CSF-1R antibody treatment at different time points after reconstitution independent of the initial overall reconstitution level. In a proof of concept experiment, enhanced human myelopoiesis was reversed by blocking mouse CSF-1 *in vivo* resulting in significantly reduced human blood monocytes and

tissue macrophages. In addition, human macrophages were functional as shown by release of inflammatory cytokines upon stimulation with LPS *in vivo*. When human macrophages were induced in tumor bearing HIS BRG mice, tumor regression was observed in two independent xenograft models compared to mice virtually lacking human tumor-associated macrophages (TAMs). In depth analysis revealed that tumors of HB2 mice were infiltrated by both M1-like CD68⁺CD204⁻ and M2-like CD68⁺CD204⁺ macrophages accompanied by a strong T cell infiltration. These results provide evidence for the key role of human macrophages in attracting and orchestrating anti-tumoral immune responses. Therefore, HB2 mice represent a novel mouse model to investigate human TAMs and the interaction with T lymphocytes in preclinical settings.

A limitation of the HB2 mouse model was the onset of graft versus host disease (GvHD) resulting in increased mortality rates. Histopathological characterization of affected HB2 animals identified granulomatous infiltrates composed of human macrophages and T cells in various tissues correlating with impaired tissue integrity, especially in the bone marrow. Strikingly, depletion of human macrophages by an α hCSF-1R antibody, but not of human T cells, prevented the GvHD-like syndromes and mortality in HB2 mice.

2. Introduction

Cancer is still one major causes of death in many areas of the world and especially in the developed countries including the United States with more than 1.5 million new cases of cancer expected to have been diagnosed in 2015¹. Although numerous mechanisms underlying cancer development have been deciphered, comprehensive strategies for the diagnosis of cancer in early stages as well as for treatment of advanced tumors are still missing. In particular, molecular and phenotypic heterogeneity between different cancer types (even within the tumor entities) complicate the establishment of consistent therapeutic approaches and foster the development of personalized cancer therapies. In this context, successful subclassification of tumors by identifying subtype-specific biomarkers has been reported for breast and pancreatic cancer^{2,3,4,5}. Targeted therapies in oncology have been consistently designed to inhibit uncontrolled proliferation of mutated tumor cells mainly by blocking survival pathways using small molecules therapeutics or antibodies. Subsequently, new therapeutic concepts were developed upon understanding the complex interaction of tumor cells with the tumor stroma, consisting of various cell types such as fibroblasts, immune cells and others⁶.

The impact of using immune cells for cancer therapy has been significantly strengthened in the last decade in clinical trials and highlighted the potency of drugs targeting human immune cells located in the tumor environment. The immune system's ability to recognize and eliminate cancerous cells has been recognized as relevant for the concept of tumor surveillance. However, immunotherapeutic approaches for treatment of cancer received only low consideration for a long period of time due to reported inefficiency of immunomodulatory drugs such as cancer vaccines in humans⁷. However, the deeper understanding of mechanisms underlying cancer immunoediting and immunosuppression did help understanding of how tumors ultimately escape the co-evolving immune response, inspiring the way for development of innovative immunotherapeutics. In particular, targeting of immune checkpoint pathways, which naturally enhance or dampen a T cell immune response, have been identified as a promising approach to redirect the body's own immune system for elimination of cancer cells. So called immune checkpoints exhibit either co-inhibitory or co-stimulatory functions, thus regulating the intensity and durability of immune responses⁸. Co-inhibitory immune checkpoints are normally required for maintenance of self-tolerance and attenuation of immune responses. However, within the tumor microenvironment co-inhibitory signals have been found to be expressed by the tumor cells, generating an immunosuppressive environment⁹. Among others, the PD-1/PD-L1 immune checkpoint axis has been studied most intensively and inhibitory antibodies targeting this pathway have been tested in clinical

trials. PD-1 is an inhibitory receptor that has been found to be highly expressed on activated tumor infiltrating T lymphocytes. Under physiological conditions T cell responses are dampened by binding of PD-1 to its ligand PD-L1 expressed by different cell types including macrophages and dendritic cells^{10,11}. Assembling of the PD-1/PD-L1 complex transmits an inhibitory signal finally leading to reduced T cell proliferation and activation^{11, 12}. Different tumors including lung, ovary, colon and melanoma were reported to express high levels of PD-L1 and to upregulate PD-L1 in response to IFN γ release by cytotoxic T lymphocytes at the lymphocyte-rich tumor margin^{13, 14, 15}. CTLA-4, another inhibitory receptor, has been shown to also regulate T cell activation but at earlier stages compared to PD-1. Its regulatory role in homeostatic and anti-tumoral immune responses was shown by loss of function and tumor growth inhibition experiments in mice, respectively^{16, 17, 18}. Although PD-1 and CTLA-4 have been most actively investigated so far, other inhibitory lymphocyte receptors such as TIM3 and LAG3 but also other classes of molecules such as indoleamine 2,3-dioxygenase (IDO), a metabolic enzyme, promote immune inhibitory effects of tumor associated immune cells and are thought to be potential cancer immunotherapy targets^{19, 20, 21, 22}. In the last decade, several clinical trials already confirmed the therapeutic potential of immune checkpoint inhibitors^{23, 24, 25}. An anti-human CTLA-4 antibody for example was the first drug to demonstrate survival benefit in patients with advanced melanoma in a randomized trial. Similarly, antibodies for the PD-1 and PD-L1 axis have already been approved by the FDA for treatment of melanoma, Hodgkin lymphoma, non-small-cell lung cancer (NSCLC) and bladder cancer^{26, 27, 28, 29}. Compared to these encouraging results achieved by activation of suppressed T cells, depletion of immunosuppressive regulatory T cells by antibodies against CD25 so far did not significantly improve outcome of cancer patients^{30, 31}. Although immune checkpoint inhibitors have been tested extensively so far, engagers of costimulatory molecules expressed on T cells such as OX40 and 4-1BB are currently evaluated in clinical trials as well. Strikingly, 12 out of 30 late-stage cancer patients treated with an OX40 agonist showed regression of at least one metastatic lesion after the first treatment round and patients with melanoma, renal cell carcinoma and ovarian cancer have been reported to benefit from treatment with a monoclonal antibody against 4-1BB^{32, 33, 34}. Based on these encouraging results of both principles, the combination of costimulatory agonists and checkpoint inhibitors is a logical step forward. Preclinical studies already confirmed that simultaneous blockage of PD-1 and OX40 or 4-1BB synergistically improves anti-tumoral immune response^{35, 36}. Although preclinical as well as clinical data obviously support the strategy to push the “costimulatory gas pedal” while releasing the “inhibitory brake”, obvious concerns regarding side effects are taken serious. Data from mouse or even primate studies might not reliably mimic the human immune responses as already seen by a study conducted in 2006: a single dose of an anti CD28 agonistic antibody was followed by an unexpectedly strong cytokine

storm finally resulting in multiorgan failure of the patients³⁷. In addition to targeting naturally occurring inhibitor or costimulatory receptors on tumor infiltrating immune cells, bispecific antibody conjugates carrying two different target moieties have been described as promising cancer immunotherapy approach by actively recruit circulating T cells to the tumor site. By simultaneously engaging CD3 expressed on T lymphocytes and tumor specific antigens these T cell recruiters have been reported to exhibit profound anti-tumoral activity in solid as well as hematological malignancies^{38, 39, 40, 41, 42}.

The suppression of anti-tumoral T cell responses represents one of the most efficient mechanisms of how cancer cells evade the human immune system. However, tumor-associated innate immune cells such as tumor-associated macrophages (TAMs) and myeloid derived suppressor cells (MDSCs) have been shown to play a major role in the immunosuppressive tumor environment in mice and men^{43, 44, 45, 46}. Macrophages are highly plastic immune cells and exhibit different functions in the body during development, tissue repair and immunity⁴⁷. As professional antigen-presenting cells, macrophages are capable of inducing adaptive immunity by providing MHC class II restricted antigens and costimulatory signals for CD4⁺ helper T cells^{48, 49}. In general, macrophages are able to act as pro-and anti-inflammatory depending on the local cytokine milieu they are exposed to⁵⁰. Pro-inflammatory macrophages, also called classically activated macrophages, are induced upon stimulation with cytokines such as INF γ and mediate anti-viral, anti-bacterial and anti-tumoral immune responses. In contrast, exposure of macrophage precursors to interleukin (IL)-4 or IL-13 results in an alternatively activated, anti-inflammatory macrophage subtype mainly responsible for wound healing^{47, 48, 51, 52}. Of note, macrophage polarization towards a specific subtype was shown to be reversible thus providing macrophages the ability to rapidly adjust to environmental changes^{53, 54, 55}. In the context of cancer the ratio of pro- and anti-inflammatory TAMs, termed M1- and M2-like TAMs, was shown to correlate with tumor growth⁵⁶. Classically activated M1-like TAMs were reported to promote anti-tumoral immune responses by secreting pro-inflammatory cytokines such as IL-1, IL-6 and IL-2, by promoting development of Th17 cells and sustaining Th1 and cytotoxic T cell responses⁵⁷. While M1-like TAMs were reported to be preferably found in early stages of tumor development, TAMs detected in late stage tumors often shifted towards an alternatively activated, anti-inflammatory phenotype^{34, 57, 58}. Preclinical studies in mice revealed these M2-like TAMs to actively promote tumor progression by suppressing immune responses and supporting angiogenesis^{59, 60, 61, 62, 63}. Among other cytokines such as CCL2, the macrophage colony stimulating factor (CSF-1) has been identified as key player utilized by tumors to attract monocytic precursor cells from the blood and to polarize them towards a M2 like phenotype^{64, 65}. CSF-1 is a highly conserved cytokine that also regulates

survival and differentiation of monocytes and macrophages across different species⁶⁶. Its important role in vertebrate ontogeny has been identified in CSF-1 knockout mice showing growth retardation, decreased fertility and osteopetrosis^{67, 68}. As a dimeric ligand, CSF-1 promotes survival of target cells like monocytes, macrophages or osteoclasts by binding to its type III protein tyrosine kinase receptor CSF-1R thereby inducing receptor dimerization and phosphorylation⁶⁹. CSF-1 has been shown to be an essential survival factor not only for tissue resident but also for M2-like tumor-associated macrophages⁷⁰. Consequently, the therapeutic effect of blocking the CSF-1 signaling pathway has been evaluated in different preclinical tumor models. In this context, release of CSF-1 by cancer cells has been shown to result in increased infiltration of M2-like TAMs thus promoting tumor progression and metastatic spread of breast cancer and neuroendocrine tumors^{71, 72, 73}. Moreover, interruption of CSF-1 signaling by blockage of colony stimulation factor 1 receptor (CSF-1R) signaling increased sensitivity of different tumor types to conventional chemo-, radio- and anti-angiogenic therapies and caused regression of established patient derived glioblastomas in mice^{71, 74, 75, 76}. Just recently, a high affinity antibody against mouse CSF-1R, called 2G2, was described to efficiently deplete TAMs in MC38 and MCA1 tumor models thereby increasing the frequency of other tumor-associated immune cells such as neutrophils, NK cells and T cells⁴⁵. Repetitive treatment of tumor bearing animals with 2G2 resulted in delayed tumor growth and in reduced number of spontaneous metastasis in the MCA1 tumor model⁴⁵. Based on these promising preclinical data and the fact that numbers of M2 like TAMs were found to correlate with poor prognosis of cancer patients the effect of blocking the CSF-1/CSF-1R pathway has been addressed in several clinical trials^{75, 77, 78, 79}. Of note, CSF-1R⁺CD163⁺ M2-like TAMs were recently shown in a Phase I study to be efficiently depleted by Emaxtuzumab, an anti-human CSF-1R antibody, in different types of solid tumors correlating with significant clinical benefit in patients with Diffuse-Type Giant Cell Tumors^{45, 80}. Interestingly, treatment of patients with Emaxtuzumab not only reduced the number of tumor promoting macrophages, but additionally increased the ratio of CD8/CD4 tumor infiltrating lymphocytes⁴⁵. Based on these results, CSF-1R blocking antibodies likely represent promising combination partners for available checkpoint inhibitors targeting T cells such as PD-L1/PD-1⁸¹. In proof of concept experiments in mice, limited efficacy of PD-L1 and CTLA-4 monotherapy has been shown to be significantly improved by combination with CSF-1R inhibitors resulting in regression of established pancreatic carcinomas⁸². Possible combinations of immunomodulatory molecules such as checkpoint and CSF-1R inhibitors, specific T cell receptor engaging therapies and conventional therapies such as chemo- or radiotherapy will improve treatment options for cancer patients in the near future^{58, 81}.

Although cancer immunotherapy has been shown to conceptually work in the clinic, evaluation of novel targets and mechanisms in preclinical stages still represent a major issue as physiological interaction of

human tumor and immune cells cannot be studied in commonly used mouse models. As a compromise, preclinical datasets for molecules such as anti-PD-1, anti-CTLA-4 and anti-CSF-1R have mainly been generated in immunocompetent mice with a fully functional mouse immune system. The major caveat of using immunocompetent mice are the profound discrepancies in both innate and adaptive immunity between mice and men, as well as the use of mouse-specific agents with differential properties to the final molecule used in human patients. For example, the CD40 agonistic antibody most frequently used in mice is the FGK45, a rat IgG2b isotype needing FcγR-mediated cross-linking for its function, while the human molecule is a so called superagonist efficiently activating CD40 without any cross-linking⁸³. Therefore, results obtained from mouse studies might not sufficiently predict actual immune responses in cancer patients. Lack of species cross-reactivity and rapid clearance of humanized antibodies represents another major drawback if using immunocompetent mouse models. Being aware of the need to reflect human immune responses in preclinical settings different, so called “humanized mouse models” have been established and utilized in the past⁸⁴. In this context the PBMC transfer model has been frequently used to study mature human immune cell function *in vivo*⁸⁵. In this model, the engraftment of human immune cells is achieved by injection of mature human peripheral blood mononuclear cells (PBMCs) into immunodeficient mice⁸⁶. Although the engraftment of certain human immune cell populations is achieved by this approach, the PBMC transfer model suffers from several major drawbacks. First of all, the injection of human PBMCs results in development of xenogeneic graft versus host disease (GvHD) leading to death of animals within several weeks^{87, 88}. The onset of GvHD was shown to be delayed in recipient mice carrying human instead of mouse MHC class II molecules, however still there remains a relatively short time frame in which mice can be analyzed⁸⁹. Moreover, the engrafted human immune system was shown to be highly artificial and did not reflect human physiological conditions. While several cell types such as human B cells, NK cells and myeloid cells do not efficiently engraft in recipient mice, engrafted human T cells exhibit a hyperactivated phenotype as shown by expression of KI67 and activation markers such as PD-1^{90, 91, 92}. Several limitations of the PBMC transfer model can be overcome by replacing mature PBMCs as source for human immune cells by human hematopoietic stem and progenitor cells (HSPCs). More than 30 years ago the ability of human HSPCs to transiently repopulate immunodeficient SCID mice has been first described, however, long term engraftment and differentiation of human stem was possible with the development of highly immunocompromised recipient mouse strains^{93, 94, 95, 96}. Until today, humanized mice generated by human HSPCs transfer (hereinafter referred to as human immune system (HIS) mice) represent the most advanced preclinical model to study human immune responses *in vivo*. HIS mice are generated by injection of multipotent human HSPCs capable of long term engraftment and multi-lineage

differentiation into preconditioned, immunodeficient mice. Human HSPCs isolated from different sources such as peripheral blood or bone marrow have been tested for their ability to engraft in immunodeficient mice. However, sufficiently high humanization levels, measured by the frequency of human CD45 positive immune cells in lymphoid organs, can only be achieved by using HSPCs from cord blood or fetal liver⁹⁷. Enrichment of human HSPCs from cord blood as well as from fetal liver samples is usually achieved by magnetic enrichment for human stem cell markers such as CD34 or CD133^{98,99}. Of note, the total CD34⁺ cord blood or fetal liver cells were found to consist of heterogeneous cell population including multipotent as well as pluripotent stem cells, the latter being characterized by the marker combination CD34⁺CD38⁻CD90⁺CD45RA⁻CD49f⁺⁹⁸. In fetal liver-derived CD34⁺ cells human hepatic progenitor cells were identified besides stem and progenitor cell populations⁹⁹. Enhanced engraftment of human HSPCs in immunodeficient mice was also reported by clearing the mouse HSC niche by myeloablative preconditioning, similarly to human patients receiving allogeneic stem cell transplants¹⁰⁰. The myeloablation in immunodeficient mice is usually performed by sublethal irradiation, chemotherapeutic treatment of newborn or adult mice or antibody mediated depletion of mouse HSPCs, while each of these approaches are equivalent alternatives^{100, 101, 102, 103, 104}. In addition, the route of administration of the human HSPCs generally depends on the age of the preconditioned animals used for humanization. While intravenous injection is the method of choice in adult mice preconditioned with chemotherapy, HSC transfer into irradiated newborns usually is carried out intra-hepatically, intravenously or intracardially^{103, 104, 105, 106}. Beside the choice between different HSPCs sources and myeloablation regimens, selection of an appropriate recipient mouse strain has been shown to represent the most critical step for successful generation of HIS mice. Among different strains reported in the literature BALB/c-RAG(2)^{-/-} Il2r γ ^{-/-} mice (BRG mice), NOD.Cg-Prkdcscid Il2rgtm1Wjl/SzJ mice (NSG mice) and NOD.Cg-Prkdcscid Il2rgtm1Sug/JicTac mice (NOG mice) have emerged as preferred recipients for human HSPCs¹⁰⁷. Based in their genetic background NOG, NSG and BRG mice are severely immunocompromised providing a permissive environment for the engraftment of xenogeneic cell types^{108, 109}. While all three strains lack a functional IL-2 receptor- γ chain required for function of mouse NK cells, absence of mature mouse B and T cells is caused by targeted knockout of the recombina-activating gene-2 (Rag2) in BRG and by the SCID mutation in NSG and NOG mice^{108, 110, 111}. The NOD mutation in the latter two strains additionally results in reduced function of mouse dendritic cells and defective mouse macrophage activity¹¹⁰. Interestingly, despite a similarly immunocompromised phenotype, human HSPCs were reported to more robustly engraft in NSG and NOG mice as compared to BRG mice as shown by higher numbers of human CD45 positive immune cells in lymphoid organs¹⁰⁰.

Several studies identified a genetic polymorphism in the signal regulatory protein α (SIRP α) to account for observed differences in reconstitution levels amongst these strains^{112, 113, 114}. In mice and men, SIRP α is mainly expressed on innate immune cells and acts as an inhibitory receptor for their effector functions¹¹⁵. Although other ligands exist, interaction of SIRP α with its widely expressed ligand CD47 has been studied most extensively. Binding of SIRP α to CD47 provides a “*don’t eat me*” signal to phagocytic cells thus allowing innate immune cells to distinguish between self and non self¹¹⁶. The majority of mouse SIRP α variants, including the Balb/c variant, were shown to generally exhibit little or no cross-reactivity to human CD47 resulting in active phagocytosis of engrafted human HSPCs by mouse macrophages in BRG mice^{117, 118, 119, 120}. In contrast, human CD47 was shown to bind with high affinity to the SIRP α variant expressed in NOD background mice preventing phagocytosis of human HSPCs in NSG and NOG mice^{113, 114}. The importance of functional SIRP α /CD47 interaction for long term engraftment of human HSPCs has been highlighted by several independent studies: The overall humanization level was reported to be enhanced in BRG mice injected with human HSPCs carrying the mouse instead of human CD47 as well as in genetically modified BRG mice expressing a NOD or the human SIRP α variant^{112, 113, 121}. Although overall humanization levels in BRG mice were consistently reported to be lower than in NSG or NOG recipients these mice are still frequently used for generation of HIS mice due to high tolerance to irradiation and superior functionality of generated human B and T cells^{93, 109, 122, 123}. The human immune cells were shown to be detectable in mice up to 40 weeks after reconstitution, with humanization peaking around 8-16 weeks after HSPC engraftment in most HIS models^{104, 106, 122}. Despite having homed to a xenogeneic environment, human HSPCs were shown to efficiently proliferate and to differentiate into multiple human hematopoietic lineages in the bone marrow of HIS mice^{109, 124}. Around week 4 to 8 after reconstitution, the differentiated human immune cells were shown to be released into the blood stream and repopulate lymphoid organs such as the spleen and the thymus^{93, 122}. In several HIS models human lymphopoiesis was shown to be functional as confirmed by detection of mature human T and B cells in spleen and blood as well as by the presence of humanized lymph nodes^{122, 124, 125, 126, 127}. The development of human B cells in the bone marrow of HIS mice was shown to largely reflect differentiation stages seen in humans, however, final maturation of peripheral B cells was reported to be blocked in HIS mice likely due to impaired interaction with human T cells^{125, 127, 128}. In contrast, other reports describe the production of human antibodies and successful class switching of Ig isotypes suggesting proper B cell maturation at least in HIS BRG mice^{122, 129}. Human CD4⁺ and CD8⁺ double positive as well as single positive thymocytes were identified in humanized thymi indicating functional positive and negative selection of human T cells in the mouse thymus comparable to the human

situation^{109,122}. The ability of human T cell receptors to interact with mouse MHC class I and II molecules and the absence of T cell dependent acute GvHD in HIS mice led to the conclusion that human T cells are exclusively restricted to mouse MHC molecules presented by mouse, thymic epithelial cells^{130, 131}. However, reported interaction of human thymocytes with human antigen presenting cells in the thymus and response of HIS mice T cells to allogenic stimuli *ex vivo* suggests restriction of human T cells on both, human and mouse MHC molecules, in HIS mice^{91, 126, 132}. The existence of human MHC-restricted T cells is also supported by the diversity of human antibodies detected in HIS BRG mice. Activation and co-stimulation of B cells by human T helper cells requires TCR engagement of peptide loaded human MHC class II molecules presented by human B cells^{125, 126, 133}. On the other hand, CD8⁺ T cells isolated from HIS mice lack human leukocyte antigen (HLA) restricted immune responses, suggesting that the selection of human CD4⁺ and CD8⁺ T cells in the mouse thymus might be carried out on both, mouse or human MHC molecules, respectively¹³⁴.

As discussed before, major parts of the human lymphoid development are frequently reported to be functionally reflected in HIS mice, however several other components of human immune system are highly underrepresented. The poor reconstitution of human innate immune cells, regulatory T cells, mast cells, platelets and erythrocytes in HIS mice was finally explained by impaired or the lack of cross-reactivity from mouse to human receptors of essential cytokines such as IL-15, CSF-1, EPO and TPO^{100,103, 124, 135, 136, 137, 138, 139, 140, 141}. Lack of human MHC restricted immune responses, underrepresentation of innate immune cells and regulatory T cells, absence of human megakaryocyte derived cell types, phagocytosis of human cells by mouse macrophages and exhaustion of transplanted stem cells are major limitations of conventional HIS mouse models such as HIS BRG or HIS NSG mice. Consequently, advanced humanized mouse models have been developed to improve function and diversity of human immune cells in HIS mice. An elaborative but significantly improved model is generated by transplantation of fetal liver and thymus fragments under the kidney capsule of preconditioned NSG mice¹⁴². Once injected with human HSPCs from the same donor these so called bone marrow-liver-thymus mice (BLT mice) were shown to provide improved overall humanization, a more diverse human immune repertoire and human T cells restricted on human MHC class molecules present in co-transplanted human thymic tissue^{131, 143, 144}. Other second generation HIS models have been generated by introducing human cytokines or molecules in NSG or BRG mice using knock-in or transgenic approaches. NSG mice expressing human instead of mouse MHC class I and II molecules were shown to mount HLA restricted and antigen-specific humoral immune responses, respectively^{134, 145}. Moreover, maintenance of human HSPCs was significantly improved in human thrombopoietin (TPO) knocking BRG mice as well as in human stem cell

factor (SCF) transgenic NSG mice^{146,147}. Different second generation of mouse models were generated to improve the reconstitution of human innate immune cell types. High frequencies of human NK cells were detected in NSG mice expressing human interleukin 2 and reconstitution of human granulocytes was improved in presence of a human granulocyte-macrophage stimulating factor (GM-CSF) variant^{140, 148}. The underrepresentation of human macrophages was always attributed to a lack of cross-reactivity of mouse CSF-1 to the human CSF-1R and therefore introduction of human CSF-1 was supposed to improve poor human myeloid development (myelopoiesis) in HIS mice¹⁴⁹. Effectively, even transient expression of human CSF-1 achieved by hydrodynamic injection restored human blood monocytes and tissue macrophages in NOG mice¹⁴¹. Knock-in of human GM-CSF in HIS NOG mice did not result in a significant increase in human monocytes, but selectively enhanced human macrophage reconstitution in the lung¹³⁵. On the other side, knock-in of human CSF-1 in HIS BRG mice systemically improved human myelopoiesis as seen by elevated numbers of CD14⁺CD33⁺ peripheral blood monocytes and human macrophage infiltration in spleen, bone marrow, skin, lung and liver^{103, 140}. A recently study published by the Flavell laboratory describes the so far most advanced humanized mouse model generated by crossing several of the described knock-in strains¹⁰⁰: The so called MISTRG mouse carries knock-in replacements for human CSF-1 (M), IL-3 (I), SIRP α (S) and thrombopoietin (T) on the BRG (RG) background. While human SIRP α and TPO expression were supposed to enhance humanization by providing phagocytic tolerance and improved maintenance of human HSPCs, co-expression of human CSF-1, GM-CSF and IL-3 was expected to enhance human myelopoiesis. In terms of engraftment, MISTRG mice exhibited higher frequencies of human immune cells in blood and BM as compared to BRG and even to NSG mice. Strikingly, reconstitution levels comparable to those in NSG mice were even detected in non-irradiated animals¹⁰⁰. Successful reconstituted without previous myeloablation was to date only observed in mouse c-kit knock-out mice, making MISTRG mice the most permissive recipients for human HSPCs reported so far¹⁵⁰. Of note, in MISTRG mice the frequency of total human monocytes was significantly increased up to 50% of total human CD45⁺ cells in blood comprising of all major monocytes subtypes found in human blood such as classical CD14⁺CD16⁻, intermediate CD14⁺CD16⁺ and non-classical CD14⁻CD16⁺ monocytes¹⁰⁰. Moreover, efficient differentiation of human monocytes was confirmed by infiltration of human macrophages in non-lymphoid tissues such as the lung, liver and colon. On a functional level, these human macrophages were shown capable of responding to LPS with cytokine release *in vivo* and phagocytosing of labeled bacteria *ex vivo*¹⁰⁰. The detection of functional human NK cells in MISTRG mice was unexpected as these innate lymphocytes so far only have been successfully generated in mice expressing human IL-2 or IL-15^{100, 148, 151}. Quantitative PCR data suggested that human NK cell development in these mice was driven by human macrophages expressing IL-15, however the formal

proof of IL-15 secretion was missing¹⁰⁰. To test of whether the presence of human macrophages and NK cells effects the growth of human xenograft tumors, Flavell and colleagues injected human melanoma cells in reconstituted MISTRG or NSG mice. Enhanced tumor growth was observed in MISTRG mice as compared to NSG mice correlating with infiltration of CD163⁺CD206⁺ human M2-like TAMs¹⁰⁰. In summary, MISTRG mice represent the first model providing enhanced humanization levels and improved reconstitution of human innate immune cells. However, even MISTRG mice still exhibit several limitations such as lack reconstitution of granulocytes, human red blood cells, regulatory T cells as well as lack of priming via a human MHC. In the context of oncoimmunology, MISTRG mice represent the first preclinical model faithfully mimicking enhanced tumor growth in presence of human M2-like tumor-associated macrophages. While most commercially available mouse strains do not efficiently support human myelopoiesis upon engraftment with human HSPCs only the knock-in replacement of human CSF-1 was reported to efficiently promote human monocyte and macrophage reconstitution in HIS mice. This fact not only seems to confirm the lack of cross-reactivity of mouse CSF-1 to the human CSF-1R but also highlights the necessity of functional CSF-1R signaling for monocyte maturation and macrophage differentiation in these mice.

The aim of this present study was primarily to enhance human myelopoiesis in non-transgenic BRG mice utilizing endogenous, mouse-derived CSF-1. In crystallography studies mouse CSF-1 was reported to actually bind to human CSF-1R but with extremely low affinity¹⁵². Thus, it could be hypothesized that the physiological concentration of mouse CSF-1 in BRG mice is simply too low to activate CSF-1 signaling in human hematopoietic cells. To evaluate of whether increased mouse CSF-1 can be harnessed to improve human myelopoiesis in non-transgenic humanized BRG mice, mouse CSF-1R was blocked by an anti-mouse CSF-1R surrogate antibody (2G2). In this context, systemically increased concentrations of CSF-1 were reported in non-human primates upon antibody mediated blockage of CSF-1R⁴⁵. In the present study the extend of human myelopoiesis was characterized in humanized BRG mice before and after antibody mediated blockage of mouse CSF-1R. The resulting human monocytes and macrophages populations were intended to be phenotypically and functionally characterized. Moreover, in case of successful reconstitution, the role of human macrophages in context of human tumor growth should be investigated. In addition, a recently published study indicates that improved human myelopoiesis negatively affects survival of humanized mice¹⁵³. Along with this finding an additional aim of this study was to reveal of whether human macrophages exhibit tolerance towards the mouse host.

3. Materials

3.1. Animals and animal facility products

C57BL/6 mice (Haplotype: H2^b)
BALB/c-RAG(2)-/- Il2ry-/- mice (Haplotype: H2^d)
Caches and cache lids
Animal feed
Water bottles
Litter for cages

Charles River, Sulzfeld
Charles River, Sulzfeld
Tecniplast, Hohenpeißenberg
ProvimiKliba AG, Kaiserau
Tecniplast, Hohenpeißenberg
Ssniff GmbH, Soest

3.2. Laboratory equipment

Autotechnicon Leica
Irradiator Type OB 29 (OBSV039)
Incubator
Digital camera Power shot
Coverslipper
Gourmet steamer
Thermometer
iBlot[®] western blot system
Isofluran vaporizer
Microscope DM500B
Microscope camera
MACSQuant[®] analyzer
MAESTRO[®] imager
Fluorescence scanner

Leica instruments GmbH, Nussloch
GSM / Gamma-Service Medical GmbH, Leipzig
Heraeus instruments, Hanau
CANON, Krefeld
Leica instruments GmbH, Nussloch
Braun GmbH, Kronberg
Oregon Scientific, Oregon (USA)
Life technologies[™], Darmstadt
Eickenmeyer Medizintechnik KG, Tuttlingen
Leica instruments GmbH, Nussloch
DEC360FX, Leica Instruments GmbH, Nussloch
Miltenyi Biotec, Bergisch Gladbach
INTAS, Göttingen
Panacom250, 3D Histotech Ltd., Budapest, Ungarn

MACS[®] cell separator
Paraffin embedding machine
Electric shaver
Rotary microtome
Caliper
Necropsy instruments
Laminar flow hood
Western blot power supply
Cell counter ViCell[®]
Centrifuges

Miltenyi Biotec, Bergisch Gladbach
Vogel GmbH, Gießen
Harotec GmbH, Berlin
Leica instruments GmbH, Nussloch
Mitutoyo Messgeräte GmbH, Neuss
B. Braun AG, Melsungen
BDK, Sonnenbühl
Life technologies[™], Darmstadt
Beckman Coulter GmbH, Krefeld
Megafuge 1.0R, Thermo Scientific, Schwerte
Centrifuge 5415C, Eppendorf, Wesseling
Leica instruments GmbH, Nussloch
3DHISTECH, Budapest (HU)
Ventana Medical Systems, Tucson (USA)
Roche Diagnostics, Basel (CH)
Eppendorf AG, Hamburg
Eppendorf AG, Hamburg
Life technologies[™], Darmstadt
TECAN, Maennedorf (CH)
Biorad, Munich
Biorad, Munich

Aperio ScanScope AT slide scanner
Pannoramic 250 Flash III Scanner
VENTANA SYMPHONY
Lumi Imager F1
Eppendorf MixMate[®]
Heating block
XCell SureLock[®] Mini-Cell gel running tank
TECAN infinite 2000 Nano Quant plate reader
Bio-Plex[®] 200 Systems
Bio-Plex Pro[™] Wash Station

3.3. Commodities/ Utensils

1 ml syringes
1,5/ 2 ml Eppendorf tubes
10/100/200/1000 µl pipet tips
15/50/250 ml falcons
SepMate™ 50 ml tubes
5 ml FACS tubes
2/5/10/25/50 ml pipet boy tips
Microvette® 300 Z EDTA coated
Microvette® 500 Z-Gel
6/12/24/96 well cell culture plates
BSA blocked NUNC streptavidin 384 well plates
DAKO pen
Precision Plus Protein™ Unstained Standard*
Histology cassettes
iBlot® Transfer Stack (Nitrocellulose)
Compensation beads anti mouse Ig, κ
MS/LS/LD magnetic separation columns
Micro-Fine™ insulin syringes (30G, 29G)
NuPAGE® Bis-Tris Gels (4-12 %)
Scalpels
Superfrost slides
40/70 µm mesh combinations
Blood lancets
Hemocytometer

B. Braun Melsungen AG, Melsungen
Eppendorf AG, Hamburg
Eppendorf AG, Hamburg
Greiner bio-one, Frickenhausen
STEMCELL Technologies™, Köln
BD Biosciences, Heidelberg
BD Biosciences, Heidelberg
Sarstedt AG & CO, Rommelsdorf
Sarstedt AG & CO, Rommelsdorf
VWR International GmbH, Ismaning
Thermo Scientific, Schwerte
DAKO, Hamburg
BIO-RAD, München
Leica Biosystems Inc., Buffalo Grove (USA)
Life Technologies™, Darmstadt
BD Biosciences, Heidelberg
Miltenyi Biotec, Bergisch Gladbach
BD Medical, Heidelberg
Life Technologies™, Darmstadt
B. Braun Aesculap AG, Tuttlingen
VWR International GmbH, Ismaning
Miltenyi Biotec, Bergisch Gladbach
WPI, Sarasota (USA)
WIS Biomed, San Mateo (Canada)

3.4. Ready to use kits

CD45 MicroBeads, mouse
Monocyte isolation kit II, human
Pierce™ BCA Protein Assay Kit
Customized BioPlex®Pro Cytokine Assay

Miltenyi Biotec, Bergisch Gladbach
Miltenyi Biotec, Bergisch Gladbach
Thermo Scientific, Schwerte
Biorad, Munich

3.5. Media and buffers histology

10x PBS
70 / 80 / 90 / 100 % Alcohol
Antibody Diluent, Dako REAL™
DAB+, Liquid
Formalin 4%
Permanent HRP Green Kit
Antigen retrieval buffers pH 6 and pH9
Permanent AP Red Kit
Eukitt® quick-hardening mounting medium
Protein block serum free
Wash buffer 10x
Hydrogen peroxide 30%
Xylol
Hämalaun Mayer

Hoffmann-La Roche GmbH, Penzberg
Hoffmann-La Roche GmbH, Penzberg
DAKO, Hamburg
DAKO, Hamburg
VWR International GmbH, Ismaning
Zytomed Systems GmbH, Berlin
DAKO, Hamburg
Zytomed Systems GmbH, Berlin
O-Kindler, Freiburg
DAKO, Hamburg
DAKO, Hamburg
Merck Millipore, Darmstadt
Merck Millipore, Darmstadt
Roth, Karlsruhe

3.6. Cell culture reagents

1 x PBS	PAN Biotech GmbH, Aidenbach
FBS (fetal bovine serum)	PAN Biotech GmbH, Aidenbach
L-Glutamine	PAN Biotech GmbH, Aidenbach
Lymphoprep™	STEMCELL Technologies™, Köln
Lympholyte®-M (Mouse)	CEDARLANE®, Hornby, Canada
PenStrep (500 x)	Hoffmann-La Roche GmbH, Penzberg
RPMI-1640	PAN Biotech GmbH, Aidenbach
DMEM	PAN Biotech GmbH, Aidenbach
Stemline 2 (HSC medium)	Sigma-Aldrich GmbH, Seelze
Trypsin/EDTA	PAN Biotech GmbH, Aidenbach
Trypan blue	Sigma-Aldrich GmbH, Seelze
X-Vivo 10 medium	Lonza

3.7. Flow cytometry reagents

Propidium Iodid	Miltenyi Biotec, Bergisch Gladbach
DAPI solution	Hoffmann-La Roche GmbH, Penzberg
Red blood cell lysis buffer (10x)	BD Pharmingen, Heidelberg
FACS buffer (MACSQuant Running Buffer)	Miltenyi Biotec, Bergisch Gladbach

3.8. Western blot reagents

LDS sample buffer	Life Technologies™, Darmstadt
SuperSignal™ West Femto Substrate	Thermo Fischer, Schwerte
SuperSignal™ West Pico Substrate	Thermo Fischer, Schwerte
SignalBoost™ Immunoreaction Enhancer Kit	Merck-Millipore, Darmstadt
NuPAGE® Antioxidant	Life Technologies™, Darmstadt
NuPAGE® Tris-Acetate SDS Running Buffer	Life Technologies™, Darmstadt
NuPAGE® Reducing agent (10x)	Life Technologies™, Darmstadt
RIPA-Puffer	Merck-Millipore, Darmstadt
PhosSTOP Phosphatase Inhibitor Cocktail Tablets	Hoffmann-La Roche GmbH, Penzberg
cOmplete Protease Inhibitor Cocktail Tablets	Hoffmann-La Roche GmbH, Penzberg
NuPAGE MOPS SDS running buffer (20x)	Life Technologies™, Darmstadt
Tween20	Merck, Darmstadt
Non-fat dried milk powder	Hoffmann-La Roche GmbH, Penzberg
EDTA solution 0.5M	Life Technologies™, Darmstadt
30% BSA solution	Miltenyi Biotec, Bergisch Gladbach

3.9. Biacore reagents

Human Antibody Capture Kit	GE Healthcare, Buckinghamshire (GB)
Mouse Antibody Capture Kit	GE Healthcare, Buckinghamshire (GB)
Series S Sensor Chip CM3 and CM5	GE Healthcare, Buckinghamshire (GB)
Buffer NaAc pH 4.5 and pH5	GE Healthcare, Buckinghamshire (GB)
Buffer HBS-N	GE Healthcare, Buckinghamshire (GB)
PBS 10x	Hoffmann-La Roche GmbH, Penzberg
Tween20	Hoffmann-La Roche GmbH, Penzberg
Human CSF-1R/Fc-Chimera	R&D Systems, Inc., Minneapolis (USA)
mouse CSF-1R/Fc-Chimera	R&D Systems, Inc., Minneapolis (USA)

human PDGFR beta/Fc-Chimera
Anti human IgG PAN

R&D Systems, Inc., Minneapolis (USA)
Hoffmann-La Roche GmbH, Penzberg

3.10. ELISA reagents

MicroCoat, 384-Well MTP, clear
StartingBlock T20
BSA fraction V
PBS
PAB<mCSF-1>Goat-IgG-Bi
MAB<mCSF-1>Rat-5A1-IgG
PAB<Rat>Goat-IgG-HRP conjugate
TMB: BM Blue POD Substrate, soluble
MaxiSorp 384-Well MTP, clear
Streptavidin-HRP Conjugate

Hoffmann-La Roche GmbH, Penzberg
Thermo Fischer, Schwerte
Hoffmann-La Roche GmbH, Penzberg
PAN Biotech GmbH, Aidenbach
R&D Systems, Inc., Minneapolis (USA)
Hoffmann-La Roche GmbH, Penzberg
R&D Systems, Inc., Minneapolis (USA)
Hoffmann-La Roche GmbH, Penzberg
VWR International GmbH, Ismaning
Hoffmann-La Roche GmbH, Penzberg

3.11. BioPlex reagents

Standard diluent
Sample diluent
Assay buffer
Wash buffer
Detection antibody diluent
Streptavidin-PE
Reference standard
Coupled magnetic beads for human IL-1b, IL-2, IL-6,
IL-10, IL-12, TNF α , MCP-1, IP-10, GM-CSF, M-CSF,
INF γ , IL-4, IL-8
Detection antibodies

Biorad, Munich
Biorad, Munich

3.12. Prepared solutions and buffer

MACS buffer
PBST wash buffer western blot and ELISA
Blocking buffer western blot
Running buffer Biacore
Dilution buffer Biacore
ELISA dilution buffer

1 x PBS, 0.5% BSA, 2mM EDTA
10x PBS, 0.1% Tween20, ddH₂O
4% non-fat dried milk powder in PBST
PBS + 0.05 % (v/v) Tween20
PBS + 0.05 % (v/v) Tween20 + 1mg/ml BSA
3% BSA/PBS 0,2%Tween20

3.13. Cytokines

Recombinant mouse CSF-1
Recombinant human CSF-1

Peprotech, Rocky Hill (USA)
Peprotech, Rocky Hill (USA)

3.14. Enzymes

DNAseI
CollagenaseIV

Hoffmann-La Roche GmbH, Penzberg
Sigma Aldrich, St.Louis (USA)

3.15. Human hematopoietic stem cells

CD34 enriched fetal liver cells

StemExpress, Placerville (USA)

3.16. Human tumor cell lines

HT29 (human colorectal carcinoma)
OVCAR5 (human ovarian carcinoma)

Hoffmann-La Roche GmbH, Penzberg
Hoffmann-La Roche GmbH, Penzberg

3.17. Fluorescence labeled antibodies

Antigen	Reactivity	Clone	Purchased from
CD3	Human	OKT3	Biolegend
CD19	Human	HIB19	Biolegend
CD20	Human	2H7	Biolegend
CD10	Human	H10a	Biolegend
HLADR-DP-DQ	Human	Tu39	Biolegend
TCR $\alpha\beta$	Human	B1	Biolegend
CD56	Human	HCD56	Biolegend
CD33	Human	WM53	Biolegend
CD14	Human	HCD14	Biolegend
CD16	Human	3G8	Biolegend
CD86	Human	IT2.2	Biolegend
CD115	Human	12-3A3-1B10	AbD serotec
CD66b	Human	G10F5	Biolegend
CD133(1)	Human	AC133	Miltenyi
CD34	Human	AC136	Miltenyi
CD11b	Human	ICRF44	Biolegend
CD117	Human	104D2	Biolegend
CD45	Human	HI30	Biolegend
CD45	Mouse	30-F11	Biolegend
F4/80	Mouse	BM8	Biolegend
CD115	Mouse	604B52E11	AbD serotec
Ly6C	Mouse	HK1.4	Biolegend
Ly6G	Mouse	1A8	Biolegend

3.18. Fluorescence labeled antibodies immunofluorescence

Antigen	Clone	Conjugate	Purchased from
Mouse IgG	Polyclonal	Alexa 488	Life Technologies™, Darmstadt
Rabbit IgG	Polyclonal	Alexa 647	Life Technologies™, Darmstadt

3.19. Primary antibodies immunohistochemistry

Antigen	Reactivity	Clone	Purchased from
CD3	Human	2GV6	Ventana Medical systems
CD20	Human	L26	Ventana Medical systems
CD45	Human	RP2/18	Ventana Medical systems
CD68	Human	Polyclonal	Sigma Aldrich, St.Louis (USA)
CD204	Human	Polyclonal	Sigma Aldrich, St.Louis (USA)
HLADR-DP-DQ	Human	CR3/43	DAKO
MHCII	Mouse	M5/114.15.2	Biolegend
F4/80	Mouse	CI:A3-1	AbD Serotec
CD45	Mouse	30-F11	BD Pharmingen

3.20. Secondary antibodies immunohistochemistry

ImPRESS® Anti-mouse IgG HRP	Vector Laboratories
ImPRESS® Anti-rabbit IgG HRP	Vector Laboratories
ImPRESS® Anti-rat IgG HRP	Vector Laboratories
Anti-mouse IgG AP	Ventana Medical systems
Mach2 double stain anti-mouse HRP + anti-rabbit AP	BIOCARE Medical
Mach2 double stain anti-mouse AP + anti-rabbit HRP	BIOCARE Medical

3.21. Western blot antibodies

Antigen	Species	Company
Human CSF-1R	Rabbit	Cell signaling
Human pCSF-1R (Y723)	Rabbit	Cell signaling
Human β -Actin	Rabbit	Cell signaling
Human pAKT	Rabbit	Cell signaling
Rabbit IgG	Goat-HRP	GE Healthcare

3.22. Therapeutic and controls animal studies

Target	Isotypes	Clone/Name	Company
Mouse CSF-1 receptor	Variable hamster, constant mouse	2G2	Hoffmann-La Roche GmbH, not commercially available
Human CSF-1 receptor	Human IgG2a	AMG820 surrogate	Reproduced from WO US2008/073611 ¹⁵⁴
Human CD3	Rat IgG2a	OKT3	Biologend
Mouse CSF-1	Rat IgG1	5A1	BioXcell
Human CSF-1	Humanized IgG	Abgenix surrogate	Reproduced from WO 2007016240 A3 ¹⁵⁵
Mouse IgG1 isotype	Mouse IgG1	MOPC-21	BioXcell
Rat IgG2a (CD3)	Rat IgG2a	RTK2758	Biologend
Xolair®	Human IgE	-	Novartis Pharma
Rat IgG1	Rat IgG1	-	BioXcell

3.23. *In vivo* substances

Lipopolysaccharides (LPS) from E. coli 0111:B4	Sigma Aldrich, St.Louis (USA)
20mM Histidin/140mM NaCl/pH6 <i>in vivo</i> buffer	Hoffmann-La Roche GmbH, Penzberg

4. Methods

4.1. Animal experiments

Pregnant female BRG mice as well as humanized BRG were kept under specific pathogen-free (SPF) conditions at the animal facility at Roche Diagnostics in Penzberg. All mouse experiments were approved by the regional government of upper Bavaria (ref. 55.2-1-54-2532-156-11, ref. 55.2-1-54-2532.2-33-12).

4.2. Preparation of human hematopoietic stem cells

Human CD34⁺ fetal liver cells (FLCs) were used as source of human hematopoietic stem cells. On the day of injection, vials of frozen FL cells were removed from liquid nitrogen and quickly thawed using a 37°C water bath. Cells were mixed by inverting the tubes and transferred to a 15 ml tube. To prevent aggregation, DNaseI was added to a final concentration of 100 µg/ml. Vials were rinsed with pre-warmed HSC medium and suspension was added drop wise to the cells. 10 ml pre-warmed HSC medium was added before centrifugation at 1400 rpm for 10 minutes. Cells were resuspended in 1ml pre-warmed HSC medium. Cell viability was determined by trypan blue exclusion using a hemacytometer and the formula: % viable cells = [1.00 – (number of blue cells ÷ number of total cells)] × 100. The formula used to finally calculate the number of viable cells per ml suspension was: Number of viable cells × 10⁴ × 1.1 = cells/mL culture. After removing ~ 2x10⁴ cells per donor for FACS analysis, FLC were centrifuged at 1400 rpm for 10 minutes and resuspended in HSC medium at ~4x10⁶ cells per ml.

4.3. Colony forming unit assay (CFC)

CFC assay was performed using human FLCs and a methylcellulose matrix according to the manufacturer's instructions. Briefly, a human FLCs stock solution was prepared by resuspending 2x10⁴ cells in 300 µl IMDM medium. The stock solution was added to 3 ml methylcellulose and mixture was vigorously vortexed. Samples were left untouched for 20 minutes until air bubbles disappeared. 1,1ml methylcellulose/cell mixture was added to a 35 mm culture plate and distributed evenly. Cells were incubated in methylcellulose for 14 days and formed colonies were analyzed using a light microscope.

4.4. Generation of human immune system BRG mice (HIS BRG mice)

Timed-pregnant BRG mice were delivered to the animal facility at gestational day 17 and were monitored daily until birth. Newborn pups (within the first three days of life) were sublethally irradiated with a dose of 2.5 Gy (250 rad) using a Cs-137 irradiator. 24h after irradiation, ~2x10⁵ human CD34⁺ FLC in 50 µl HSC media were injected intra-hepatically using a 29-gauge needle.

4.5. Blood and serum sampling

Blood sampling for flow cytometry and serum extraction was carried out at different time points after reconstitution and at day of necropsy by puncture of the Vena facialis using a lancet. Sample take for flow cytometry were immediately transferred to EDTA coated Z tubes to prevent aggregation. Separation of serum was carried out by centrifugation of whole blood in a gel microvette at 10000 rpm for 10 minutes at 4°C. Serum samples were stored at -20°C or at -80°C until further analysis.

4.6. Tissue sampling

Mice were sacrificed by cervical dislocation before tissue collection. Depending on the downstream application, organs were stored in sterile RPMI medium containing 2% FBS for flow cytometry or trimmed using a scalpel blade and transferred to 4% formalin solution for immunohistochemistry (IHC).

4.7. Preparation of single cell suspensions for flow cytometry

4.7.1. Blood

Equal volume of whole blood from each mouse was transferred from EDTA coated Z tubes to a 5 ml FACS tube. For analysis of white blood cells, erythrocytes were lysed by adding 1ml 1x RBC lysis buffer per 50 µl whole blood for 15 minutes at room temperature. Upon centrifugation at 1200 rpm for 5 minutes, cell pellets were resuspended in 50 µl FACS buffer per FACS staining (e.g. for 4 different FACS stains 200µl FACS buffer were added to each sample). To prevent unspecific binding of FACS antibodies by mouse or human Fc receptors, each sample was incubated for 15 minutes at 4°C with 1.25 µg anti-mouse and anti-human FcR block according to manufacturer's instructions. Heparinized human whole blood was collected from healthy volunteers at the Roche medical service in Penzberg. Single cell suspensions from human blood aliquots were prepared like mouse aliquots but without adding mouse FcR block.

4.7.2. Spleen and bone marrow

Femurs and spleen fragments were first rinsed with RPMI + 2% FBS using a 22-gauge needle. Remaining tissue fragments were processed through a 70/30 µm filter mesh combination and cell suspension was centrifuged at 1200 rpm for 5 minutes. RBC lysis was performed by resuspending the pellet in 1 ml 1x RBC lysis buffer and incubation at room temperature for 20 seconds. RBC lysis was stopped by adding 10 ml PBS. Cell suspension was filtered through a 70/30 µm filter mesh combination and centrifuged at 1200 rpm for 5 minutes. Pellets were resuspended in 10 ml PBS and cell number per ml was determined using the MACSQuant flow cytometer. For each FACS staining 1×10^6 cells were incubated for 15 minutes at 4°C with 1.25 µg anti-mouse and anti-human FcR block according to manufacturer's instructions

4.7.3. Thymus and lymph nodes

Thymus and lymph node samples were processed like spleen and bone marrow (4.7.2) but without the initial rinsing step at the beginning.

4.7.4. Liver and lung

Liver and lung samples were mechanically dissociated using a scalpel blade. Fragments were digested by adding 5 ml digestion medium (RPMI +5%FBS + 100 U/ml collagenase IV+ 0.02 mg/ml DNase I) for 40 minutes at 37°C. Digested tissue was filtered and processed through a 70 µm mesh. Samples were centrifuged at 1200 rpm for 5 minutes and resuspended in 15 ml PBS. To remove debris, liver samples were additionally centrifuged at 30g for 5 minutes and supernatants transferred to new 50 ml tubes. Liver supernatants and lung samples were centrifuged at 1200 rpm for 5 minutes. Pellets were resuspended in 15 ml PBS and cell numbers per ml were calculated using the MACSQuant flow cytometer. Subsequently, mononuclear cells were isolated by density gradient centrifugation: Upon centrifugation at 1200 rpm for 5 minutes pellets were resuspended in 15 ml 40% Percoll in RPMI (cell concentration < 1×10^7). This suspension was then carefully overlaid onto 15 ml 70% Percoll in PBS. Mononuclear cells were collected from the interphase and transferred to new 50 ml tubes. Cells were washed twice in 10 ml RPMI + 2% FBS, then pellets were resuspended in 10 ml PBS (liver) or 5ml PBS (lung) and cell numbers per ml were calculated using the MACSQuant flow cytometer. For each FACS staining 1×10^6 cells were incubated for 15 minutes at 4°C with 1.25 µg anti-mouse and anti-human FcR block according to manufacturer's instructions

4.8. Tumor cell expansion *in vitro*

The human tumor cell lines OVCAR5 and HT29 were grown in DMEM + 10% FBS. Cultures were maintained at 37°C in a humidified atmosphere with 5% CO₂. Cells were harvested upon incubation with trypsin/EDTA for 4 minutes. Enzymatic reaction was stopped by adding DMEM + 10% FBS and cell number as well as cell viability were determined using the ViCell cell counter. Upon centrifugation at 1200 rpm for 10 minutes, cells were resuspended at 5×10^7 cells per ml in PBS.

4.9. Flow cytometry

Fluorescence activated cell sorting (FACS) was performed on the MACSQuant flow cytometer equipped with a violet (405nm), a blue (488nm) and a red (638nm) laser allowing the detection of 8 different fluorochromes simultaneously. To perform multicolor analysis, instrument settings (compensations) were generated for each individual stain using anti-mouse IgG compensation beads in combination with

the MACSQuant multicolor compensation modus. In most FACS experiments, unless otherwise stated, 1µg of each fluorochrome conjugated was added to up to 1×10^6 cells. Only few antibodies (e.g. human HLA-DR/DP/DQ) needed titration due to exceptionally high antigen expression. Labeling of cells was performed by adding 50 µl of the respective antibody cocktails to single cell suspensions containing Fc block. Mixtures were incubated at 4°C and protected from light for 20 minutes. Unbound antibodies were removed by washing the cells twice in FACS buffer. Finally cell pellets were resuspended in 100 µl FACS buffer. To exclude dead cells from the analysis, DAPI or Propidium Iodide were added to each sample right before the measurement using the MACSQuant auto-labeling modus. Analysis of acquired FACS data was carried out using the FlowJo software. The general gating strategy for each FACS experiment was based on the following three parameters: identification of target cells by appropriate FCS-SSC setting, exclusion of cell aggregates by FSC-A and FSC-H blot and of dead cells by gating on DAPI/PI negative cells. Only these pre-gated cells were finally analyzed for expression of specific antigens tagged with a certain fluorochrome such as phycoerythrin (PE).

4.10. Tissue processing for histology and immunohistochemistry

For IHC analysis trimmed organs were fixed in 4% formalin in PBS for 24h. Formalin fixed tissues were dehydrated and infiltrated by paraffin using the following program on an automated tissue processor (autotechnicon):

A	3x Ethanol 70%	90 minutes	RT
B	2x Ethanol 95%	90 minutes	RT
C	2x Ethanol 100%	90 minutes	RT
D	2x Xylol 100%	90 minutes	RT
E	4x Paraffin	60 minutes	60°C

Tissue samples were permanently wrapped in paraffin using an embedding machine. Paraffin tissue blocks were cut into 2.5 µm thick sections using a rotary microtome and sections were loaded onto Superfrost glass slides. Upon dehydration over night at 37°C tissue sections were stored at 4°C until further staining.

4.11. Staining of paraffin embedded tissue sections

For histological analysis of tissue morphology paraffin embedded tissue sections were subjected to automated hematoxylin and eosin staining (H&E staining) performed by the Ventana Symphony System.

Immunohistochemical stainings of tissue sections were done manually. First, paraffin embedded tissue sections were deparaffinized and hydrated using the following steps:

A	3x Xylol 100%	5 minutes	RT
B	2x Ethanol 100%	2 minutes	RT
C	1x Ethanol 90%	2 minutes	RT
D	1x Ethanol 80%	2 minutes	RT
E	2x Ethanol 70%	2 minutes	RT
F	1x deionized water	20 seconds	RT

To perform heat induced antigen retrieval (HIER) slides were boiled at 97°C for 20 minutes in antigen retrieval buffer at pH6 and cooled down to 60°C afterwards. Slides were washed twice for 1 min in deionized water, followed by another minute in 1x PBS. Endogenous peroxidases were blocked by incubation in PBS + 0.3% H₂O₂ for 10 minutes. Slides were washed twice 1x PBS for 2 minutes and twice in wash buffer for additional 2 minutes. Unspecific binding sites were blocked using serum free blocking solutions for 20 minutes. Primary antibodies were added at given concentrations (Table 1) for 1h at room temperature. Slides were washed trice in wash buffer for 2 minutes each. Appropriate secondary antibodies coupled to horse-radish peroxidase (HRP) or alkaline phosphatase (AP) were added (Table 1) and incubated at room temperature for 20 minutes. Slides were washed trice in wash buffer for 2 minutes. Chromogen stainings were developed by adding HRP or AP substrates to the slides. Chromogen reactions were stopped in deionized water as soon as color development was sufficiently strong without background detection. The choice of chromogens and the order in which they are developed on the slides were varied in case of single or double staining. However, if triple staining was performed using two antibodies from species 1 and a third from species 2, DAB substrate was used for the first antibody from species 1 , permanent red for antibody from species 2 and permanent green for second antibody from species 1. The reason for this particular order is based on the ability of the HRP substrate DAB to block the Fc part of the respective primary antibody. In this way two primary antibodies from the same species can be developed with the enzyme HRP on the same slide. Chromogen stained slides were counterstained with Hämalaun solution for 30 seconds. Reaction was stopped in tap water and slides were rinsed in running tap water for 10 minutes. Slides were tried at 60°C for 30 minutes and cooled down to room temperature. Upon three 5 minutes wash steps in 100% xylol slides were permanently covered with Eukitt medium using a coverslipper machine. Slides were scanned using the Aperio ScanScope scanner and analyzed either with the Aperio Image Scope or the Definiens software.

Table 1 Immunohistochemical stainings (h: human, m: mouse)

Staining	HIER	Dilution	2nd antibody	Chromogen
mCD45/hCD45	pH6	1:50/ none	anti rat-HRP/ anti-mouse HRP	Histogreen/ DAB
hCD68/ hCD3	pH6	1:500/ none	anti rabbit-HRP/ anti-rabbit HRP	DAB/ PermRed
hCD68/hCD3/hCD20	pH6	1:100/ none/ none	anti mouse-HRP/ anti rabbit-AP/ anti mouse-HRP	DAB/ PermRed/ Histogreen
hCD204/ hCD3	pH6	1:100/ none	anti rabbit-HRP/ anti-rabbit HRP	DAB/ PermRed
hMHCII/mMHCII	pH6	1:100/ 1:50	anti mouse-HRP/ anti rat-HRP	Histogreen/ DAB

4.12. Western blot

8x10⁶ isolated human CD14⁺ cells were seeded per T25 cm² flask in X-Vivo 10 medium and incubated at 37°C for 3 hours for attachment. Cells were washed once in pre-warmed PBS. X-Vivo 10 medium was supplemented with either human CSF-1 at 100 ng/ml or mouse CSF-1 at 100 ng/ml, 500 ng/ml or 5000 ng/ml was added for 5 or 15 minutes, respectively. X-Vivo medium supplemented with 0.05% BSA served as control condition. After stimulation, cells were washed twice with ice cold PBS and flasks were put on ice. Adherent cells were scraped off the dish using a cold plastic cell scraper and cell lysis was performed by incubation of scraped cells in 150 µl RIPA buffer containing protease and phosphatase inhibitors for 15 minutes at 4°C. Cell lysates were centrifuged at 14000 rpm for 30 minutes and supernatants were frozen at -80°C until analysis. Protein concentrations of thawed samples were determined using BCA assay according to the manufacturer's instructions. Approximately 10 µg protein per sample was reduced by adding NUPAGE LDS sample buffer, NUPAGE reducing agent and deionized water up to 50 µl and heated at 70°C for 10 minutes. According to the manufacturer's instructions 4-12% Bis-Tris gels were placed in the XCell *SureLock*[®] Mini-Cell gel running tank and the chamber was filled with 1x NUPAGE MOPS running buffer. 50 µl of each reduced sample and 10 µl of the protein standard were loaded onto the gel. Gels were run at 120V for 90 minutes. Gels were removed from the plastic cover and rinsed once in deionized water. Using the iBlot system proteins were transferred to a nitrocellulose membrane in 9 minutes according to manufacturer's instructions. Membranes were incubated for 1h at room temperature in blocking buffer. The following primary antibodies were diluted 1:1000 in signal enhancer solution 1 and added onto the blocked membranes: anti-human CSF-1R, anti-human pCSF-1R (Y723) and

anti-human pAKT. Anti-human β -Actin antibody was added and served as a loading control. Membranes were incubated overnight at 4°C on an orbital shaker and washed three times 10 minutes in TBST at room temperature. A secondary HRP coupled antibody was diluted 1:500 in signal enhancer solutions 2 and added on the membranes for 1h at room temperature. Membranes were washed 3x in PBST and 1x in PBS and wrapped in a plastic foil. Femto western blot substrate was added onto the membranes and chemoluminescence signals were detected using a lumi imager system. In some cases, membranes were washed in PBST once and reprobed with additional primary antibodies following the same protocol.

4.13. ELISA for detection of total mouse CSF-1

To detect total, α mCSF-1 bound and unbound, mouse CSF-1 in sera of mice, streptavidin coated microplates were incubated with 30 μ l/well 1 μ g/ml PAB<mCSF-1>Goat-IgG-Bi in StartingBlock for 60 minutes at room temperature. In the meantime seven standards were prepared by serial 1:2 dilution of a mouse CSF-1 stock solution starting from 3.6 ng/ml in StartingBlock. Serum samples were diluted using StartingBlock 1:3, 1:60 and 1:1000 and 5A1 detection antibody at a final concentration of 37.5 μ g/ml. Plates were washed three times in 100 μ l PBST. 20 μ l prediluted 5A1 detection antibody was added to each well and 10 μ l standard, serum sample or blank in triplicates. Mixtures were incubated 120 minutes at room temperature and washed three times in 100 μ l PBST. PAB<Rat>Goat-IgG-HRP was diluted 1:800 in 3% BSA/PBS 0.2% Tween20 and 30 μ l were added per well for 60 minutes incubation at room temperature. Plates were washed three times in 100 μ l PBST before 30 μ l of BM blue substrate was added. Reaction was stopped by adding 25 μ l 1M H₂SO₄ and absorbance was determined at 450 nm using a plate reader.

4.14. ELISA for detection of unbound mouse CSF-1

To detect free mouse CSF-1 in sera of α mCSF-1 treated mice (4.21.6), 384-well microplates were coated by adding 2 μ g/ml anti-mouse CSF-1 coating antibody clone 5A1 in 30 μ l total volume per well followed by overnight incubation at 4°C on a plate shaker. Coated plates were blocked for 40 minutes at room temperature with 100 μ l StartingBlock per well and washed three times in 100 μ l PBST. Seven standards were prepared by serial 1:2 dilution of a mouse CSF-1 stock solution starting from 0.16 ng/ml. Serum samples of animals treated with anti-CSF-1R clone 2G2 were diluted 1:20000 and of HIS BRG control mice 1:40 in StartingBlock. 30 μ l of each sample, standard and blank (StartingBlock) were transferred in triplicates to coated plates and incubated for 20 minutes at room temperature. Plates were washed three times in 100 μ l PBST and incubated with 30 μ l biotinylated detection antibody prediluted in StartingBlock at 0.6 μ g/ml for 60 minutes at room temperature. After another washing step in TBST, 30 μ l streptavidin-HRP prediluted 1:7500 in 3% BSA/PBS 0.2% Tween20 were added onto the plates and incubated for 30-60

minutes at room temperature. Plates were washed three times in 100 μ l PBST before 30 μ l of BM blue substrate was added. Reaction was stopped by adding 25 μ l 1M H₂SO₄ and absorbance was measured at 450 nm using a plate reader.

4.15. Bioplex

To measure levels of different human cytokines in sera of LPS treated HIS BRG control and HB2 mice Bioplex Pro Cytokine Assay was performed. Firstly, serum samples of HIS BRG control mice were diluted 1:4 and those of HB2 mice 1:30 in BioPlex dilution buffer. Subsequent steps were carried out in accordance with the manufacturer's protocol. Briefly, 50 μ l of respective beads were added to pre-moistened wells of filter plates. After two washing steps, 50 μ l standard, sample or blank were added to the wells. All samples and standards were run in duplicates. Incubation was carried out at room temperature using a shaker at 850 rpm. Plates were washed three times in wash buffer before addition of 25 μ l detection antibody. Plates were incubated for 30 minutes at room temperature. After another wash run 50 μ l streptavidin-PE was added for 10 minutes at room temperature. Plates were washed again and finally 125 μ l assay buffer was added. Plates were shook for 30 seconds at 850 rpm and analyzed on the BioPlex plate reader system. Cytokine concentrations were finally quantified on the basis of a unique standard curve for each analyte.

4.16. Biacore analysis

All experiments were performed on T200 Instrument (Biacore T200 Control SW V 2.0). Standard amine coupling was carried in HBS-N buffer according to the manufacturer's instructions. Activation was performed by a mixture of EDC/NHS. Capture molecules were diluted in coupling buffer containing 10 mM sodium acetate pH 4.5 or 5.0. Finally, residual activated carboxyl groups were blocked by injection of ethanolamine. To measure receptor-ligand interactions, human and mouse CSF-1R/Fc-chimeras were captured via amine coupled α human Fc- or α mouse Fc antibodies. Coupling of both capture antibodies was performed at 25 μ g/ml. Human PDGFR was used and captured as negative control. Series with increasing concentrations of the CSF-1 were injected with an association phase of 180 s followed by a dissociation phase of 600 s (mouse CSF-1) or 3600 s (human CSF-1). Mouse and human CSF-1 was analyzed at concentrations of 0.46-1000nM and 100nM, respectively. Interaction partners were analyzed in duplicates on a CM3 sensor chip at 37°C. To determine the affinity of mouse CSF-1 to human CSF-1R in solution, both components were pre-incubated at concentrations of 0.78-1600nM and 4nM, respectively. An anti-human CSF-1R antibody, RG7155, was captured by amine coupling at 50 μ g/ml. All samples were analyzed with an association phase of 180s and dissociation phase of 300s using a flow rate of 50 μ l/min.

The dissociation constant (K_D) of mouse CSF-1 to human CSF-1R was finally calculated by determining the EC50 inhibition using a 4-parameter fit calibration curve and a sigmoidal dose-response-model. Incubation mixes of mouse CSF-1 without human CSF-1R were used as negative controls ($c = 1600, 100, 0.78 \text{ nM}$). Collected data were evaluated using the Biacore T200 Evaluation SW V2.0 (GE) according to the manufacturer's instructions. The Langmuir fit was adjusted to the full range of the association and dissociation intervals. Binding signals were double referenced against blank buffer and a flow cell containing no or inactive ligand. Kinetic constants were calculated from fitting to a 1:1 Langmuir binding model ($R_I = 0$) in BiaEvaluation. Listed K_D values represent apparent affinity values, i.e. avidity values, due to bivalent binding of dimeric CSF to receptors unless stated otherwise.

4.17. Isolation of human PBMCs from human whole blood

Heparinized blood was collected from healthy volunteers at the Roche medical service in Penzberg. Human peripheral blood mononuclear cells (PBMCs) were isolated from whole blood by density gradient centrifugation using SepMate™ tubes in combination with Lymphoprep™ medium according to the manufacturer's instructions. Briefly, whole blood was diluted in equal volume of 1x PBS and overlaid carefully onto the insert of the SepMate™ tubes previously filled with 15 ml Lymphoprep™ medium through the central hole of the insert. Tubes were centrifuged for 10 minutes at 1200x g with break on. PBMCs were harvested by pouring the top layer into a new tube. Cells were washed two times in 1x PBS to remove remaining platelets and purity of target cells was determined by FACS analysis. Cells were either frozen at -80°C or used immediately for functional assays.

4.18. Enrichment of human monocytes from human PBMCs

Untouched magnetic enrichment of human CD14^+ peripheral blood monocytes was performed using the human monocyte isolation kit II. Briefly, $30 \mu\text{l}$ per 10^7 PBMCs were incubated at 4°C for 10 minutes with $10 \mu\text{l}$ human FcR blocking reagent and $10 \mu\text{l}$ biotin-antibody cocktail as instructed by the manufacturer. Subsequently, $30 \mu\text{l}$ MACS buffer and $20 \mu\text{l}$ anti-biotin microbeads cocktail per 10^7 cells were added and incubated for another 15 minutes at 4°C . Samples were washed twice on MACS buffer and up to 10^8 labeled PBMCs in $500 \mu\text{l}$ MACS buffer were loaded onto LS columns that have been prepared by adding 3 ml MACS buffer. The eluate contains the CD14 enriched fraction and was collected and columns were washed by adding 3x 3 ml MACS buffer always collecting the elution buffer. Enriched cells were washed twice in MACS buffer and counted. Purity of enriched peripheral blood monocytes was determined by FACS analysis using CD14 staining. $5\text{-}10 \times 10^6$ cell aliquots were finally re-suspended in 1ml freezing medium and frozen at $-1^\circ\text{C}/\text{min}$ in a -80°C freezer. Cells were stored at -80°C until analysis.

4.19. Isolation of human monocytes from bone marrow of humanized mice

Single cell suspensions from femurs of humanized mice were prepared and counted as described in 4.7.2. For isolation of human CD14⁺ monocytes from bone marrow single cell suspensions, highly abundant mouse immune cells were depleted by positive selection using the mouse CD45 microbeads in combination with LD columns according to the manufacturer's instructions. Briefly, up to 10⁷ bone marrow cells were re-suspended in 90 µl MACS buffer, mixed with 10 µl of anti-mouse CD45 microbeads and incubated for 15 minutes at 4°C. Samples were washed twice in 2 ml MACS buffer. Up to 10⁸ cells were taken up in 500 µl MACS buffer and loaded onto LD columns that have been prepared by adding 2 ml MACS buffer. The flow through (mouse CD45 depleted fraction) was collected and columns were washed by adding 2x 1 ml MACS buffer always collecting the flow trough. Mouse CD45 depleted cells were washed twice in MACS buffer and depletion success was determined by FACS analysis. Enrichment of human monocytes from mouse CD45 depleted bone marrow cells was performed using the monocyte isolation kit described in 4.18. Purity of CD14 positive bone marrow-derived monocytes was determined by FACS analysis. 5-10x10⁶ cells were finally aliquoted in 1ml freezing medium and frozen at -1°C/min in a -80°C freezer. Cells were stored at -80°C until analysis.

4.20. Monocyte differentiation assays

CD14⁺ monocytes isolated from human PMBCs or HIS BRG bone marrows were seeded in 96-well plates at a density of 5x10⁴ cells per well in 200 µl medium. Cells were incubated for 10 day in X-Vivo 10 medium supplemented with human CSF-1 at 100 ng/ml, mouse CSF-1 at 100 ng/ml, 500 ng/ml or 5000 ng/ml. To assess monocyte differentiation, cell morphology was analyzed daily using a light microscope. Differentiated macrophages were finally detached for 30 minutes at 4°C in ice cold PBS+5 mM EDTA and prepared for flow cytometric analysis using human FcR block. Blocked samples were incubated with different fluorescence labeled antibodies, washed twice in FACS buffer and analyzed on the MACSQuant analyzer.

4.21. *In vivo* experiments

4.21.1. Calculation of humanization level in lymphoid organs of HIS BRG mice

FACS analysis was used to determine the frequency of human immune cells or humanization level in lymphoid organs of humanized mice. Single cell suspensions were prepared from thymus, lymph nodes, spleen or bone marrow as described in 4.7.2 and 4.7.3. Cells were Fc-blocked and stained with human and mouse CD45 antibodies using the FACS protocol described in 4.9. Except on erythrocytes and platelets, CD45 is expressed on all hematopoietic cells in mice and men. Mouse and human specific CD45

variants allow initial distinction of mouse from human immune cells in lymphoid organs of HIS mice. To determine the level of humanization in HIS BRG mice the frequency of human CD45⁺ cells in total, mouse and human, CD45⁺ cells and was calculated by the formula: $100 * ((\% \text{ human CD45} / (\text{human CD45} + \text{mouse CD45}))$). Mice with humanization level >2% were termed “non-humanized” and excluded from further analysis.

4.21.2. Group allocation of HIS BRG mice for *in vivo* studies

Group allocation of HIS BRG mice to different treatment groups was performed manually for all *in vivo* studies performed based on the following parameters (priority in descending order): level of human CD45 (“humanization level”), frequency of monocytes within human CD45⁺ cells, frequency of T cells within human CD45⁺ cells, stem cell donor used for reconstitution. Group allocation of HIS BRG mice was always performed 7-10 days before starting the study to ensure the mice to recover from the last blood sampling procedure. *In vivo* studies were generally started 12-18 weeks after HSC transfer to ensure the establishment of a human immune system.

4.21.3. Generation of HB2 mice by depletion of mouse macrophages in HIS BRG mice

Depletion of mouse macrophages in HIS BRG mice was started on week 14 after HSC transfer by four consecutive weekly intraperitoneal injections of the monoclonal anti-mouse CSF-1R antibody clone 2G2 at 30 mg/kg per injection (1q7dx4) (Table 2). Instead of 2G2 control mice received a mouse IgG1 isotype antibody (MOPC-21) using the same treatment regimen.

Table 2 Treatment groups mouse CSF-1R blockage study in HIS BRG mice

Group	Number of animals	Compounds	Dose	Route of administration	Treatment regimen
1	8	MOPC-21	30 mg/kg	i.p.	1q7dx5
2	8	2G2	30 mg/kg	i.p.	1q7dx5

Blood samples were taken weekly (~ 50 µl blood/mouse per week) and analyzed by flow cytometry for reconstitution and CD14⁺ cell content. Mice were monitored daily and systemic GvHD was assessed by incorporating five clinical parameters initially described by Cooke et al.¹⁵⁶. Mice were sacrificed in the course of the study upon the appearance of the following symptoms: body weight loss > 20%, decreased activity, obvious hunching, ruffled fur texture, abnormal skin integrity. Mice were sacrificed 7 days after the last 2G2 injection (total treatment time: 28 days) by cervical dislocation. Blood, spleen and bone

marrow samples were prepared for FACS analysis as described before. Tissue sections of spleen, bone marrow, thymus, colon, liver, lung and lymph nodes were fixed in 4% formalin in PBS and processed for immunohistochemistry as described in 4.10. Monoclonal antibodies against specific mouse and human surface antigens were finally used to evaluate the depletion of mouse macrophage and its effect on human immune cells in various tissues.

4.21.4. Survival study: Simultaneous depletion of mouse macrophages and human T cells

In this survival study, HIS BRG mice were manually allocated 16 weeks after reconstitution into three different treatment groups (Table 3). Similar to the regimen in 4.21.3, Group 2 was injected with four consecutive doses of the 2G2 antibody alone. Group 3 was treated with 2G2 antibody and in addition with an anti-human CD3 (α hCD3) T cell depleting antibody at 5 mg/kg twice a week. Control group 1 received non-binding isotype matched antibodies using the same treatment regimen.

Blood samples were taken once per week (~ 50 μ l blood/mouse) and analyzed by FACS analysis. Mice were monitored daily and scored by the same criteria as mentioned in 4.21.3. Mice were sacrificed 7 days after the last 2G2 injection by cervical dislocation (total treatment time: 42 days). Blood and tissue sampling was performed as mentioned in 4.21.3 The average overall survival in these groups was calculated and plotted using the GraphPad Prism software.

Table 3 Treatment groups human T cell depletion study in HB2 mice

Group	Number of animals	Compounds	Dose	Route of administration	Treatment regimen
1	12	MOPC-21 + Rat IgG2a	30 mg/kg + 5 mg/kg	i.p. i.p.	1q7dx5 + 2q7dx5
2	12	2G2	30 mg/kg	i.p.	1q7dx5
3	12	2G2 + α hCD3	30 mg/kg + 5 mg/kg	i.p. i.p.	1q7dx5 + 2q7dx5

4.21.5. Survival study: Simultaneous depletion of mouse and human macrophages

In this survival study, HIS BRG mice were manually allocated 18 weeks after reconstitution into three different treatment groups (Table 4). Group 2 was treated with four consecutive weekly doses of 2G2 as described in 4.21.3. In addition to 2G2, group 3 was simultaneously treated with a human CSF-1R blocking antibody (α hCSF-1R) once a week at 10 mg/kg. Control group 1 received non-binding isotype matched antibodies using the same treatment regimen.

Table 4 Treatment groups human macrophage depletion study in HB2 mice

Group	Number of animals	Compounds	Dose	Route of administration	Treatment regimen
1	10	MOPC-21 + Xolair	30 mg/kg + 10 mg/kg	i.p. i.p.	1q7dx10 + 1q7dx10
2	10	2G2	30 mg/kg	i.p.	1q7dx10
3	10	2G2 + α hCSF-1R	30 mg/kg + 10 mg/kg	i.p. i.p.	1q7dx10 + 1q7dx10

Blood samples were taken once a week (~ 50 μ l blood/mouse) and analyzed by FACS analysis. Mice were monitored daily and scored by the same criteria as mentioned in 4.21.3. Mice were sacrificed 7 days after the last 2G2 injection (total treatment time: 79 days) by cervical dislocation. Blood and tissue sampling was performed as mentioned in 4.21.3. The average overall survival in these groups was calculated and Kaplan-Meier plots were generated using GraphPad Prism 6 software.

4.21.6. Blockage of mouse or human CSF-1 *in vivo*

Table 5 Treatment groups mouse and human CSF-1 blockage study

Group	No animals	Compound	Dosing	Route of administration	Adm. mode
1	10	MOPC-21 + Rat IgG + Xolair	30 mg/kg + 1 mg/mouse + 10 mg/kg	i.p. i.p. i.p.	1q7dx4 + 1q1d/2q7d4x 1q7dx4
2	10	2G2	30 mg/kg	i.p.	1q7dx4
3	10	2G2 + α mCSF-1	30 mg/kg + 1 mg/mouse	i.p. i.p.	1q7dx4 + 1q1d /2q7d4x
4	10	2G2 + α hCSF-1	30 mg/kg + 10 mg/kg	i.p. i.p.	1q7dx4 + 1q7dx4

In this study, HIS BRG mice were manually allocated 14 weeks after reconstitution into 5 different treatment groups (Table 5). Group 2 was dosed with 2G2 as described in 4.21.3. Next to 2G2, group 3 was additionally injected with anti-mouse CSF-1 antibody clone 5A1 (α mCSF-1) and group 4 with anti-human CSF-1 (α hCSF-1) antibody in indicated treatment intervals and at indicated time points. Control group 1 received non-binding isotype matched antibodies using the same treatment regimen. Blood samples were taken once a week (~ 50 μ l blood/mouse) and analyzed by flow cytometry. Mice were monitored daily and scored by the same criteria as mentioned in 4.21.3. Mice were sacrificed 7 days after the last 2G2 injection (total treatment time: 28 days) by cervical dislocation. Blood and tissue sampling was performed as mentioned in 4.21.3 and also included FACS analysis of lung and liver tissues.

4.21.7. Response of HB2 mice to stimulation with LPS *in vivo*

To test the functionality of human macrophages *in vivo*, HB2 mice were generated by injecting HIS BRG mice 20 weeks after HSC transfer using four consecutive doses of 2G2 as described in 4.21.3. HIS BRG mice injected with same doses of MOPC-21 isotype control served as reference control. HIS BRG control mice as well as HB2 mice were intraperitoneally injected with 35 µg LPS per mouse. 2 hours after injection sera were taken and subjected to Bioplex analysis to determine levels of several different human cytokines.

4.21.8. Tumor growth in HIS BRG and HB2 mice

Comparison of tumor growth kinetics between HIS BRG control and HB2 mice was carried out using the human colorectal carcinoma cell line HT29 or the human ovarian carcinoma cell line OVCAR5. To generate human xenograft tumors 2×10^6 HT29 or 3×10^6 OVCAR5 tumor cells were resuspended in 100 µl PBS and injected in the right flank of isofluran anesthetized mice at 14 weeks after reconstitution. As soon as tumors were palpable, growth was monitored twice a week by perpendicular caliper measurement and tumor volume was calculated using the following formula: $\text{volume} = 0.5 \times \text{length}^2 \times \text{width}$. Moreover, body weight was controlled daily using a laboratory scale. Animals were removed from the study as soon as one of the following termination criteria was reached: Tumor size $> 1500 \text{ mm}^3$, tumor ulceration, physical impairment or body weight loss $> 20\%$. At day of necropsy tumors were carefully removed and pictures were taken using a digital camera. Upon termination, tumors were fixed in 4% formalin and processed for immunohistochemistry as described in 4.21.3

4.22. Workflow for Definiens image analysis

Quantification of human immune cells on chromogen stained immunohistochemistry slides was performed using the Definiens software. Chromogen signals on each slide were quantified by detection of the percent area coverage in respective regions of interest (ROIs). Briefly, scanned slides were opened in the Definiens developer tissue studio software and the “dual staining flexible chromogens” mode was selected. Cytoplasm was chosen as area of chromogen detection for most markers analyzed. An image that had counterstain, both markers and white space was initially used to “train” the software. After all parameters were assigned, ROIs were determined using the tissue background separation tool and modified using the polygon selection tool. The latter one was specifically used to delete specific areas within the ROIs, vessels for example. Sample areas were selected to represent various areas of the tissue. Using the marker area detection tool, thresholds for each of the assigned markers were adjusted to get the most accurate representation of the stainings. Settings were finally applied to all images to be

analyzed and acquired data were exported to Excel. Statistical analysis was performed with the GraphPad Prism 6 software.

4.23. Statistical analyses

Statistical analysis was performed with the GraphPad Prism 6 software. Two-tailed unpaired Student's T-test was used for comparison of two data sets using a confidence interval of 95% (Statistical significance: $P < 0.05$). More than two data sets were analyzed by one-way ANOVA followed by Tukey's test comparing the mean of each data set with every other mean with a confidence interval of 95% (Statistical significance: $P < 0.05$). The level of statistical significance was described using defined parameters (Table 6) and only significant results are shown on the graphs generated.

Table 6 Parameters to describe level of statistical significance

< 0.0001	Extremely significant	****
0.0001 to 0.001	Extremely significant	***
0.001 to 0.01	Very significant	**
0.01 to 0.05	Significant	*
≥ 0.05	Not significant	ns

5. Results

5.1. Characterization of CD34-enriched fetal liver cells

The generation of HIS mice was achieved by injecting human CD34-enriched fetal liver cells (FLCs) into pre-conditioned, newborn BRG mice. To initially confirm that the purchased cells contain human HSPCs capable of long term engraftment and multi-lineage differentiation, FLCs from different donors were subjected to phenotypic and functional characterization *in vitro* and *in vivo*. Phenotyping of FLCs by flow cytometry revealed the bulk of cells were positive for the common human HSC marker CD34 (Figure 1A + Supplementary Figure 1A). While CD34 was found to be consistently expressed among all donors tested, the frequency of cells simultaneously expressing human HSC markers CD133 and c-kit (CD117) ranged from 36% to 64% (Figure 1B + Supplementary Figure 1B). Low numbers of long term repopulating cells (LTRCs) defined by the marker combination $CD34^+CD38^-CD90^+CD45RA^-CD49f^+$ were detected in all FLCs samples tested (Figure 1C and Supplementary Figure 1C-E). Next, human FLCs functionality was tested: The self-renewal capability along with the ability to differentiate into multiple lineages for replenishment all cell types of the human hematopoietic system. To verify the presence of multipotent HSPCs, FLCs were analyzed using a colony forming cell (CFC) assay *in vitro*. This test allows evaluation of the differentiation potential of applied cell types by colony formation in a three dimensional matrix

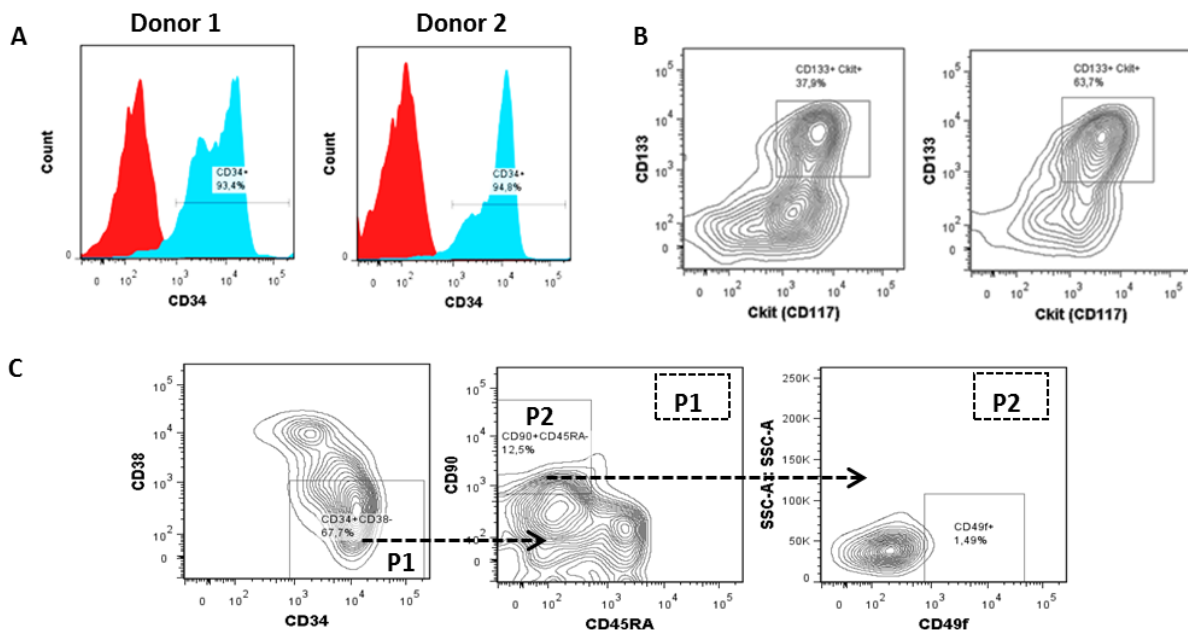


Figure 1: Phenotyping of human CD34 enriched FLCs using FACS analysis

FLCs were stained using monoclonal antibodies directed against indicated surface markers and analyzed by flow cytometry. (A) FLCs of two representative donors are shown for HSC marker CD34 (blue), the matching isotype control was used as reference (red). (B) Frequency of CD133 and CD117 (c-kit) double positive FLCs within CD34 positive population shown in A. (C) Gating strategy for human long-term repopulating cells (LTRCs), applied to FLCs from one representative donor; the frequency of each subpopulation is based on the parental gate shown on the top right of each plot, P1 and P2, respectively.

supplemented with human cytokines. In summary, human FLCs efficiently differentiated into multipotential progenitor cells (CFU-GEMM) as well as into all myeloid lineage committed progenitor cells (CFU-GM, CFU-M, CFU-G, CFU-E, BFU-E) as confirmed by formation of respective colonies (Figure 2). The CFC assay suggested that FLCs exhibit multi-lineage differentiation potential however it does not cover lymphoid differentiation. To test the lymphoid and myeloid differentiation potential, human FLCs were intra-hepatically injected into sublethally irradiated, newborn BRG mice. Engraftment and differentiation of human FLCs *in vivo* was assessed two weeks after injection by flow cytometry by detection of human CD45⁺ immune cells in bone marrow aspirates (Figure 3). Strikingly, human CD34⁺CD38⁻ HSPCs as well as lymphoid and myeloid progenitor cells could be identified as early as 14 days after injection. Efficient differentiation of FLCs into lymphoid restricted progenitor cells was confirmed by detection of CD7⁺CD2⁻ pro-T1, CD7⁺CD2⁺ pro-T2 T cells and of CD19⁺CD10⁺ immature B cells (Figure 3). The presence of human CD33⁺CD14^{-/+} myeloid as well as of human CD123⁺ and CD11c⁺ dendritic cell precursors verified myeloid differentiation (Figure 3). Based on the functional validation *in vitro* and *in vivo* human FLCs were confirmed to contain human HSPCs required for generation of HIS BRG mice.

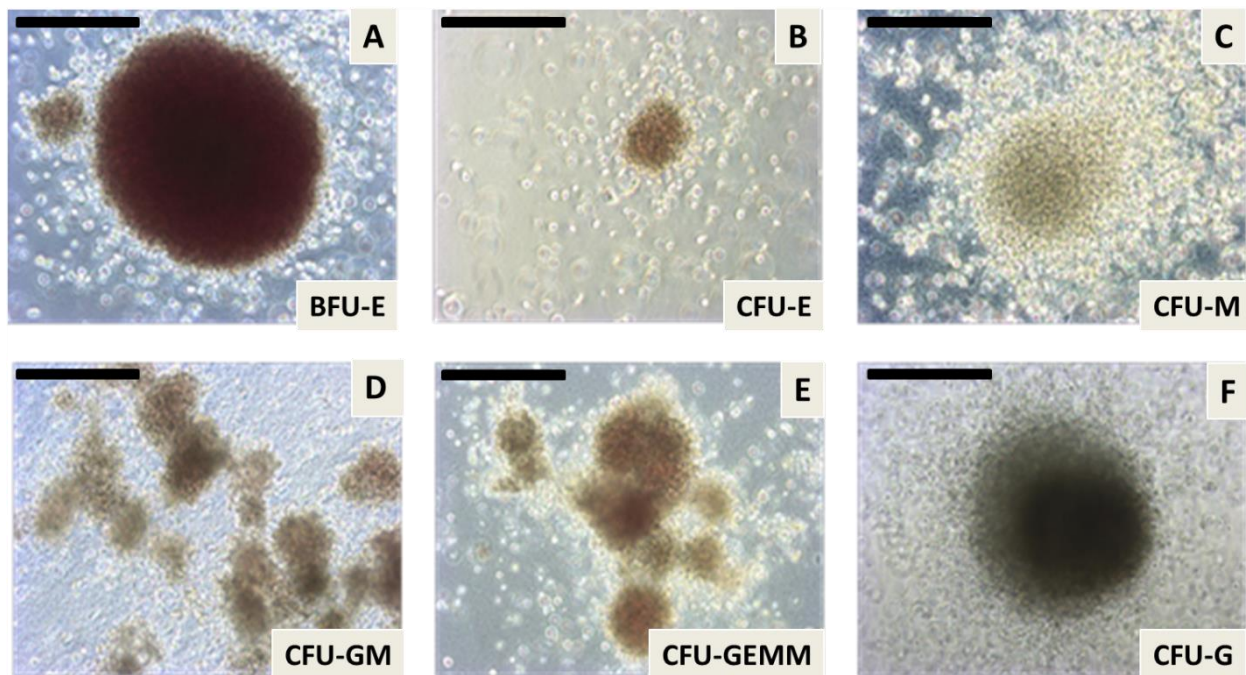


Figure 2: Colony types formed by FLCs in the colony formation cell (CFC) assay

Representative pictures of different colony types formed by FLCs incubated for 14 days in methylcellulose (scale bars represent 500 μ m length). (A) Burst forming unit-erythroid. (B) Colony forming unit-erythroid. (C) Colony forming unit-macrophage. (D) Colony forming unit-granulocyte, macrophage. (E) Colony forming unit granulocyte, erythroid, macrophage, megakaryocyte. (F) Colony forming unit-granulocyte.

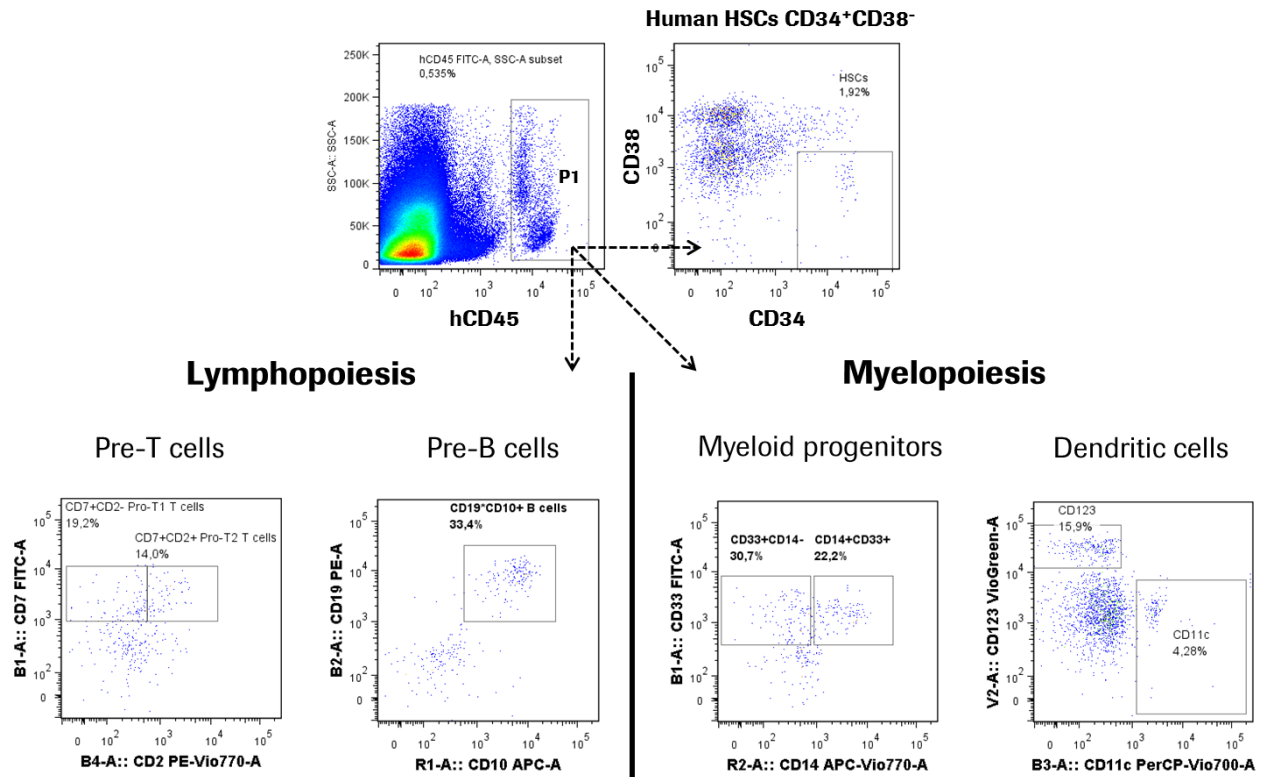


Figure 3: Engraftment and differentiation of human FLCs in the bone marrow of newborn BRG mice

Bone marrow aspirates from HIS BRG mice were analyzed by flow cytometry for presence of human CD45 positive immune cells (P1) 2 weeks after reconstitution. Different subsets of human immune cells were identified by staining for the indicated surface markers. The frequency of each subpopulation is based on the parental gate shown on the top right of each plot.

5.2. Characterization of lymphoid organs in HIS BRG mice

To test whether engrafted human FLCs were capable of establishing a human like immune system, newborn BRG mice were intra-hepatically injected with cells from four different donors and primary as well as secondary lymphoid organs were analyzed at different time points after reconstitution.

5.2.1. Peripheral blood

Analysis of peripheral blood is described as reliable readout to determine the success of humanization in reconstituted HIS mice^{100,122}. Thus, blood samples of HIS BRG mice were analyzed 8 weeks, 12 weeks and 18 weeks after FLCs injection using flow cytometry. The humanization level given in percentage reflects the frequency of human CD45 positive cells among total, mouse and human, immune cells in the peripheral blood. At every time point analyzed, mouse immune cells were found to dominate within the leukocyte compartment as seen by the average frequency of human CD45 positive cells being less than 50% (Figure 4A). Moreover, the frequency of human leukocytes in peripheral blood was found to significantly decrease over time. While the level of humanization averaged more than 30% at 8 weeks

upon reconstitution only half of this humanization level was observed 10 weeks later (Figure 4A). In contrast to the calculated frequencies, human CD45⁺ cell counts peaked 13 weeks after reconstitution however also significantly declined within the following 5 weeks (Supplementary Figure 2A). In general, high variation of humanization levels were observed among individual animals at each time point analyzed (Figure 4A). To test whether the observed divergence was dependent on the HSC donor used, the average frequency of human CD45 positive cells was analyzed in blood of mouse batches derived from a single FLC donor 8 weeks after reconstitution (Figure 4B). Strikingly, the average level of humanization ranged from below 20% in mice derived from donor 1 to over 40% in mice derived from donor 3. In addition, high variability in humanization was also observed in individual mice derived from the same FLC donor (Figure 4B). Detailed phenotyping of the human white blood cells (WBCs) revealed the majority of human CD45⁺ cells were lymphocytes, whereas the myeloid lineages were underrepresented (Figure 4C-F). Effectively, human CD3⁺T and CD19⁺ B cells were found to account for more than 80% of all human leukocytes at all three time points tested, while human innate immune cells such as CD11b⁺ myeloid cells and CD56⁺ NK cells averaged less than 15% or were virtually absent, respectively (Figure 4C + Figure 4E-F). While the frequency of human CD3⁺ T cells was relatively constant over time, human B cells proportionally decreased and human myeloid cells increased 18 weeks after reconstitution (Figure 4E+F). Counts of human peripheral blood T cells, B cells and monocytes peaked 13 weeks after reconstitution and declined from there on (Supplementary Figure 2). The analysis of cell counts also revealed that a significant drop of human CD3⁺ and CD19⁺ counts between week 13 and 18 is responsible for increased frequencies of human myeloid cells described before (Figure 4E + Supplementary Figure 2). In general, human leucocyte counts calculated in blood of HIS BRG mice were 100-1000 fold lower as compared to human individuals and 50-500 fold lower as compared to immunocompetent mice. In clear contrast to HIS BRG mice, CD11b⁺ myeloid cells clearly dominate over CD3⁺ and CD19⁺ lymphoid cells in human whole blood samples analyzed (Figure 4F). Moreover, a defined population of human NK cells can be detected in human peripheral blood, but not in blood of HIS BRG mice (Figure 4F).

Taken together, human leukocytes were detected at variable levels in blood of HIS BRG mice at different time points after reconstitution. Whereas in human blood myeloid cell types clearly dominate over T and B cells low frequency of these cell types was detected in blood of HIS BRG. Humanization levels calculated in blood were highly variable and donor dependent resulting in a very heterogenous population of HIS BRG mice. As a consequence for subsequent experiments, mice were allocated to specific groups using multiple criteria as described (4.21.2) to balance this variability. Despite the

presence of human immune cells in peripheral blood is a valuable readout for humanization, structural and cellular analyses of primary and secondary lymphoid organs were performed in addition.

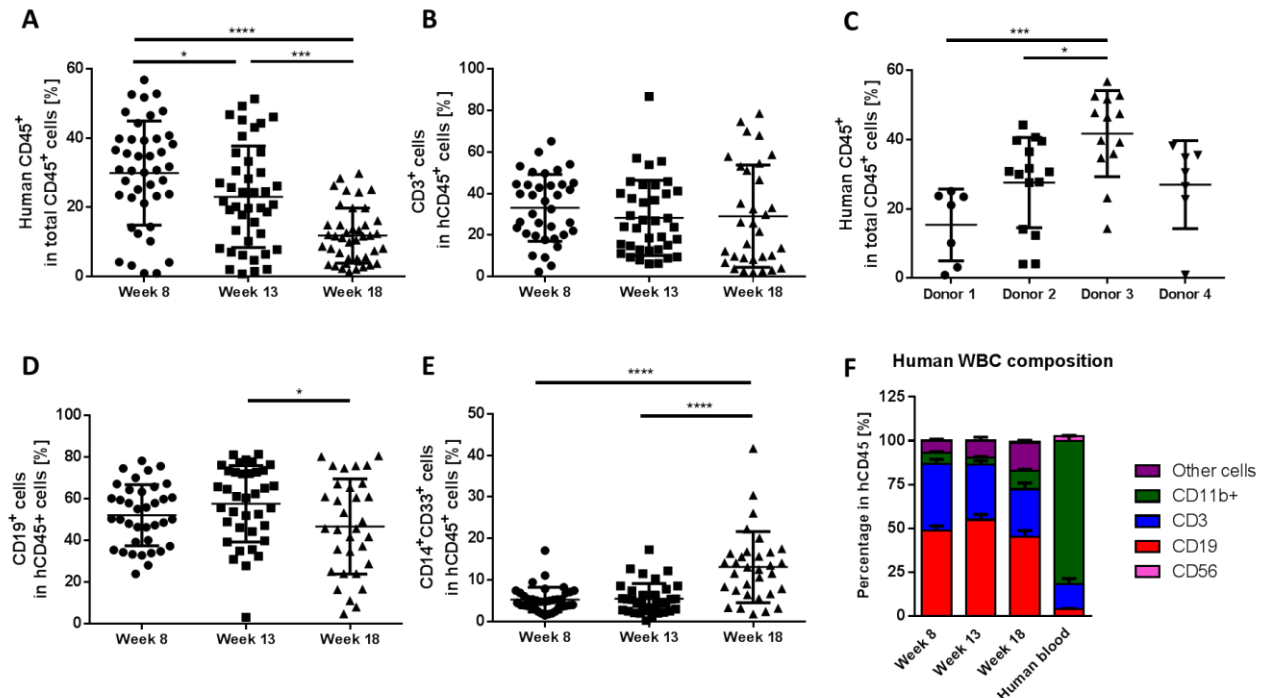


Figure 4: Analysis of human white blood cell composition in peripheral blood of HIS BRG mice

(A) Frequencies of human hematopoietic cells among total (mouse and human) CD45⁺ cells in peripheral blood of HIS BRG mice at indicated time points after reconstitution. Each symbol represents an individual mouse, black bars indicate mean values \pm SEM (n= 42 mice; one-way analysis of variance (ANOVA) followed by Tukey's test (* $p < 0.05$)). (B) Frequencies of human immune cells among total CD45⁺ cells in peripheral blood of HIS BRG mice 8 weeks after reconstitution with indicated HSC donors (n= 7-15 mice; mean \pm SEM, one-way ANOVA; * $p < 0.05$ Tukey's test). (C-E) Frequency of human T cells (CD3⁺), B cells (CD19⁺) and myeloid cells (CD11b⁺) among human immune cells in peripheral blood of HIS BRG mice at indicated time points after reconstitution (n= 42 mice; mean \pm SEM, one-way ANOVA; * $p < 0.05$ Tukey's test). (F) Composition of human white blood cells in peripheral blood of HIS BRG mice compared to healthy human volunteers (n = 42 mice; n = 3 human donors; mean \pm SEM).

5.2.2. Bone marrow

The presence of human hematopoietic cells in peripheral blood proves the release of differentiated human leukocytes from the bone marrow. Human FLCs have been shown to give rise to lymphoid as well as myeloid progenitors 2 weeks after intrahepatic injection (Figure 3), however with a strong bias towards lymphoid cell type. This raises the question whether advanced myeloid differentiation is impaired in HIS BRG mice. To address this, human white blood cell composition was analyzed in the bone marrow of HIS BRG mice 8 to 15 weeks after HSC transfer. To visually confirm humanization of the bone marrow in HIS BRG mice, human and mouse immune cells were stained simultaneously by immunohistochemistry (IHC) on representative longitudinal bone marrow sections. Co-staining of human and mouse CD45 identified high numbers of human cells to populate the mouse bone marrow even 12

weeks after reconstitution (Figure 5A). Human CD45 positive cells were evenly distributed throughout the bone marrow and mixed with mouse CD45 positive immune cells (Figure 5A, insert). To more accurately determine the frequency of human cells within the bone marrow, single cell suspensions stained for mouse and human CD45 were analyzed by flow cytometry (Figure 5C). On average, approximately every fourth immune cell in the bone marrow was identified to be of human origin (Figure 5C). Among human CD45⁺ white blood cells CD19⁺B cells were the most abundant cell type, whereas frequencies of CD11b⁺ myeloid cells and especially CD3⁻CD7⁺T cell precursors were lower (Figure 5D). Within the human CD11b⁺ myeloid compartment, monocytic as well as granulocytic cell types were identified in form of CD33⁺CD14⁻ monocytic precursors and differentiated CD33⁺CD14⁺ monocytes as well as of CD16⁺CD15⁺ neutrophils, respectively (Figure 5B). In depth phenotyping of human B populations in the bone marrow revealed several differentiation stages of human B cells to be reflected. The majority of human B cells expressed CD19 but no immunoglobulin M (IgM), thus representing very early B cell precursors called pre-B cells (Figure 5E). Furthermore, CD19⁺IgM⁺ immature as well as CD19⁺IgM⁺IgD⁺

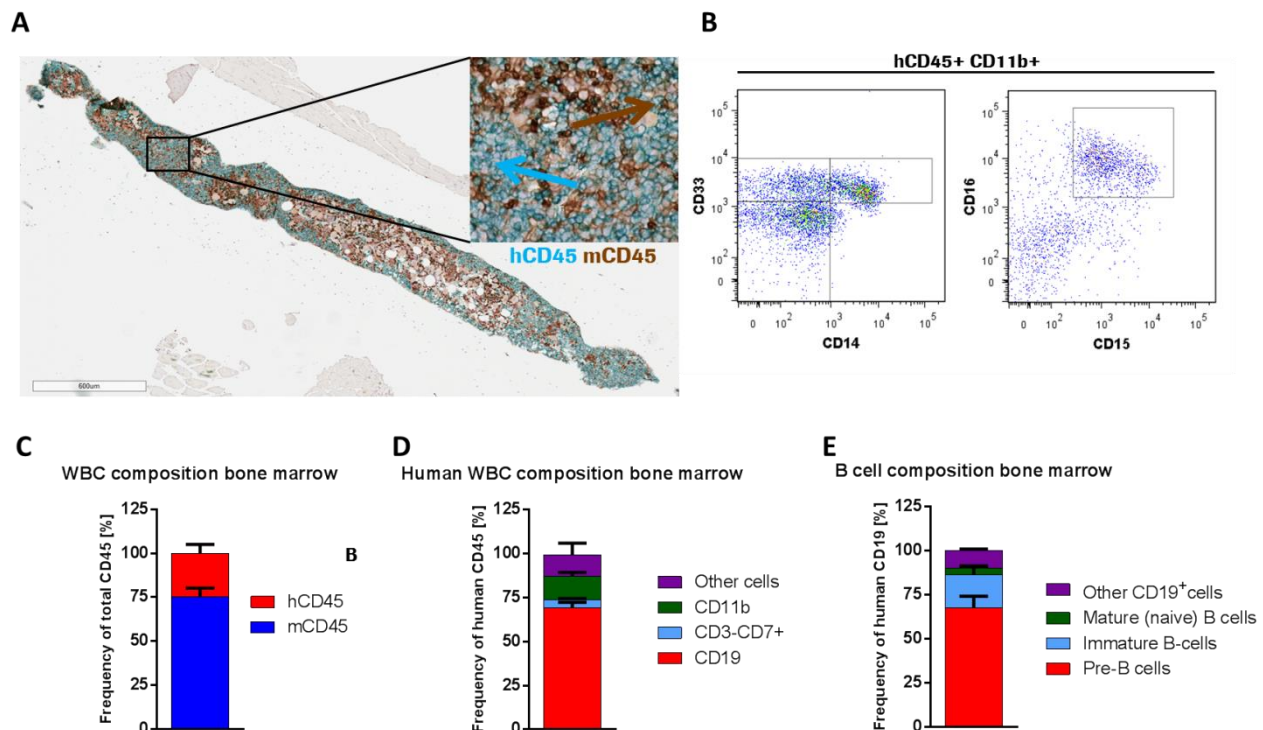


Figure 5: Morphological and cellular characterization of the bone marrow in HIS BRG mice

(A) Paraffin embedded femur section was double-stained for human (purple) and mouse (brown) CD45⁺ cells 12 weeks after reconstitution; data are representative of 18 samples (BM: Bone marrow, B: Bone). (B) Representative flow cytometry analysis of myeloid markers as indicated within human CD45⁺CD11b⁺ bone marrow cells. (C) Frequency of human and mouse leukocytes of total human and mouse CD45⁺ cells in bone marrow aspirates of humanized mice 8-15 weeks after reconstitution (n=18 mice; n=2 FLC donors; mean ± SEM; hCD45: human CD45; mCD45: mouseCD45). (D) Frequencies of cell types indicated among human CD45⁺ cells in BM aspirates of HIS BRG mice 8 to 15 weeks after reconstitution (n=14 mice; n=2 human donors; mean ± SEM) (E) Frequency of CD19⁺IgM⁻ pre-B cells, CD19⁺IgM⁺ immature B cells and CD19⁺IgM⁺IgD⁺ mature B cells in human CD19⁺ bone marrow cells of HIS BRG mice 8 to 15 weeks after reconstitution (n=12 mice; n=2 human donors; mean ± SEM).

mature B cells were detected in bone marrow was well (Figure 5E).

In summary, humanization of the bone marrow in HIS BRG mice was durable for at least 15 weeks after reconstitution despite the continued dominance of mouse immune cells over the human counterpart. Efficient lymphopoiesis as well as myelopoiesis was detected at different time points after reconstitution as confirmed by detection of human B and T cells as well as of monocytic and granulocytic precursor cells, respectively. The differentiation of human pre-B cells into immature and mature B cells has been described to correlate with surface expression of human IgM and IgD dependent on the developmental stages of human B cell maturation, which were found to be reflected in HIS BRG mice.

5.2.3. Thymus

Whereas in men B cell development is mainly restricted to the bone marrow, maturation of thymocytes takes place in another specialized primary lymphoid organ, the thymus. Detection of mature human T cells in blood indicates that human T cell development in HIS BRG mice is functional and that thymocytes may undergo similar developmental stages. However, human T cell differentiation and selection requires intact thymic structures usually not present in immunodeficient BRG mice due to diminished mouse T cell development. As already reported in other HIS mouse models two thymic lobes were detectable in front of the trachea of most HIS BRG mice at different time points after reconstitution¹⁵⁷ (Figure 6A). While humanized thymi were structurally very similar to those found in immunocompetent C57BL/6 mice, they were much smaller in size (Supplementary Figure 3A). In contrast to bone marrow and blood, more than 90% of leukocytes colonizing the thymus were of human origin as confirmed by expression of human CD45 (Figure 6B). The majority of human immune cells in humanized thymi stained positive for surface markers CD4 and/or CD8 and thus represented either double or single positive human thymocytes (Figure 6C). Surprisingly, also CD19⁺ human B cells were consistently detected in thymi of HIS BRG mice (Figure 6C). Using the same gating strategy as for the bone marrow, the majority of intrathymic B cells was be classified as immature pre-B cells due to lack of human IgM expression (Supplementary Figure 3B). In humans, CD4 and CD8 double positive immature thymocytes undergo positive and negative selection in the thymus before being released as CD4 or CD8 single positive T cell into the periphery¹⁵⁸. Human thymopoiesis is a well understood process including defined maturational stages each of which is characterized by expression of specific surface markers¹⁵⁹. To address whether these developmental stages of thymus maturation can be reflected in a mouse thymic structure, expression of surface markers CD69, CD1a, CD3, T cell receptor $\alpha\beta$ and CD44 was detected on CD4 and CD8 single as well as double positive thymocytes isolated from thymi of HIS BRG mice by FACS.

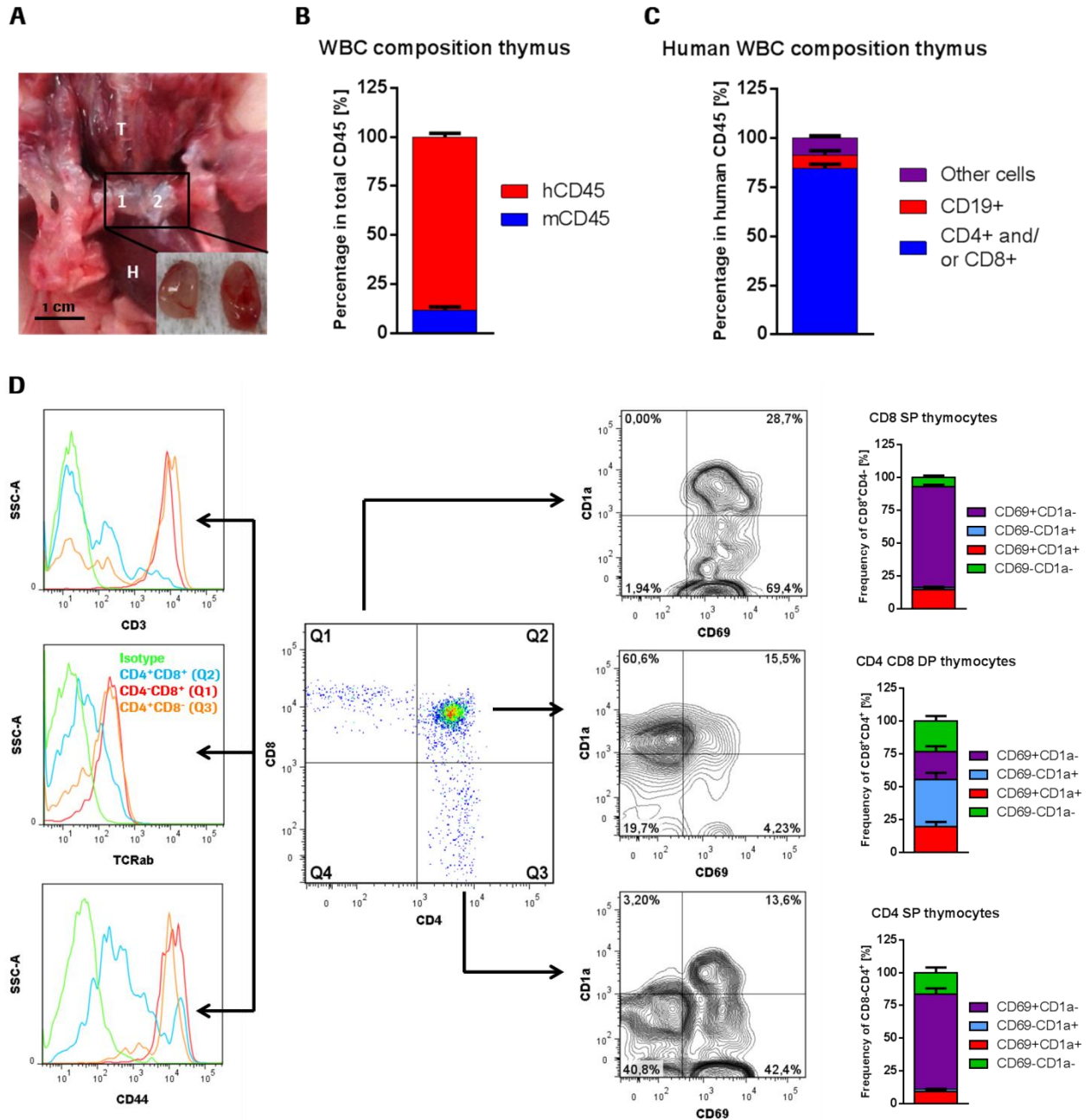


Figure 6: Thymus characterization in HIS BRG mice

(A) Localization of two (1,2) thymic lobes above the heart (H) and in front of the trachea (T) in a HIS BRG mouse 12 weeks after reconstitution; thymic lobes were removed and picture was taken at higher magnification (insert). (B) Frequency of human and mouse leukocytes within total CD45⁺ cells in thymus samples of HIS BRG mice 8-15 weeks after reconstitution (n=18 mice; n=2 human donors; error bars, SEM; hCD45: human CD45; mCD45: mouse CD45). (C) Frequency of indicated human leukocyte populations within human CD45⁺ cells in thymus samples of HIS BRG mice 8-15 weeks after reconstitution (n=18 mice; n=2 human donors; error bars, SEM) (D) Thymus samples from HIS BRG mice analyzed by flow cytometry 12 weeks after intrahepatic transfer of human FLCs. (Center) Expression of human CD4 and CD8 surface antigens within human CD45⁺ cells. (Right) Representative FACS plots and frequencies (bar charts) of CD69 and CD1a expression within CD4⁺CD8⁺ (Q2), CD4⁺CD8⁻ (Q3) and CD4⁻CD8⁺ (Q1) thymocytes; the frequency of each subpopulation is based on the parent gate shown on the top right of each plot. (Left) Overlaid histograms representing expression level of indicates markers on CD4⁺CD8⁺ (blue), CD4⁺CD8⁻ (orange) and CD4⁻CD8⁺ (red) thymocytes; expression level relative to non-specific isotype antibodies (green).

More than 50% of CD4⁺CD8⁺ thymocytes were found to express CD1a, while less than 15% of single positive CD4 and CD8 T cells expressed CD1a (Figure 6). For the early activation marker CD69, more than 85% of CD4 and CD8 single positive cells co-expressed this, but it was only detected on approximately 20% of double positive thymocytes. Moreover, CD4⁺CD8⁺ thymocytes had lower expression level of CD3, CD44 and T cell receptor $\alpha\beta$ compared to CD4 and CD8 single thymocytes (Figure 6). Positive and negative selection of immature thymocytes is usually facilitated by MHC molecules presented by specialized thymic epithelial cells and immune cells characterized by simultaneous expression of MHC class I and II molecules in the thymus. Successful genetic rearrangement and expression of TCR α and TCR β suggests that human thymocytes have efficiently interacted with MHC molecules in the mouse thymus. To evaluate whether a chimeric thymus provides a proper environment for human thymocyte selection, mouse and human MHC class II expression was detected by IHC (Figure 7). As expected, mouse MHCII⁺ cells were detected in the thymus forming an epithelial like grid (Figure 7). Interestingly, high numbers of human MHC class II⁺ cells were present in the thymus as well. Cells positive for human MHC

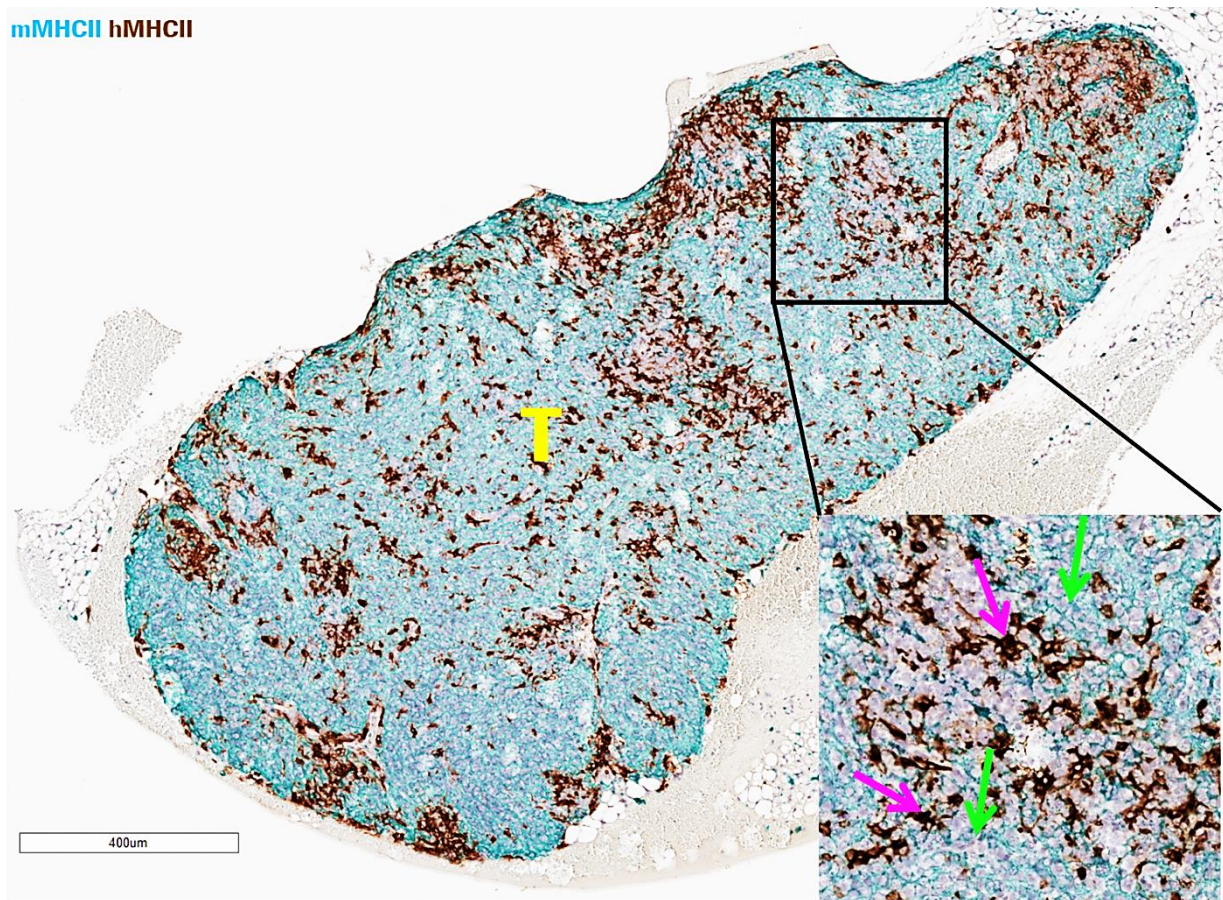


Figure 7: Expression of human and mouse MHC class II molecules in the thymus of HIS BRG mice

Paraffin embedded sections of a humanized thymus (T) double-stained with monoclonal antibodies against human and mouse MHCII 12 weeks after reconstitution; Insert: Higher magnification of indicated thymus area demonstrating human (pink arrows) and mouse (green arrows) MHC class II co-expression in humanized thymus; Data are representative of 18 samples.

class II appeared to be a more heterogenous population with stretched epithelial like cells and roundish lymphocyte like cell types (Figure 7), while mouse MHC class II⁺ cells were more uniformly shaped. Mouse MHC class II⁺ cells were equally distributed throughout the thymus and human MHC class II⁺ cells tend to cluster in certain areas devoid of mouse MHC class II expression (Figure 7). In principle, the presence of human antigen-presenting cells in the thymus enables selection of human CD4⁺CD8⁺ thymocytes on human MHC molecules. To visually verify the interaction of human MHC class II⁺ cells with human thymocytes, specific co-localization of both cell types was evaluated by fluorescence microscopy (Figure 8). As expected, the merged fluorescence images suggest only few interactions of human CD8⁺ and human MHC class II⁺ cells (Figure 8B) and CD8⁺ thymocytes seem to be evenly distributed throughout the thymic tissue. In contrast, most CD4⁺ thymocytes cluster in specific areas of the thymus and were generally found in close proximity to human MHC class II⁺ cells, indicating direct interaction of both cell types (Figure 8A).

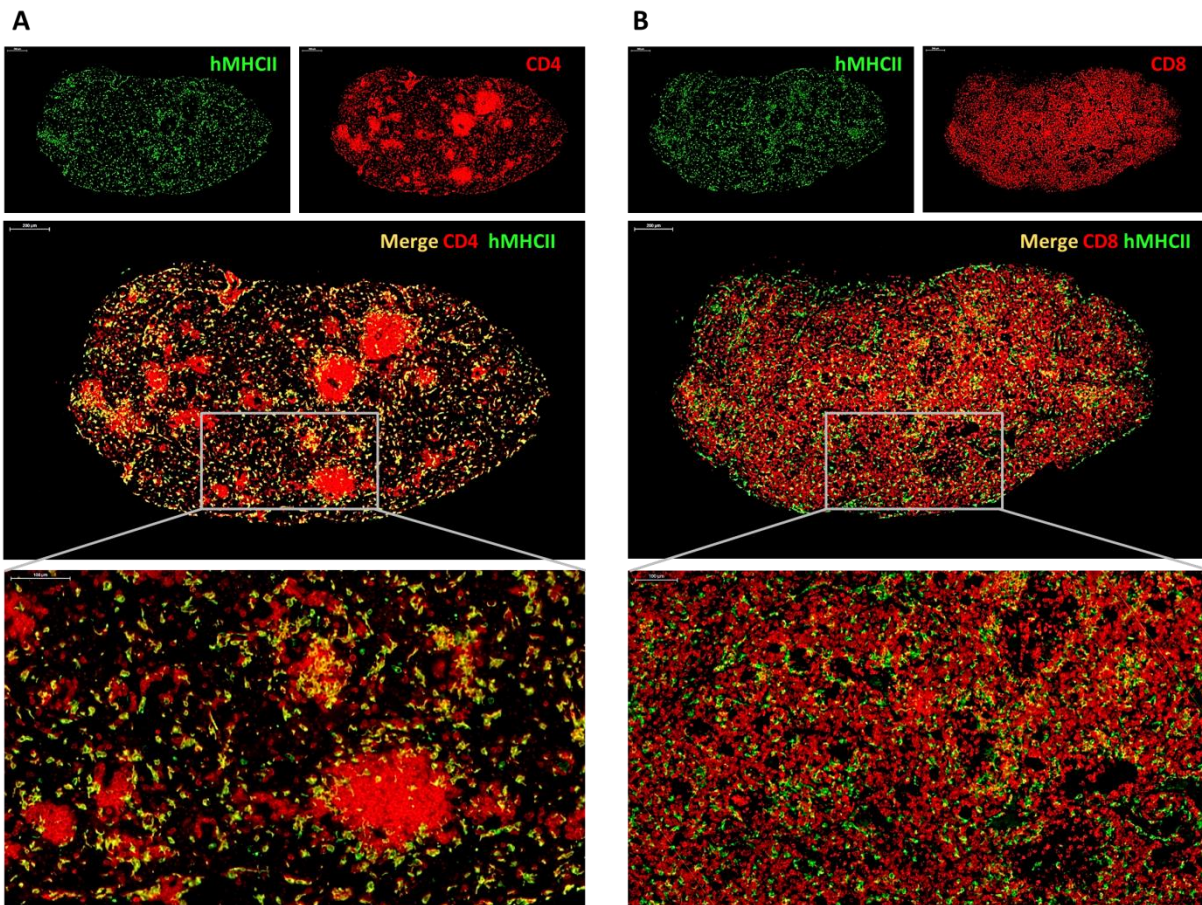


Figure 8: Co-localization of human antigen presenting cells and human thymocytes in thymus of humanized mice
Paraffin embedded sections of a humanized thymus double-stained with monoclonal antibodies against human MHCII and human CD4 (A) or human CD8 (B); human MHCII and CD4/CD8 were visualized using Alexa488 (green) and Alexa647 (red) conjugated secondary antibodies, respectively; colocalization of indicated marker was achieved by simultaneous detection of both fluorescent signals (yellow).

Taken together, thymopoiesis in *de novo* generated thymic structures exhibited remarkable similarities to the human situation in accordance to the performed phenotypic analysis. Therefore, human lymphoid development in primary lymphoid organs has been shown to reflect in HIS BRG mice.

5.2.4. Lymph nodes

Immunodeficient BRG mice generally lack distinct lymph node structures as functional knockout of the Rag2 gene inhibits development of functional mouse lymphocytes. In contrast, defined lymph nodes were regularly detected in BRG mice reconstituted with human FLCs. While mesenteric lymph nodes were present in the intestinal connective tissue of most HIS BRG mice cervical, axial and inguinal lymph nodes were only sporadically observed (Figure 9A). Although flow cytometry analysis revealed the average frequency of human leukocytes to exceed 70% (Figure 9E) highly variable humanization levels were detected in lymph nodes of individual mice as confirmed by IHC (Figure 9 B+C). Consistent with previously characterized lymphoid organs the majority of human leukocytes isolated from lymph nodes were lymphoid cell types with CD3⁺ T cells accounting for more than 50% (Figure 9 D+F). Extremely low numbers of human CD33⁺CD14⁻ myeloid precursor cells and CD14⁺ monocytes detected in mesenteric lymph nodes indicate that human myeloid cells indeed do not efficiently differentiate in lymphoid organs of HIS mice (Figure 9F). Frequencies of leukocyte populations calculated by FACS analysis were visually reflected on lymph node tissue sections (Figure 9D and F). Whereas CD3⁺ T cells were found to be distributed all over the lymph node tissue CD20⁺ B cells rather clustered in distinct areas. Co-localization of human B and T cells suggests that both lymphocytes populations might actively interact with each other. However, if compared to follicular like structures found in human lymph nodes cellular organization in lymph nodes of HIS BRG mice was rather chaotic (Figure 9D + Supplementary Figure 4). Furthermore, in contrast to human lymphocytes CD68⁺ human macrophages could only be sparsely detected in lymph nodes of HIS BRG mice at any time point after reconstitution (Figure 9D + Supplementary Figure 4A). In summary, mesenteric lymph nodes were efficiently generated in HIS BRG mice. Detailed cellular analysis revealed the frequency of human immune cells to significantly differ in lymph node samples of individual mice. As already observed in blood and the bone marrow human T and B lymphocytes were found at high frequencies in lymph node tissues while human myeloid cell types were clearly underrepresented. Although direct interaction of human immune cells in lymph nodes of HIS BRG mice is likely, lack of follicular like organization might explain the absence of humoral immune responses in conventional HIS mouse models. Beside the lymph nodes the spleen is another secondary lymphoid organ in which defined follicles are formed in humans.

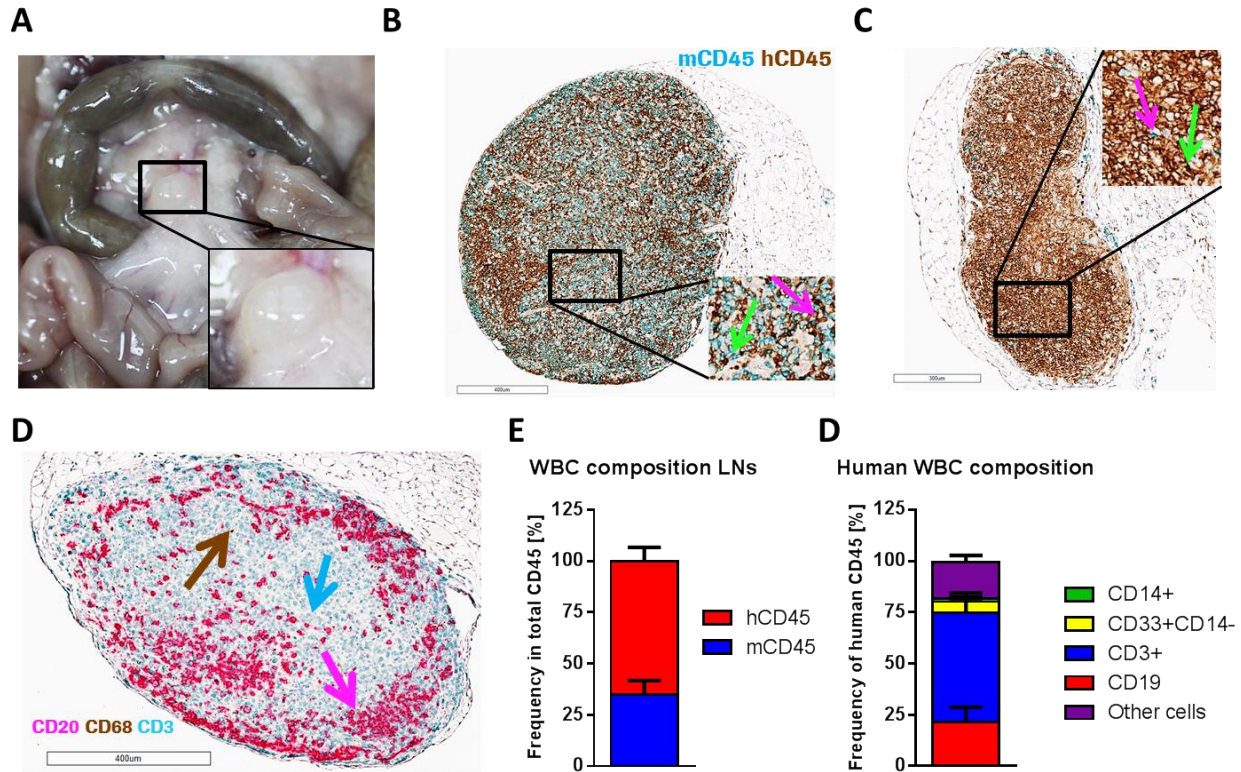


Figure 9: Morphological and cellular characterization of mesenteric lymph nodes in HIS BRG mice

(A) Localization of one representative mesenteric lymph node in the connective fatty tissue of the small intestine in of a representative humanized mouse at 12 weeks after reconstitution; Insert: same lymph node at higher magnification. (B+C) Paraffin embedded lymph node sections of two representative mice double-stained for human (purple) and mouse (brown) CD45⁺ cells 12 weeks after reconstitution; Inserts: Higher magnification of indicated lymph node area demonstrating human (pink arrows) and mouse (green arrows) CD45⁺ cells. (D) Representative lymph node section triple-stained for human CD3 (purple), CD68 (brown) and CD20 (pink) 12 weeks after reconstitution. (E+F) Frequency of human and mouse leukocytes within total CD45⁺ cells (E) and of indicated human leukocyte populations within human CD45⁺ cells (F) in lymph node samples of HIS BRG mice 8-15 weeks after reconstitution (n=7 mice; n=2 human donors; error bars, mean + SEM; hCD45: human CD45; mCD45: mouse CD45).

5.2.5. Spleen

In contrast to *de novo* formed lymph nodes in HIS BRG mice, splenic structures preexisted in immunodeficient BRG mice (Figure 10A left). To test whether human leukocytes successfully repopulated the spleen with characteristic follicular-like structures, samples of humanized mice were characterized at different time points after reconstitution. In general, spleens from HIS BRG mice were markedly enlarged compared to spleens from non-humanized BRG mice at every time point analyzed (Figure 10A). On a cellular basis, the vast majority of leukocytes in humanized spleens were found to be of mouse origin expressing mouse CD45 (Figure 10D). In contrast, the average frequency of human immune cells was below 20% as detected by flow cytometry (Figure 10D). Co-staining of mouse and human CD45 on

splenic tissues sections visually confirmed the dominating mouse compartment over human immune cells in HIS BRG mice (Figure 10B). Similar to what was observed in peripheral blood and lymph nodes (Figure 4 + Figure 9), human leukocytes isolated from spleen samples were clearly biased towards the lymphoid lineage at any time point after reconstitution (Figure 10E). More concretely, B and T lymphocytes account for more than 70% of all human white blood cells, while CD33⁺CD14⁻ myeloid precursors as well as CD14⁺ monocytes did sum up to approximately 15 % (Figure 10F). In contrast to lymph nodes, human cells were found to be organized in follicular-like structures in the spleen (Figure 10C). However, in contrast to human splenic follicles, those found in HIS BRG mice lack a clear cellular organization. In the human spleen lymphocyte populations are located in distinct areas of the follicles. Similar to what was observed in human lymph nodes (Figure 9) B cells were found in the germinal center of splenic follicles while T cells were mainly located in the surrounding area (Supplementary Figure 4). In

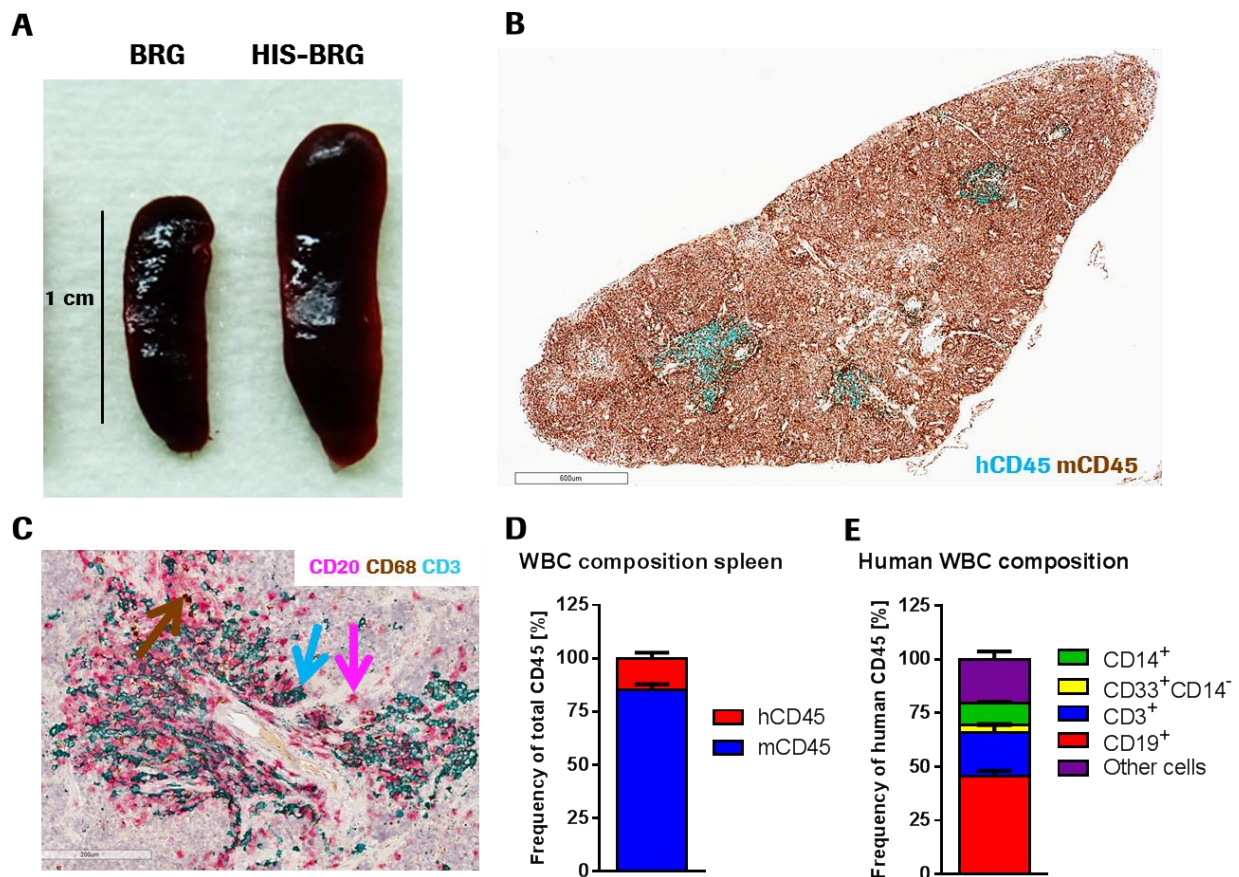


Figure 10: Morphological and cellular characterization of the spleen in HIS BRG mice

(A) Spleen size of BRG and HIS BRG mice. (B+C) Paraffin embedded spleen section double-stained for human (purple) and mouse (brown) CD45⁺ cells 12 weeks after reconstitution. (C) Representative spleen section triple-stained for CD3 (purple), CD68 (brown) and CD20 (pink) 12 weeks after reconstitution. (D+E) Frequency of human and mouse leukocytes within total CD45⁺ cells (D) and of indicated human leukocyte populations within human CD45⁺ cells (E) in spleen samples of HIS BRG mice 8-15 weeks after reconstitution (n=7 mice; n=2 human donors; error bars, SEM; hCD45: human CD45; mCD45: mouse CD45).

contrast to this well organized structure, human B and T lymphocytes were rather mixed up in splenic follicles of HIS BRG mice (Figure 10C). Another obvious difference was the overall frequency of human CD68 positive macrophages. While in human spleens, CD68 positive cells are found in splenic follicles as well as in the remaining spleen tissue, they were only sparsely detectable or even absent in spleen samples of HIS BRG mice (Figure 10C + Supplementary Figure 4).

Taken together, human multipotent CD34⁺ fetal liver cells were shown to engraft and differentiate in newborn and sublethally irradiated BRG mice. Generated HIS BRG mice were shown to finally developing a chimeric immune system consisting of innate mouse and mainly lymphoid human leukocytes. Both primary lymphoid organs, bone marrow and thymus, were able to provide a permissive environment for human B cell and T cell maturation, respectively. B cells underwent human-like maturation steps from pre- to mature B cells in the bone marrow. Similar to human thymopoiesis, immature T cells underwent positive and negative selection in thymus of HIS BRG mice. Human lymphocytes released from primary lymphoid organs were found to efficiently repopulate lymph nodes and the spleen. Although human B and T cells were found in close proximity to each other in both lymphoid organs, defined follicular structures as seen in humans were not detected. While human lymphopoiesis is well reflected in HIS BRG mice observed underrepresentation of human innate immune cells clearly represents a major limitation of this model. While monocyte, granulocyte and dendritic cell precursors were readily detectable in the bone marrow of HIS BRG mice only low numbers of mature myeloid cell types were present in blood, lymph nodes and spleen. As human antigen-presenting cells are necessarily required for innate as well as adaptive immunity, e.g. for the initiation of anti-tumoral immune responses, it is doubtful if HIS BRG mice represent an suitable model to study human anti-tumor immune responses *in vivo*.

5.3. Cross reactivity of mouse CSF-1 on human CSF-1 receptor

Flavell et al initially demonstrated in 2011 that replacement of mouse by human macrophage colony stimulating factor (CSF-1) significantly improves the development of human monocytes and macrophages in HIS BRG mice¹⁰³. Mouse CSF-1 has been reported repeatedly to lack biological activity on human CSF-1R¹⁴⁹, and data derived from the human CSF-1 knock-in mice obviously confirmed this hypothesis *in vivo*^{100, 103}. Mouse CSF-1 however was confirmed to indeed bind to human CSF-1R but with very low affinity of μM ¹⁵². This led to the hypothesis, that mouse CSF-1 is principally capable of activating CSF-1R signaling in human cells. Therefore, we tested binding of mouse CSF-1 to human CSF-1R by two different types of Biacore measurements. First of all, a so called surface plasmon resonance (SPR)

approach was applied to determine the affinity of free mouse CSF-1 to immobilized human and mouse CSF-1R. For each concentration of mouse CSF-1 a characteristic sensogram was generated comprising of different binding phases. In the initial association phase ligands attach to the receptor reflected by increasing response rates. The association phase is followed by an equilibrium phase characterized by a constant response rate over a certain time. Decreased response rates finally indicate detachment of the ligand from the receptor (Figure 11A+B). As expected, mouse CSF-1 was found to tightly bind to its cognate receptor as seen by consistent response rates over time even at very low concentrations (Figure 11A), resulting in an extremely high affinity of 2.7 pM (Figure 11A). In contrast, mouse CSF-1 was shown

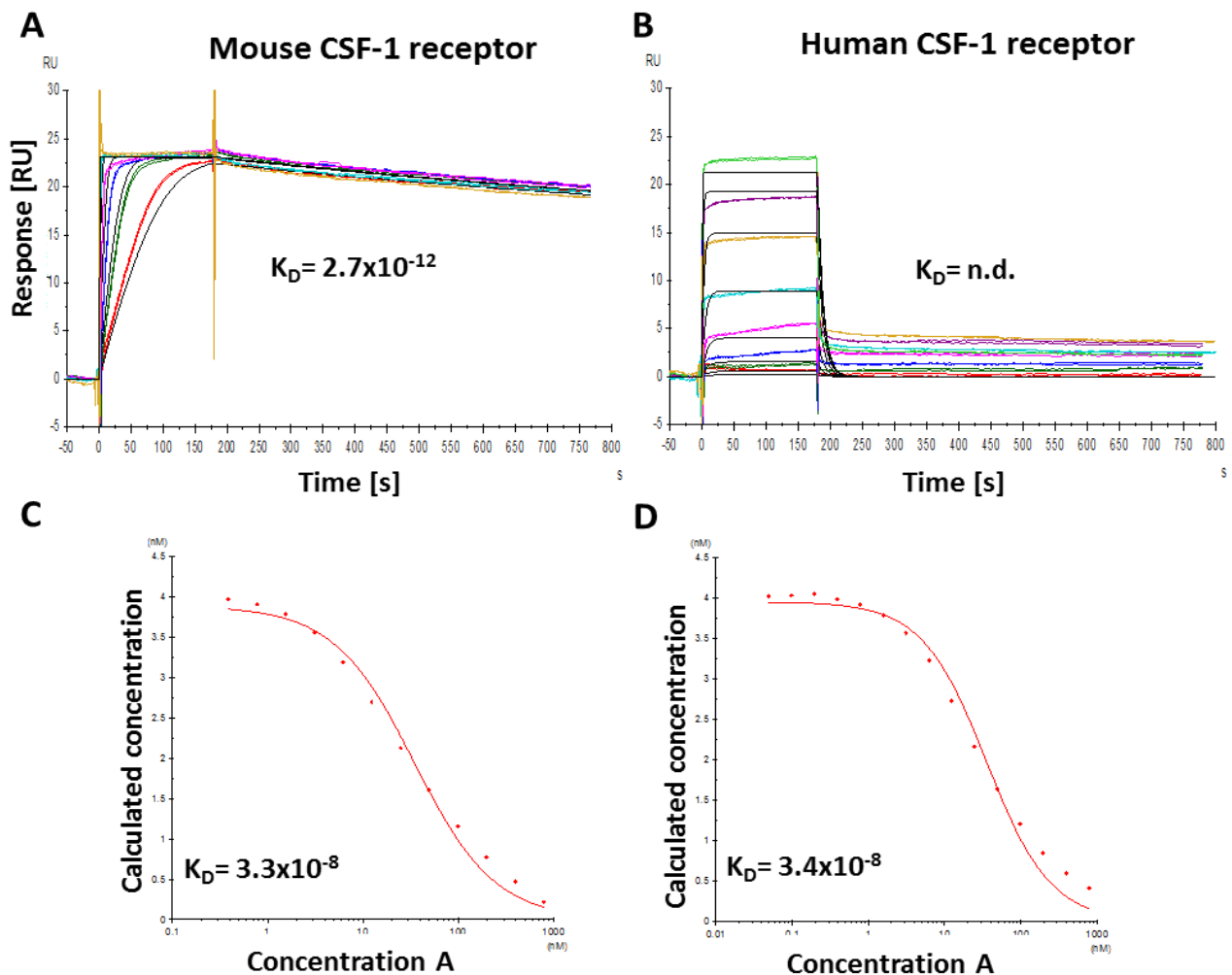


Figure 11: Biacore analysis of mouse CSF-1 and human or mouse CSF-1R

(A) Affinity of mouse CSF-1 to immobilized mouse CSF-1R as measured by the response rate over time with each colored line representing a specific mouse CSF-1 concentration. (B) Affinity of mouse CSF-1 to immobilized human CSF-1R as measured by the response over time; different colors indicate different mouse CSF-1 concentrations tested. (C+D) Inhibition curves of two independent affinity in solution measurements determining the affinity of mouse CSF-1 (concentration A) and human CSF-1R in solution (K_D : Dissociation constant).

to bind to human CSF-1R only at very high concentrations and only for a relatively short time (Figure 11B). This fast-on/fast-off binding behavior did not allow calculation of affinity by steady state equilibrium kinetics, therefore an affinity in solution assay was performed in addition. In this assay format human CSF-1R was preincubated with increasing concentrations of mouse CSF-1 in solution and unbound CSF-1R was detected by an immobilized anti-human CSF-1R capture antibody. Figure 11C represents the dose response or inhibition curves from two independent measurements. Both data sets confirmed independently, that increasing concentrations of mouse CSF-1 correlated with decreasing amounts of free human CSF-1R. A calibration curve was finally used to determine the average affinity of the mouse ligand to the human receptor. The resulting affinity of 33.5 nM revealed that mouse CSF-1 can bind to human CSF-1R but with a more than 12,000 fold lower affinity compared to its cognate receptor.

Taken together, mouse CSF-1 was shown to indeed bind to human CSF-1R, however very low affinity results in rapid dissociation of the receptor ligand complex. Next, human peripheral blood monocytes were stimulated *in vitro* with different concentrations of mouse CSF-1 to determine whether human CSF-1R can still dimerize and induce phosphorylation. Western blot analysis was performed to evaluate CSF-1R phosphorylation and downstream AKT using beta actin as loading control. Human monocytes were stimulated for 5 minutes with human CSF-1 served as positive control. As reported before,

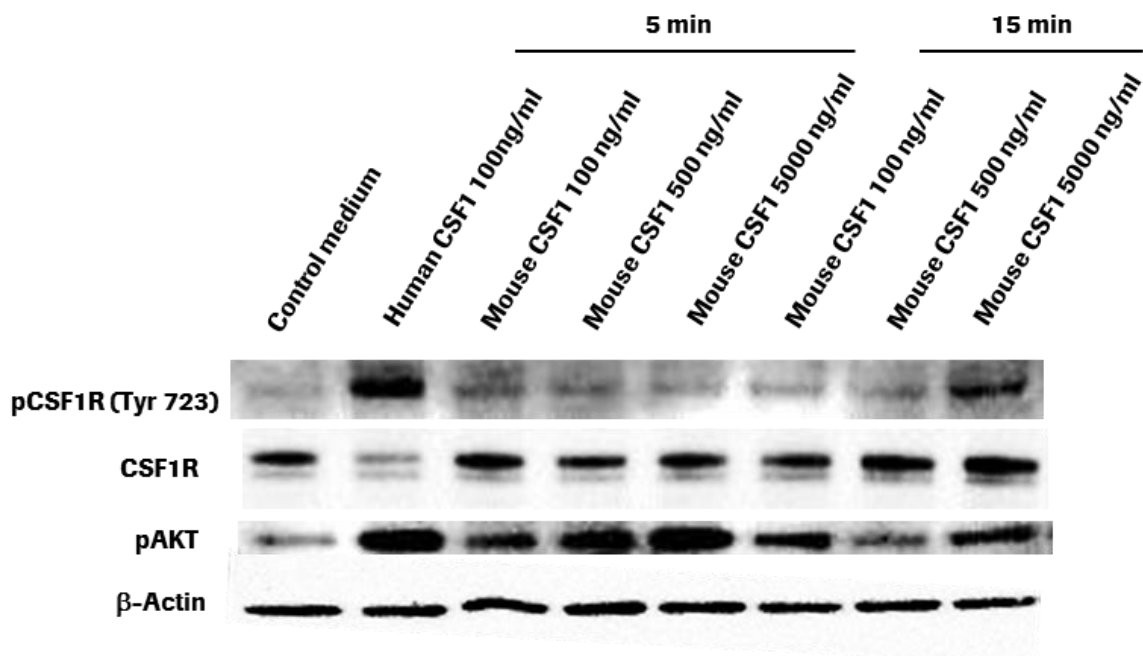


Figure 12: Analysis of CSF-1R signaling in human monocytes stimulated with mouse and human CSF-1

Human CD14⁺ monocytes were isolated from a single human blood donor by density gradient centrifugation and stimulated with indicated concentrations of human or mouse CSF-1 for 5 or 15 minutes; protein lysates were separated by SDS PAGE and blotted onto a nitrocellulose membrane; membranes were probed with antibodies directed against pCSF-1R, total CSF-1R or pAKT. β -Actin was used on each membrane as loading control (representative sample chosen).

phosphorylation of CSF-1R and AKT in monocytes stimulated with human CSF-1 was accompanied by reduced protein level of total CSF-1R¹⁶⁰ (Figure 12). Strikingly, stimulation of human monocytes with 5 $\mu\text{g/ml}$ mouse CSF-1 for 15 minutes resulted in activation of CSF-1R signaling cascade as determined by phosphorylation of CSF-1R and AKT (Figure 12). However, level of total CSF-1R was not decreased upon stimulation using mouse CSF-1. No CSF-1R phosphorylation was observed in human monocytes stimulated with CSF-1 for only 5 minutes, but a dose dependent phosphorylation of AKT was detected, which indicates that a non-detectable CSF-1R signaling might happen after all.

5.4. Biological activity of mouse CSF-1 on human CSF-1R

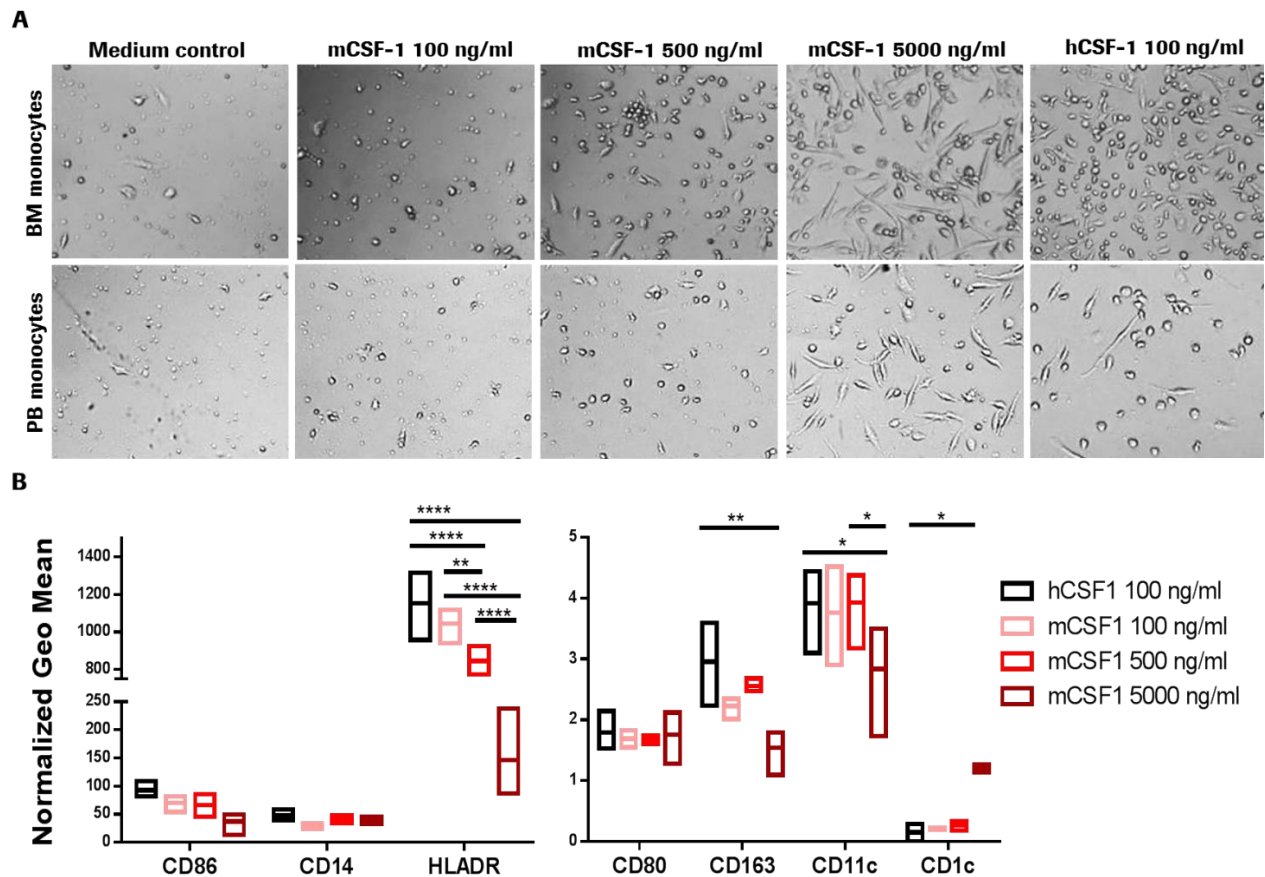


Figure 13: Differentiation of human monocytes upon stimulation with mouse CSF-1 *in vitro*

(A) Human monocytes were isolated from peripheral blood (PB monocytes) or bone marrow of HIS BRG mice (BM monocytes) by density gradient centrifugation and magnetic enrichment of CD14⁺; cells were seeded in media containing indicated concentrations of mouse or human CSF-1 for 8 days. Morphology was assessed using a light microscope; media without supplements was used as reference control. (B) Human peripheral blood monocytes from 3 human blood donors were differentiated as described in A and analyzed by flow cytometry for expression of indicated surface markers; absolute staining intensities were calculated by normalizing to the matching isotype control (n= 3; mean \pm SEM; one-way analysis of variance (ANOVA) per marker followed by Tukey's test (*P < 0.05)).

Next, it was evaluated of whether CSF-1R signaling activated by mouse CSF-1 is sufficient to induce differentiation of human monocytes into macrophages *in vitro*. CD14⁺ monocytes isolated from peripheral blood of human donors and from bone marrow aspirates of HIS BRG mice were incubated for 8 days with various concentrations of mouse CSF-1. Human bone marrow monocytes from HIS BRG mice were enriched by first depleting mouse CD45⁺ cells followed by magnetic enrichment for human CD14 cells. Purity of human CD14 positive cells finally accounted to 84% (Supplementary Figure 5). As expected human peripheral blood monocytes survived and differentiated upon stimulation with human CSF-1 as shown by presence of stretched and roundish cell types at day 8 (Figure 13A). Comparable results were

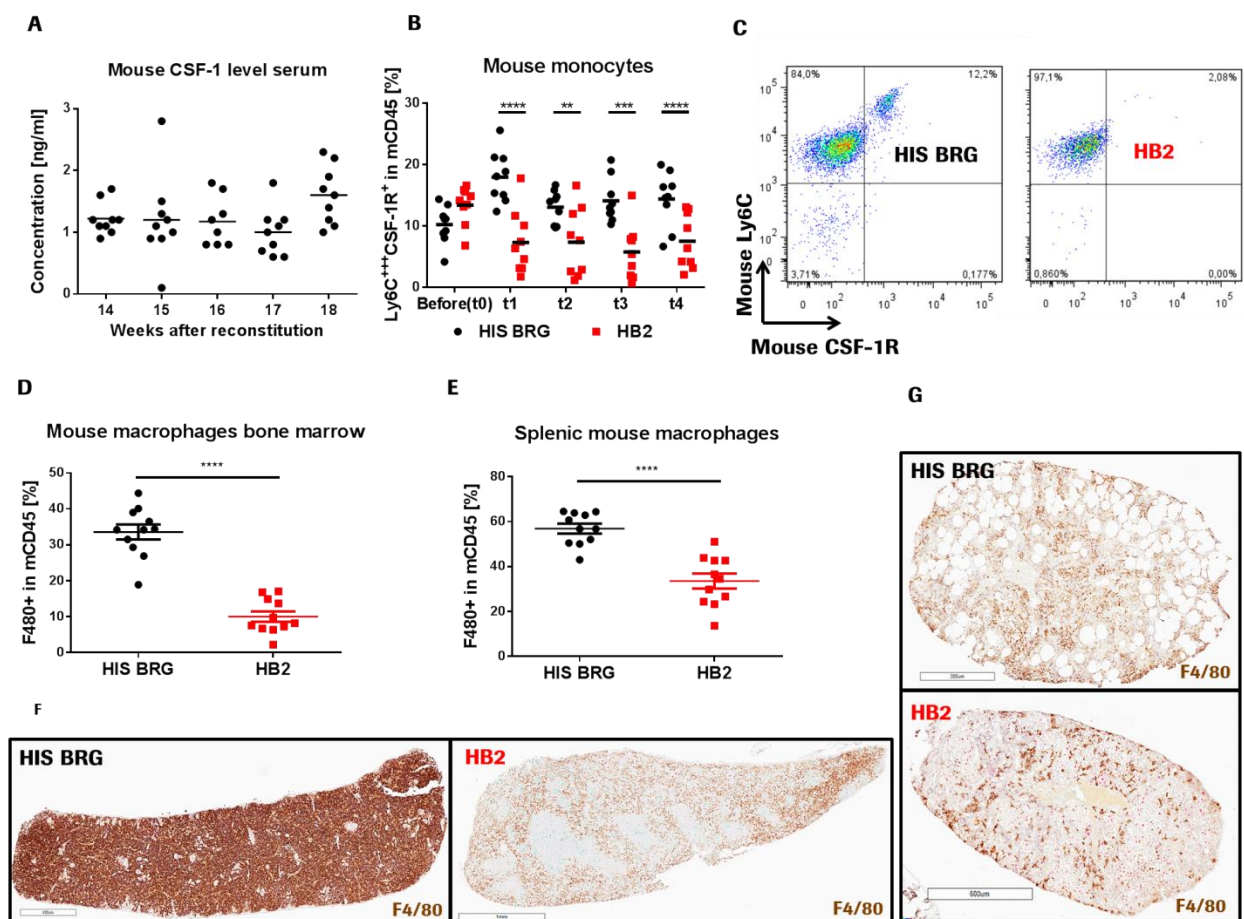


Figure 14: Depletion of mouse monocytes and macrophages in HIS BRG mice

Humanized mice were injected with 4 consecutive doses of 2G2 (anti-mouse CSF-1R) or the matching mouse IgG1 isotype (MOPC-21) at 30 mg/kg/week. Different parameters were analyzed before (t0) and during (t1-t4) the treatment in peripheral blood and at day of necropsy (t4) in spleen and bone marrow. (A) Level of mouse CSF-1 in serum of HIS BRG mice at different time points after reconstitution as measured by ELISA (n=8-9 mice). (B) Frequency of Ly6C⁺⁺⁺CSF-1R⁺ mouse monocytes within mouse CD45⁺ cells in HIS BRG mice injected with 4 doses of MOPC-21 (HIS BRG) or 2G2 (HB2) antibody (n= 8-10 mice; mean ± SEM, separate unpaired Student's t-test per time point; *p < 0.05). (C) Representative FACS blot comparing the frequency of Ly6C⁺⁺⁺CSF-1R⁺ mouse monocytes in control and 2G2 mice. (D+E) Frequency of F4/80 positive mouse macrophages within mouse CD45⁺ cells in bone marrow or spleen of HIS BRG and HB2 mice as determined by FACS analysis (n= 8-9 mice; mean ± SEM, unpaired Student's t-test; Mean). (F+G) Immunohistochemical staining of mouse F4/80 on representative spleen or bone marrow sections of humanized mice injected with 4 doses of control (MOPC-21) or anti-mouse CSF-1R (2G2) antibody.

achieved if cells were cultured with mouse CSF-1 at 5 $\mu\text{g}/\text{ml}$ while lower CSF-1 concentrations not sufficiently support human monocyte survival and differentiation (Figure 13A). Human bone marrow-derived monocytes survived and differentiated similarly when incubated with human CSF-1 or mouse CSF-1 at 5 $\mu\text{g}/\text{ml}$ (Figure 13). Survival of both human monocyte populations positive correlated with increasing concentrations of mouse CSF-1 and was dose dependent (Figure 13A). To further phenotypically classify differentiated blood monocytes, expression of several myeloid markers were analyzed by flow cytometry after 8 days of *in vitro* culture. Expression levels of co-stimulatory molecules CD86 and CD80, as well as CD14 were only low expressed in all conditions analyzed (Figure 13B). In comparison to monocytes differentiated with human CSF-1, expression of human MHCII decreased in dose dependent manner in cultures containing mouse CSF-1 (Figure 13B). Expression levels of M2 scavenger receptor CD163, the dendritic cell marker CD1c and pan myeloid marker CD11c were rather comparable in monocytes cultured with either human or mouse CSF-1 at low to intermediate concentrations. In contrast, CD163 and CD11c were significantly downregulated and CD1c upregulated on cells differentiated with 5 $\mu\text{g}/\text{ml}$ mouse CSF-1 (Figure 13B).

To sum up the *in vitro* results obtained, mouse CSF-1 was shown to bind to human CSF-1R with a $\sim 12,000$ fold lower affinity than to its cognate receptor and with a fast-on/fast-off binding kinetic. Nevertheless, it was able to induce CSF-1R signaling as shown by phosphorylation of CSF-1R and downstream AKT in human peripheral blood as well as in bone marrow derived monocytes. Activation of CSF-1R signaling in human blood monocytes correlated with survival and differentiation in dose dependent manner. Cells differentiated with low to mid nanogram concentrations of mouse CSF-1 phenotypically resembled human CSF-1 treated monocytes but showed decreased survival. Using the highest mouse CSF-1 concentration on the hand correlated with enhanced survival and differentiation into a morphological similar but phenotypical different phenotype.

5.5. Induction of supraphysiological mouse CSF-1 levels in HIS BRG mice

After showing that mouse CSF-1 is cross-reactive to the human CSF-1R, it is still questionable why human monocytes and macrophage are underrepresented in HIS BRG mice. Differentiation and survival of human monocytes was shown to be dose dependent, therefore it is reasonable to presume that mouse CSF-1 levels present in humanized BRG are not sufficient to promote human myelopoiesis. Sera from HIS BRG mice were analyzed for mouse CSF-1 levels 14 to 18 weeks after reconstitution (Figure 14A). These time points were chosen because the overall humanization levels is expected to peak within this time (Figure 4). The average concentration of mouse CSF-1 in sera of HIS BRG mice ranged from 1-2 ng/ml,

which seems to be insufficient for driving human monocyte survival and differentiation (Figure 14A). CSF-1 signaling is not only required for terminal differentiation but also for maturation of monocytes precursors in the bone marrow. Therefore, a dramatic increase in mouse CSF-1 in HIS BRG mice could improve human monocyte as well as human macrophage reconstitution. Mouse CSF-1 is known to be produced by different cell types including endothelial cells, bone marrow stromal cells and fibroblast while it is mainly consumed by monocytes, macrophages and osteoclasts¹⁶¹. One way to elevate mouse CSF-1 levels in HIS BRG mice is the blockade of CSF-1R, which is crucial for the high turn-over rate of CSF-1 and has been shown to result in dramatically increased CSF-1 levels in non-human primates and mice^{45, 162}. 2G2, an anti-mouse CSF-1R antibody, was recently reported to efficiently deplete CSF-1R positive tumor associated macrophages in immunocompetent mice⁴⁵. This antibody efficiently blocks mouse CSF-1R, thereby inducing abnormal high CSF-1 levels (Ries & Hoves, unpublished data). Consequently, HIS BRG mice were treated with 2G2 at 30 mg/kg per week for four consecutive injections. As a reference control, another group of HIS BRG mice received the matching mouse IgG1 isotype control antibody (MOPC-21) instead of 2G2. HIS BRG mice subjected to the described 2G2 treatment regimen are hereinafter referred to as HB2 mice and control animals receiving the matching mouse IgG1 isotype control as HIS BRG mice. The effect of 2G2 was monitored in the blood by detecting the frequency of mouse monocytes after each single injection (Figure 14B). Strikingly, already the first injection of 2G2 significantly reduced Ly6C⁺⁺⁺CSF-1R⁺ mouse monocytes in blood (t1) and these decreased monocyte frequencies could be maintained throughout the treatment period (t2-t4). In contrast, injection of MOPC-21 isotype antibody did not significantly alter mouse monocyte frequencies (Figure 14B+C). To test whether 2G2 injection reduced the amount of tissue resident mouse macrophages as well, spleen and bone marrow samples were stained for mouse macrophage specific marker F4/80 by flow cytometry and IHC. The frequency of mouse macrophages was remarkably reduced by more than 20% in bone marrow samples of 2G2 treated HIS BRG mice (Figure 14D). This result was visually confirmed by decreased numbers of F4/80⁺ cells in bone marrow section of representative animals (Figure 14G). Similarly, splenic macrophages were efficiently diminished upon treatment with 2G2 compared to control mice (Figure 14E). Although the relative reduction was comparable in both lymphoid organs, mouse macrophages still accounted for more than 30% of all mouse immune cells in the spleen (Figure 14D+E). Nevertheless, the efficiency of 2G2 in reducing the number of tissue macrophages was much more obvious in spleen than in bone marrow samples (Figure 14F). To confirm, that the blockade of CSF-1R positive mouse cells resulted in a systemic increase of mouse CSF-1, serum samples of 2G2 and MOPC-21 treated HIS BRG mice were subjected to ELISA measurements. The concentration of mouse CSF-1 concentrations in sera of MOPC-21 treated animals did not exceed 3ng/ml at any time point

(Figure 15A). Strikingly, treatment with a single dose of 2G2 increased the serum concentration of mouse CSF-1 more than 500 fold and repetitive treatment even more than 1000 fold with individual mice exceeding 1500 ng/ml (Figure 15A). Taken together, systemic blockade of CSF-1R and the reduction of host macrophages and monocytes resulted in supraphysiological levels of mouse CSF-1 in sera of HIS BRG mice.

5.6. Induction of human monocytes and macrophages in HIS BRG mice

To evaluate whether supraphysiological mouse CSF-1 levels in HB2 mice are sufficient to allow human myelopoiesis, peripheral blood was analyzed at the same time points as described before (Figure 14). Strikingly, in mice being treated with 2G2, counts of human total leukocyte were significantly increased

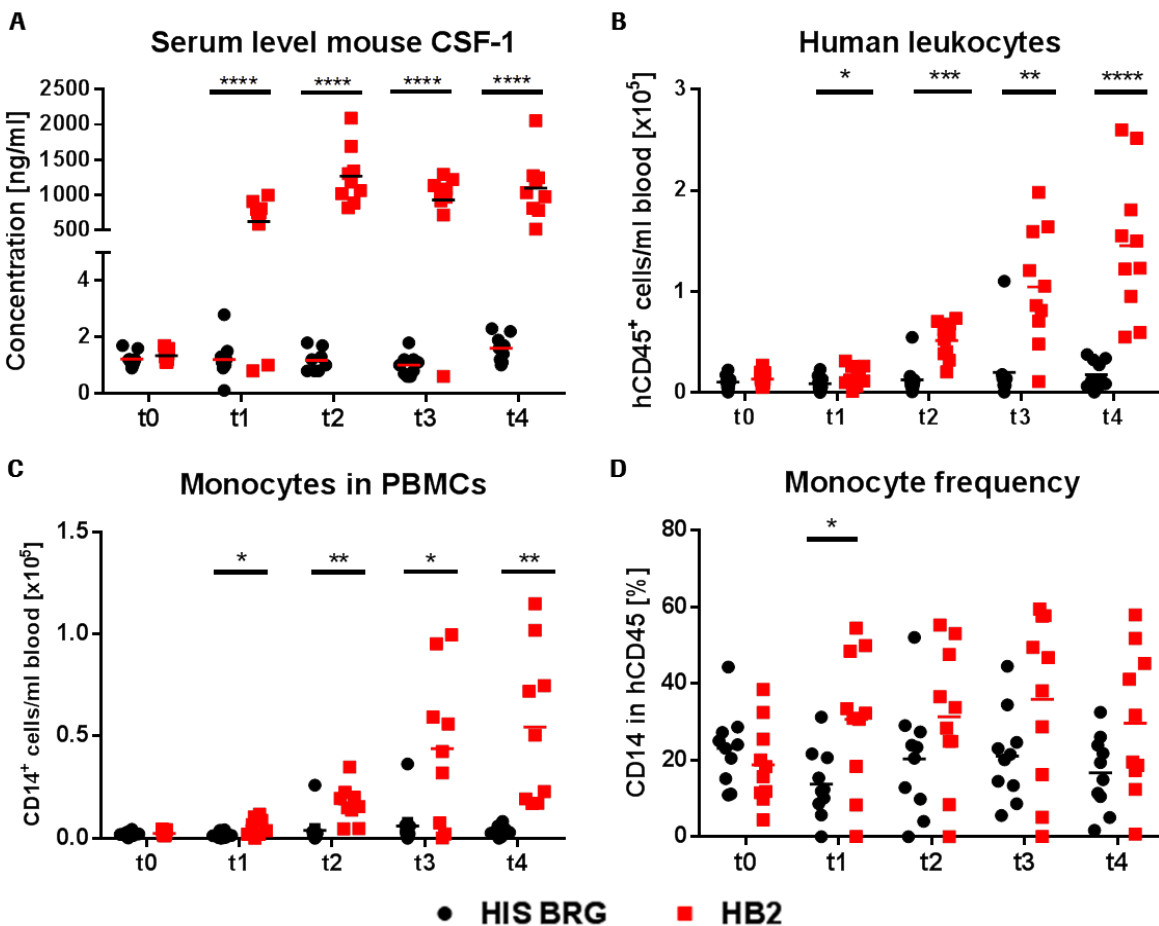


Figure 15: Blood analysis in HB2 mice

Humanized mice were injected with 4 consecutive doses of 2G2 (HB2) or MOPC-21 (HIS BRG) at 30 mg/kg/week and different parameters in peripheral blood were analyzed before (t0) and after (t1-t4) single injections. (A) Concentration of mouse CSF-1 was analyzed in sera of humanized mice at indicated time points using mouse specific CSF-1 ELISA (n= 8-10 mice; mean; one separate unpaired Student's t-test per time point; *P < 0.05). (B+C) Human CD45⁺ and human CD14⁺ counts per ml of peripheral blood (n= 8-10 mice; mean; separate unpaired Student's t-test per time point; *p < 0.05). (D) Frequency of human CD14⁺ cells among human CD45⁺ cells (n= 8-10 mice; mean; separate unpaired Student's t-test per time point; *p < 0.05).

over time as compared to control animals (Figure 15B). At time point of necropsy (t4), counts of human CD45 positive cells were increased more than 8 fold in peripheral blood of HB2 mice (Figure 15B). While human monocyte counts were as shown before constantly low in HIS BRG mice (Figure 4), a significant amplification of human CD14 positive cells was detected in HB2 mice (Figure 15C). Upon termination at t4, human monocytes were 16 fold higher in HB2 mice as compared to HIS BRG control mice (Figure 15C). These increased total numbers were also reflected by consistently higher frequency of CD14 positive cells within human white blood cells (Figure 15D). Subsequently, human monocytes detected in HB2 mice were phenotypically compared to monocytes isolated from human blood donors. Similar to human blood, classical CD14⁺⁺⁺CD16⁻, intermediated CD14⁺⁺⁺CD16⁺ as well as CD14^{+/-}CD16⁺ non-classical monocytes were detectable in HB2 mice (Figure 16). Whereas classical monocytes clearly dominated over intermediate and non-classical subtypes in human blood, all three populations were evenly represented in 2G2 treated mice (Figure 16A). Monocytes were further characterized by staining of activation markers MHCII and CD86 as well as of human CSF-1R (CD115) on CD14⁺CD33⁺ cells. Compared

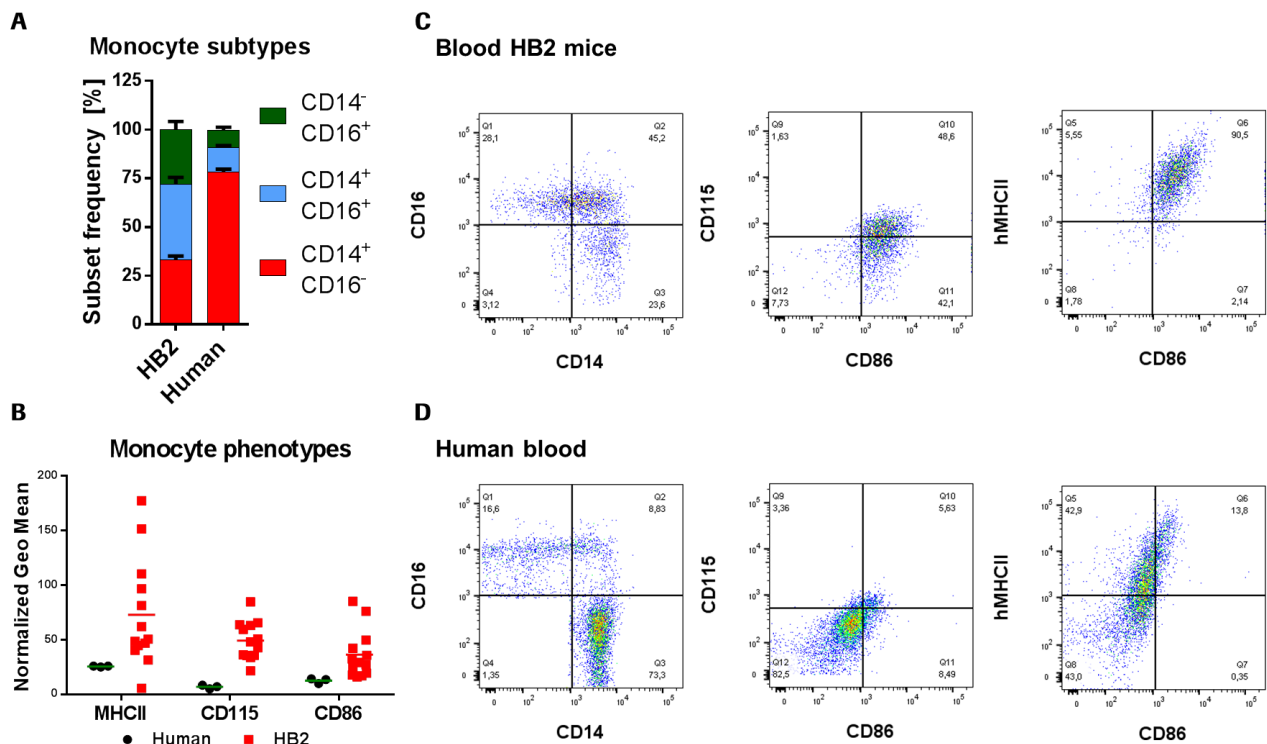


Figure 16: Phenotyping of human monocytes in HB2 mice

HIS BRG mice were treated with 4 consecutive doses of anti-mouse CSF-1R antibody and monocyte phenotypes were compared to blood samples from human donors. (A) Frequencies of the indicated cell populations among hCD45⁺CD14⁺CD16⁺ peripheral blood mononuclear cells of 2G2 treated HIS mice and human donors (n=19 mice; n=3 human donors; mean + SEM). (B) Expression of indicated markers on hCD45⁺CD14⁺CD33⁺ cells in peripheral blood of HB2 mice and human donors; signal intensities were normalized to geometric mean of the matching isotype control. (C/D) FACS staining of indicated makers in peripheral blood of a representative HB2 mouse (C) and a representative human donor (D).

to human blood, expression of MHCII, CD115 and CD86 was elevated ~ 50 fold, 8 fold and 3 fold on HB2 monocytes, respectively on monocytes isolated from HB2 mice (Figure 16C-D). To test whether improved reconstitution of monocytes was accompanied by terminal differentiation of human tissue human macrophages, lymphoid as well as non-lymphoid organs of HB2 mice were stained by IHC for human macrophage specific pan-maker CD68. In line with previous reports, most tissues in HIS BRG mice lack presence of tissue infiltrating human macrophages except for bone marrow and spleen (Figure 17 HIS BRG panel). In HB2 mice, CD68⁺ positive cells were detected in all lymphoid as well as non-lymphoid tissues (Figure 17 HB2 panel). In non-lymphoid organs high numbers of human macrophages were detected in the lung and the liver while colon and skin were moderately infiltrated (Figure 17). CD68 positive cells were evenly distributed in the bone marrow and rather randomly distributed in lymph nodes of HB2 mice (Figure 17). In contrast, human macrophages found in spleen of HB2 mice were mainly located in areas of splenic follicles composed of human CD20⁺ B and CD3⁺ T cells (Figure 17). Due to the limiting self-renewal potential of human HSPCs used to generate HIS mice, usability of this model

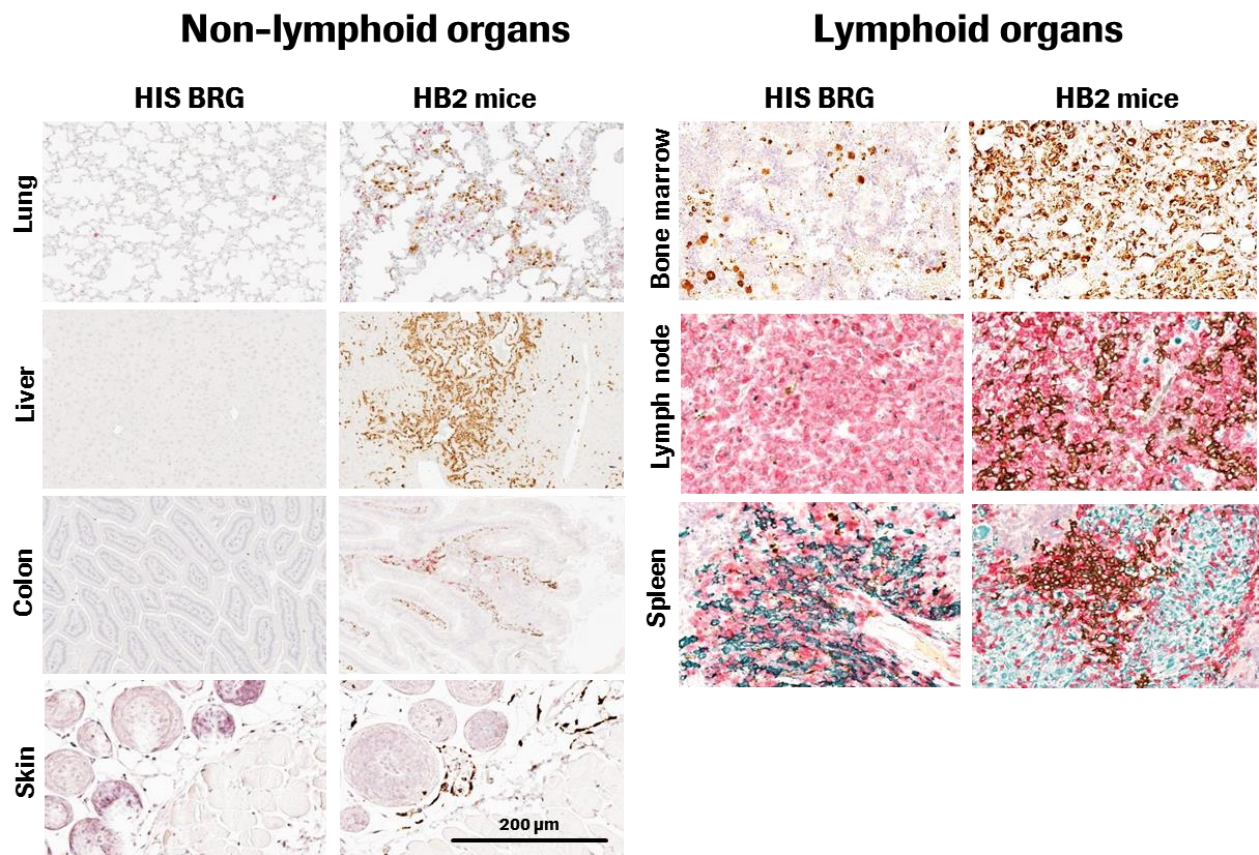


Figure 17: Infiltration of human macrophages in lymphoid and non-lymphoid tissues of HB2 mice

Formalin fixed non-lymphoid (A) and lymphoid (B) organs of HIS BRG control mice (HIS BRG mice) and HIS BRG mice treated with 4 consecutive doses of 2G2 (HB2 mice) were stained for indicated human markers by immunohistochemistry. Representative pictures of each staining and organs were chosen. Human macrophages: CD68 positive cells (brown); human T cells: CD3 positive cells (pink); human B cells: CD20 positive cells (purple).

is generally restricted to a certain time window after reconstitution. To test whether induction of human macrophages is time-dependent, HIS BRG mice with comparable humanization levels were treated with 4 consecutive doses of 2G2 at different time points after reconstitution (Figure 18). In general, frequencies of total human immune cells as well as human monocytes in human CD45⁺ cells increased at any time point after reconstitution in peripheral blood upon treatment with 2G2 (Figure 18A+B). However, differences in humanization levels and monocytes frequencies before and after treatment were reduced, the later animals were injected with 2G2 (Figure 18A+B). Strikingly, human macrophages could be successfully induced at every time point after reconstitution as shown by infiltration of human CD68⁺ cells in liver of representative animals (Figure 18C). Interestingly, even in mice previously declared as “non-humanized” based on very low hCD45⁺ frequencies (below 2 %) in peripheral blood, human macrophages could be induced (Figure 18C).

In summary, it was demonstrated here for the first time that repetitive injection of HIS BRG with an anti-mouse CSF-1R antibody significantly improves reconstitution of human peripheral blood monocytes as well as human tissue infiltrating macrophages at different time points after reconstitution.

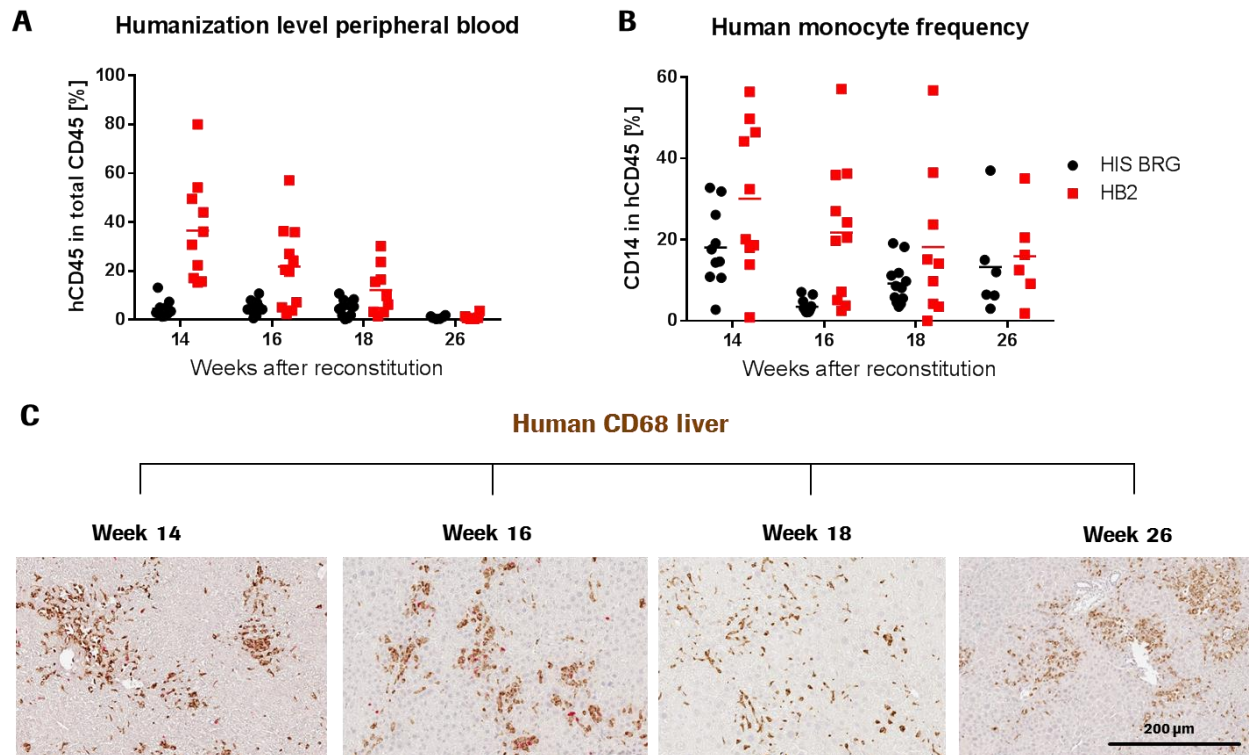


Figure 18: Time independent induction of human macrophages in HB2 mice

HIS BRG mice were treated at different time points after reconstitution (weeks after reconstitution) with 4 consecutive doses of 2G2 to become HB2 mice. The frequency of human CD45⁺ in total CD45⁺ cells (A) as well as the frequency of human CD14⁺ monocytes (B) was determined before (HIS BRG) and after (HB2) 2G2 treatment in peripheral blood of HIS BRG mice. (C) Presence of human macrophages was verified by immunohistochemical staining of human CD68 in liver samples of in HB2 mice.

5.7. Inhibition of human myelopoiesis in HB2 mice

Next we tested, whether supraphysiological mouse CSF-1 level generated upon blocking CSF-1R drive the improved human myelopoiesis in HB2 mice *in vivo* by antibody-mediated inhibition of mouse CSF-1. HIS BRG mice were simultaneously injected with 2G2 in presence or absence of an anti-mouse CSF-1 antibody (α mCSF-1, clone 5A1¹⁶³). To rule out, that improved myelopoiesis in HB2 mice was induced by human CSF-1 secreted by the macrophages themselves, another group of HIS BRG animals was co-injected with 2G2 and an anti-human CSF-1 antibody (α hCSF-1). To test if co-administration of α mCSF-1 reduced supraphysiological mouse CSF-1 levels, unbound mouse CSF-1 was measured in sera of mice of the different treatment groups by ELISA (Figure 19A). As expected, mouse CSF-1 concentrations were consistently increased \sim 1000 fold in sera of HB2 mice as compared to control HIS BRG mice. Remarkably, co-injection of α mCSF-1 reduced serum concentrations of unbound mouse CSF-1 to the control level (Figure 19A). As expected, co-injection of α hCSF-1 did not significantly influence the serum concentration of free mouse CSF-1 (Figure 19A). Although mouse CSF-1 complexed with α mCSF-1 was reported to lose its biological activity¹⁶⁴, total mouse CSF-1, free as well as complexed, was determined in sera as well. In control and α hCSF-1 treated mice total and free mouse CSF-1 levels were congruent (Figure 19A+B). However, concentrations of complexed mouse CSF-1 were more than 150 fold increased in α mCSF-1 treated mice at time point of necropsy as compare to HIS BRG control animals (Figure 19B, t4). Nevertheless, reduction of free as well as total mouse CSF-1 in α mCSF-1 treated HB2 mice was sufficiently high to evaluate its relevance for human myelopoiesis. As reported before (Figure 15), human monocyte counts were significantly increased up to 5×10^4 cells per ml blood in mice treated with 2G2 compared to control HIS BRG mice (Figure 19C). Although CD14⁺CD33⁺ counts tend to slightly decrease during α hCSF-1 treatment their total number was not significantly changed over time (Figure 19C). In contrast, co-injection of α mCSF-1 reduced human monocyte numbers by more than 60% (Figure 19 C, t4). Enhanced infiltration of human macrophages was observed in several non-lymphoid organs of HB2 mice, but the differences were most obvious in liver and lung (Figure 19 D-F). To compare the effect of blocking mouse or human CSF-1 on macrophage numbers in liver and lung, human CD68 positive cells were quantified based on IHC stain tissue sections. As compared to control animals, human macrophage counts were significantly increased in lung and liver of HB2 animals (Figure 19 D-F). In both organs, 2G2 induced increase was significantly reversed by blockage of mouse but not of human CSF-1 (Figure 19 D+F). Of note, human macrophages neither in the lung nor in the liver were reduced to control level by α mCSF-1 treatment (Figure 19 D+F), suggesting that autocrine production of human CSF-1 does

contribute to human macrophage survival and differentiation as well. In summary, these data clearly underline the fundamental role of supraphysiological mouse CSF-1 for human myelopoiesis in HB2 mice.

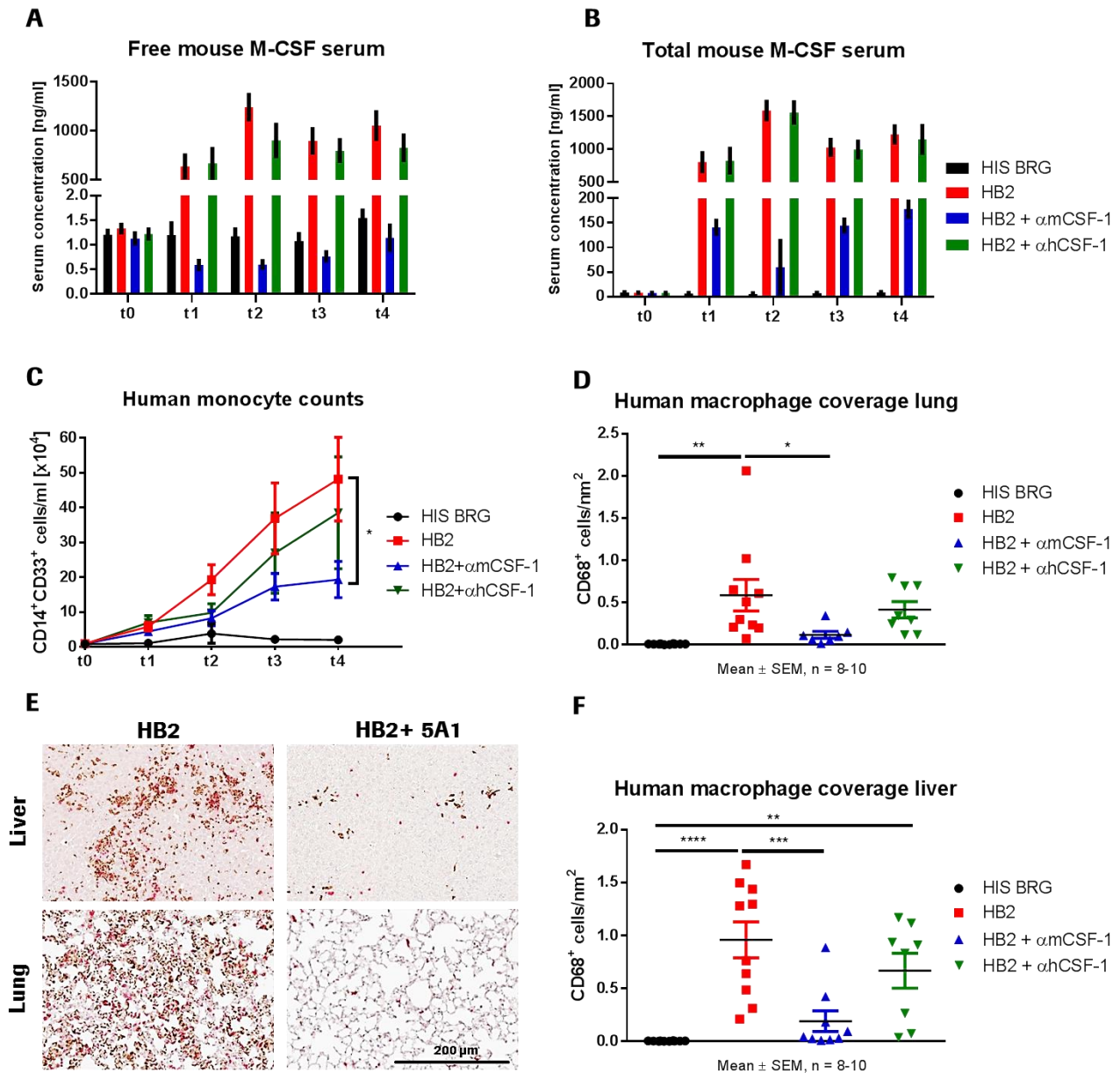


Figure 19: Diminished human myelopoiesis in HB2 mice upon blockage of mouse CSF-1

HIS BRG mice were injected with four weekly doses of isotype (HIS BRG), 2G2 (HB2), 2G2 plus anti-mouse CSF-1 (HB2+ α mCSF-1) or 2G2 plus anti-human CSF-1 (HB2+ α hCSF-1) antibodies. (A+B) Serum samples were taken weekly and concentration of free (unbound) (A) or total (B) mouse CSF-1 was determined by ELISA (n=7-9, mean \pm SEM). (C) Human CD33+CD14+ monocyte counts in peripheral blood before (0 weeks of treatment) and during (1-4 weeks of treatment) respective antibody treatments (n=9-10, mean \pm SEM; one t-test per time point; *P<0.05 Student's t-test). (E) Representative IHC staining of human CD68⁺ macrophages (brown) in lung and liver tissue of HB2 and α mCSF-1 treated HB2 mice at time point of necropsy (t4). (D+F) Quantification of CD68⁺ cells in IHC stained lung (D) and liver (F) sections of individual mice using the Definiens software (n= 8-10 mice; mean \pm SEM, one-way ANOVA, ; *P < 0.05 Tukey's test).

5.8. Functionality of human macrophages in HB2 mice *in vivo*

Human macrophages from HB2 mice resemble morphologically and phenotypically those found in humans, however their functionality needs to be validated. For this reason, the cytokine response of human macrophages in HB2 mice was tested *in vivo* by injection of the TLR4 agonist LPS. Sera of mice were taken 90 minutes after LPS injection and analyzed for presence of different human, pro-inflammatory cytokines by multiplex ELISA. Pro-inflammatory cytokines associated with monocytes/macrophages TNF α , IL-6, IL-1 β , MCP-1 and IP-10 were significantly elevated in sera of HB2 mice upon LPS stimulation compare to HIS BRG mice (Figure 20). Human TNF α levels were remarkably high as seen by an average concentration of ~500 ng/ml and in individual mice even 1 μ g/ml TNF α was detected (Figure 20). Serum concentrations of human IL-6, human MCP-1 and human IP-10 levels were much lower but still in a low nanogram range (Figure 20). Compared to all other cytokines, human IL1 β was significantly increased in HB2 mice but the overall serum concentration was more than tenfold lower (Figure 20). Although on average, all human cytokines were significantly increased the intensity of cytokine response to LPS was very heterogenous among individual HB2 mice (Figure 20). In summary, release of human pro-inflammatory cytokines in response to TLR4 stimulation provided first evidence for functionality of human macrophages in HB2 mice *in vivo*.

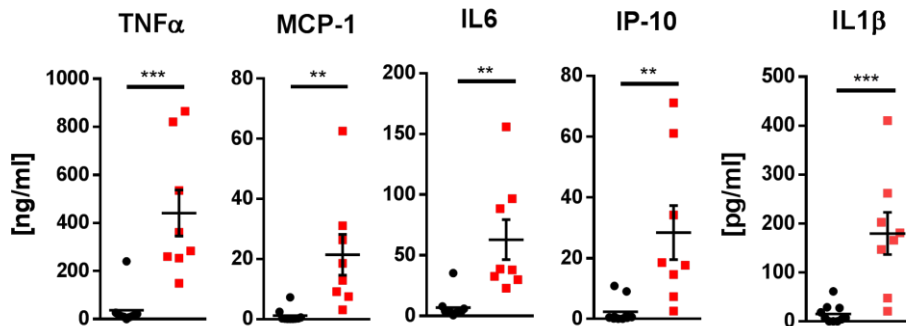


Figure 20: Cytokine response of human macrophages in HB2 mice upon stimulation with LPS *in vivo*

HIS BRG mice were treated with four consecutive weekly doses of mouse IgG1 isotype control (HIS BRG mice, black) or 2G2 (HB2 mice, red) and injected with 35 μ g LPS/mouse. Sera were taken 2 hours after injection and indicated human cytokines were quantified using BioPlex analysis (n=7-8 mice; one-way ANOVA, ; *P < 0.05 Tukey's test)

5.9. Growth of human xenograft tumor cells in HIS BRG and HB2 mice

The complexity of how tumor-associated macrophages influence cancer development and progression still has not been fully deciphered yet, in fact TAMs were proven to exhibit a bilateral role by either inhibiting or promoting tumor growth. HIS BRG mice generally open the possibility to investigate the growth of human tumor cells in the presence of an existing human immune system. However,

comprehensive data evaluating the growth of different tumor models in HIS BRG mice are lacking. To assess tumor growth in humanized and non-humanized BRG mice, the following tumor lines were used: the ovarian epithelial carcinoma cell line OVCAR5 and the colorectal adenocarcinoma cell line HT29. Cell

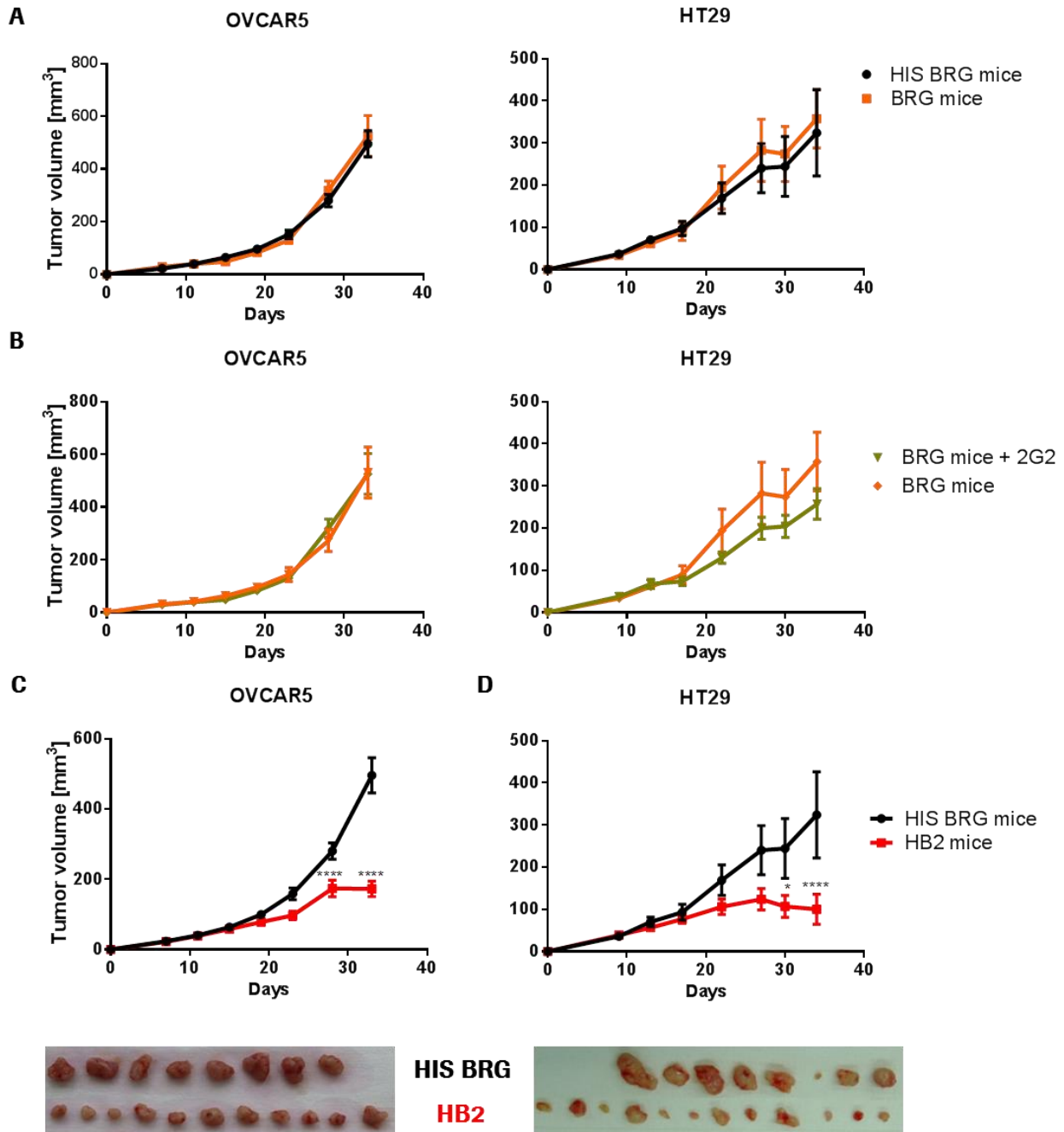


Figure 21: Growth of human tumor cell lines in HIS BRG and HB2 mice

HT29 and Ovar5 tumors were inoculated subcutaneously in the right flank and tumor volumes were detected over time by Caliper measurement. (A) Tumor growth of HT29 and Ovar5 in BRG and HIS BRG mice (n=8; Mean ± SEM). (B) Tumor growth kinetics of HT29 and Ovar5 in non-humanized BRG mice treated with 4 consecutive weekly doses of isotype (orange) or 2G2 (green) antibody at 30mg/kg starting 5 days after inoculation (n=8; Mean ± SEM). (C+D) Tumor growth kinetics of HT29 and Ovar5 in HIS BRG and HB2 mice (n=8; Mean ± SEM) and pictures of explanted corresponding tumors

lines were injected subcutaneously in HIS BRG mice and tumor growth was monitored by caliper measurements over time. Interestingly, growth kinetics of both tumor cell lines was found to be indistinguishable in BRG and HIS BRG mice (Figure 21A). Macrophages were previously reported to efficiently induce anti-tumoral responses in humans. Hence the improved human myelopoiesis in HB2 mice was therefore assumed to influence growth of human tumor cell lines. The generation of HB2 mice is accompanied by depletion of mouse macrophages, which potentially might have an impact on the engraftment and growth of the human xenografts. Therefore, the impact of 2G2 treatment was first evaluated on HT29 and OVCAR5 growth in non-humanized BRG mice. Tumor growth was found to be not significantly changed upon treatment with 2G2 although HT29 tumors tend to grow a little slower from day 18 after inoculation (Figure 21B). To finally reveal whether the presence of human macrophages affects HT29 and OVCAR5 tumor growth, animals were treated with 2G2 or isotype control 5 days after tumor cell inoculation. Until day 20 both tumor lines, HT29 and OVCAR5, grew comparably in HIS BRG and HB2 mice, but from there on HB2 mice showed a significantly inhibited growth (Figure 21C+D + Supplementary Figure 6 Supplementary Figure 6). As a result, tumors grown in HB2 mice were significantly smaller than those derived from HIS BRG mice at time point of necropsy (Figure 21C). Although growth kinetics of both tumor cell lines were comparable in HB2 and HIS BRG mice, intragroup variation of tumor volumes at time point necropsy was higher in HT29 than in OVCAR5 tumors (Figure 21C+D + Supplementary Figure 6). Nevertheless it was demonstrated here for the first time that growth of human tumor cells lines is significantly inhibited in mice with an established human immune system. Mouse macrophages were significantly reduced in HB2 mice suggesting that these cells have not contributed to tumor growth inhibition. The anti-tumoral immune response was most likely initiated by components of the human immune system. Human T cells and macrophages were found to be the most abundant effector populations in HB2, representative sections of representative OVCAR5 tumors were co-stained by IHC for human CD68 and CD3. Both markers were only sporadically detected in tumor tissue derived from HIS BRG mice, suggesting that generally neither human T cells nor macrophages were actively infiltrating into the control tumors (Figure 22A). In contrast, high numbers of CD68 and CD3 positive cells were detected mainly at the boundary but also inside tumors derived from HB2 mice (Figure 22C). Interestingly, CD204⁺CD68⁺ double positive as well as CD204⁻CD68⁺ single positive macrophages were detected indicating different subsets of human macrophages have differentiated in the tumor tissue (Figure 22B+C). Whereas CD204⁻CD68⁺ cells tended to locate at the tumor border, CD204⁺CD68⁺ macrophages were more detected inside the tumor mass (Figure 22B+C). Human CD3⁺ T cells were found to generally co-localize with CD68⁺ single positive macrophages cells and were

composed of CD3⁺CD8⁻ negative as well as CD3⁺CD8⁺ cells indicating helper as well as cytotoxic T cells being present in OVCAR5 tumors (Figure 22D).

In summary, tumor growth inhibition observed in HB2 mice was found to correlate with unprecedented infiltration of different subtypes of human macrophages and T cells. Based in these results, HB2 mice

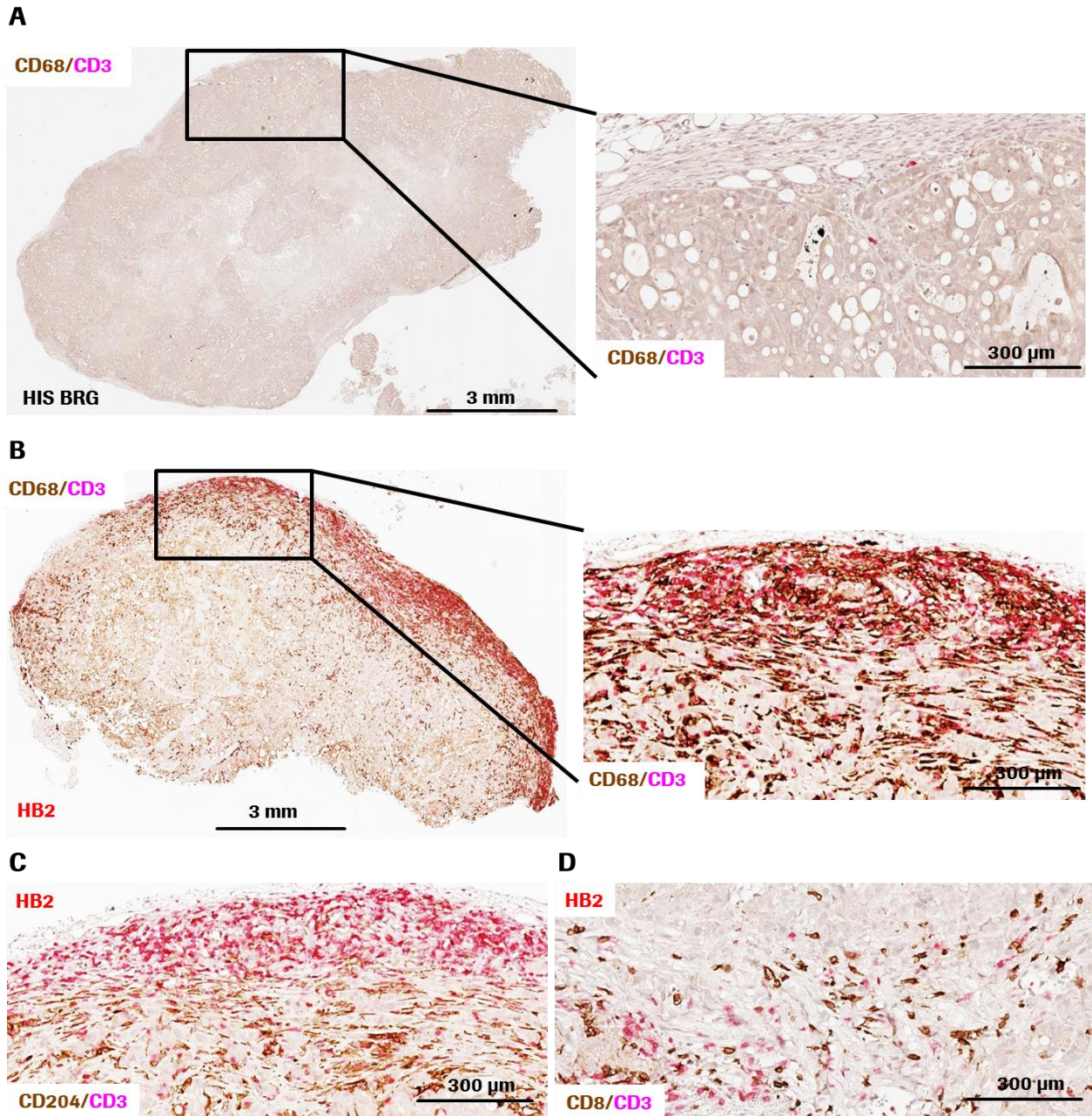


Figure 22: Phenotyping of human tumor infiltrating immune cells

Sections of OVCAR5 tumors from HB2 and HIS BRG mice were simultaneously stained for different human specific immune cell markers by immunohistochemistry. (A+B) Representative OVCAR5 tumors isolated from HIS BRG (A) or HB2 (B) mice were co-stained for human CD68 positive macrophages (brown) and human CD3 positive T cells (pink); on the right: indicated tumor areas are depicted at higher magnification. (C+D) Consecutive section of HB2-derived OVCAR5 tumor (B) stained for human CD204 positive M2-like macrophages and human CD3 positive T cells. (D) Total human T cells (CD3) and human cytotoxic T cells (CD8) co-stained on section of OVCAR5 tumor stain in B and C.

represent a unique *in vivo* model for studying interaction of human tumor cells with human infiltrating immune cells.

5.10. Human macrophages mediate graft versus host disease in HB2 mice

When treating HIS BRG mice with 2G2, some animals developed a ruffled fur, showed signs of disorientation, a hunchbacked position as well as signs of anemia as seen by pale tails, ears and paws and blood (Figure 23A). These general signs of distress were accompanied by significant body weight loss and in consequence in almost 30% decreased overall survival of HB2 mice as compared to control animals during the treatment period (Figure 23B). Pathological analysis of affected HB2 mice by hematoxylin and eosin (H&E) confirmed GvHD symptoms in these mice (Figure 23C): In lymphoid and non-lymphoid organs of HB2 mice these symptoms showed granuloma formation at different degrees. Granulomas were characterized by accumulation of large cytoplasmic cells forming multinucleated

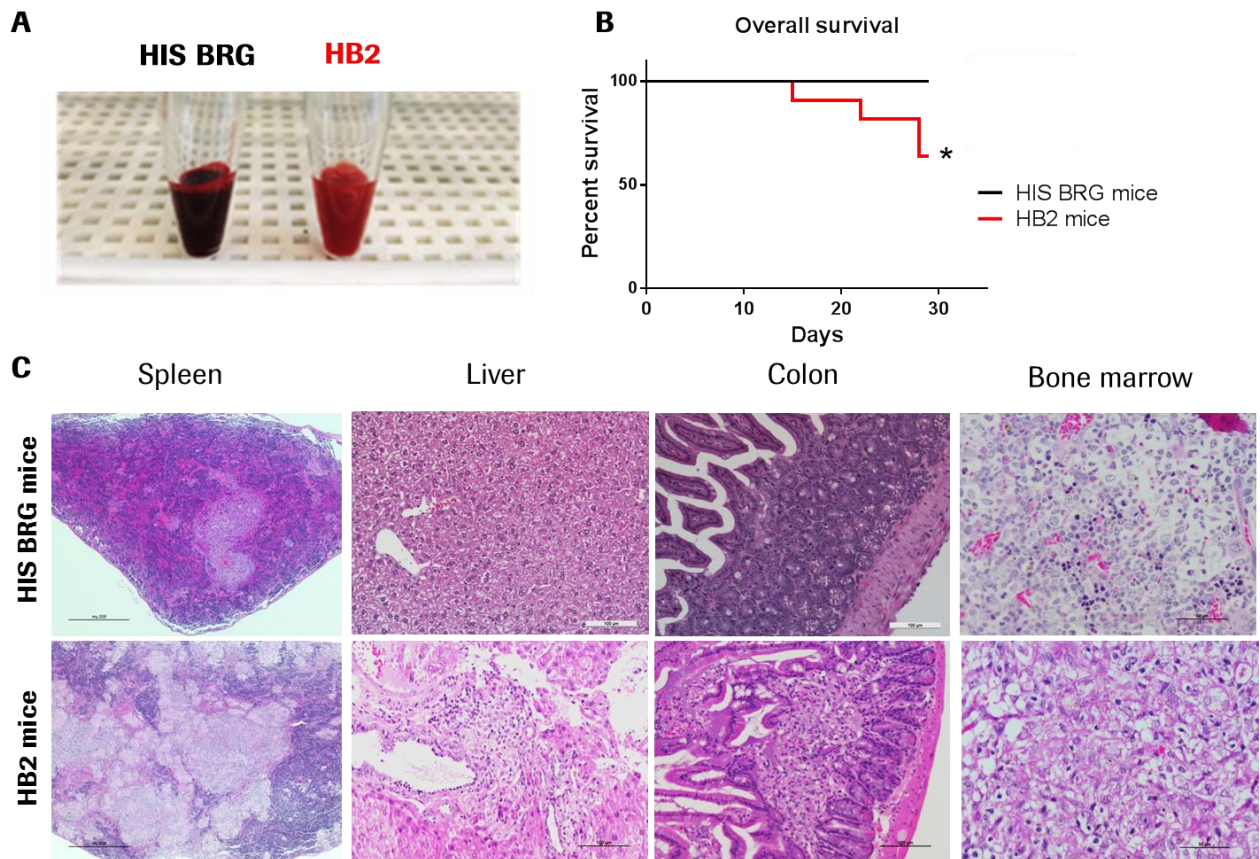


Figure 23: Characterization of graft versus host disease in HB2 mice

HIS BRG mice were treated with four consecutive, weekly doses of mouse IgG1 isotype control (HIS BRG mice) or anti-mouse CSF-1R antibody (HB2 mice) at 30 mg/kg. (A) Representative whole blood samples from HIS BRG and HB2 mice. (B) Overall survival of HIS BRG control and HB2 mice during the treatment period as analyzed by Kaplan Meier (n=14, Log-rank Mantel-Cox test) (C) Sections of indicated tissues removed from HIS BRG or HB2 mice stained with H&E staining.

aggregate-like structures, which were virtually absent in all tissues of control HIS BRG mice (Figure 23C). Granuloma formation was less pronounced in liver and colon; however, bone marrow and spleen samples appeared virtually perforated by granulomatous infiltrates (Figure 23C). In the bone marrow, multifocal granulomas even replaced hematopoietic tissue leading to loss of tissue integrity (Figure 23C). Formation of granulomas in various tissues was found to be the most significant pathological difference between HIS BRG mice and affected HB2 mice. Thus cellular components of these infiltrates were suspected to cause the increased mortality. Therefore, tissue sections containing granulomatous infiltrates were subjected to immunohistochemical analysis. Strikingly, in areas of granuloma formation human CD68⁺ macrophages and human CD3⁺ T cells were co-located strongly suggesting one or both cell types to cause GvHD like symptoms in HB2 mice (Figure 24A). In two subsequent *in vivo* studies either human T cells or human macrophages were depleted in HB2 mice: Human T cells were depleted by a human CD3 blocking antibody (α hCD3), a co-receptor of the T cell receptor complex, which was described to efficiently deplete human T cells in human peripheral blood lymphocyte transfer models¹⁶⁵. However, the depletion of human macrophages has never been reported in preclinical animal models, but TAM depletion has been shown for cancer patients⁴⁵. Similarly to the human patient situation, an anti-human CSF-1R antibody was chosen for depletion of CSF-1R⁺ myeloid cells (US2008/073611¹⁵⁴). Parameters applied to evaluate progression of GvHD were fur texture, body weight, anemia, mobility and general behavior. As shown before, the mortality of HB2 mice was increased in comparison to HIS BRG mice in both independent studies (Figure 24B+C). Human T cells were efficiently depleted in HB2 mice upon α hCD3 injection, as demonstrated by the absence of CD3 positive cells in analyzed liver sections (Figure 24D). Surprisingly, depletion of human T cells did not improve but rather decreases overall survival of HB2 mice (Figure 24B). Strikingly, systemic depletion of human macrophages by α hCSF-1R injection (confirmed by representative staining of respective liver samples, Figure 24E) significantly improved overall survival of HB2 mice (Figure 24C). Of note, human T cells were not detected in liver samples of HB2 mice depleted of human macrophages but vice versa (Figure 24D+E). In summary, improvement of human myelopoiesis in HIS BRG mice results in increased mortality correlating with GvHD symptoms in affected animals. Multifocal granulomas were detected in various organs of animals suffering from GvHD and were formed by human macrophages and human T cells. Treatment with an α hCSF-1R antibody rescued HB2 mice from developing GvHD, implicating that human macrophages play a major role in the increased mortality rates, not T cells.

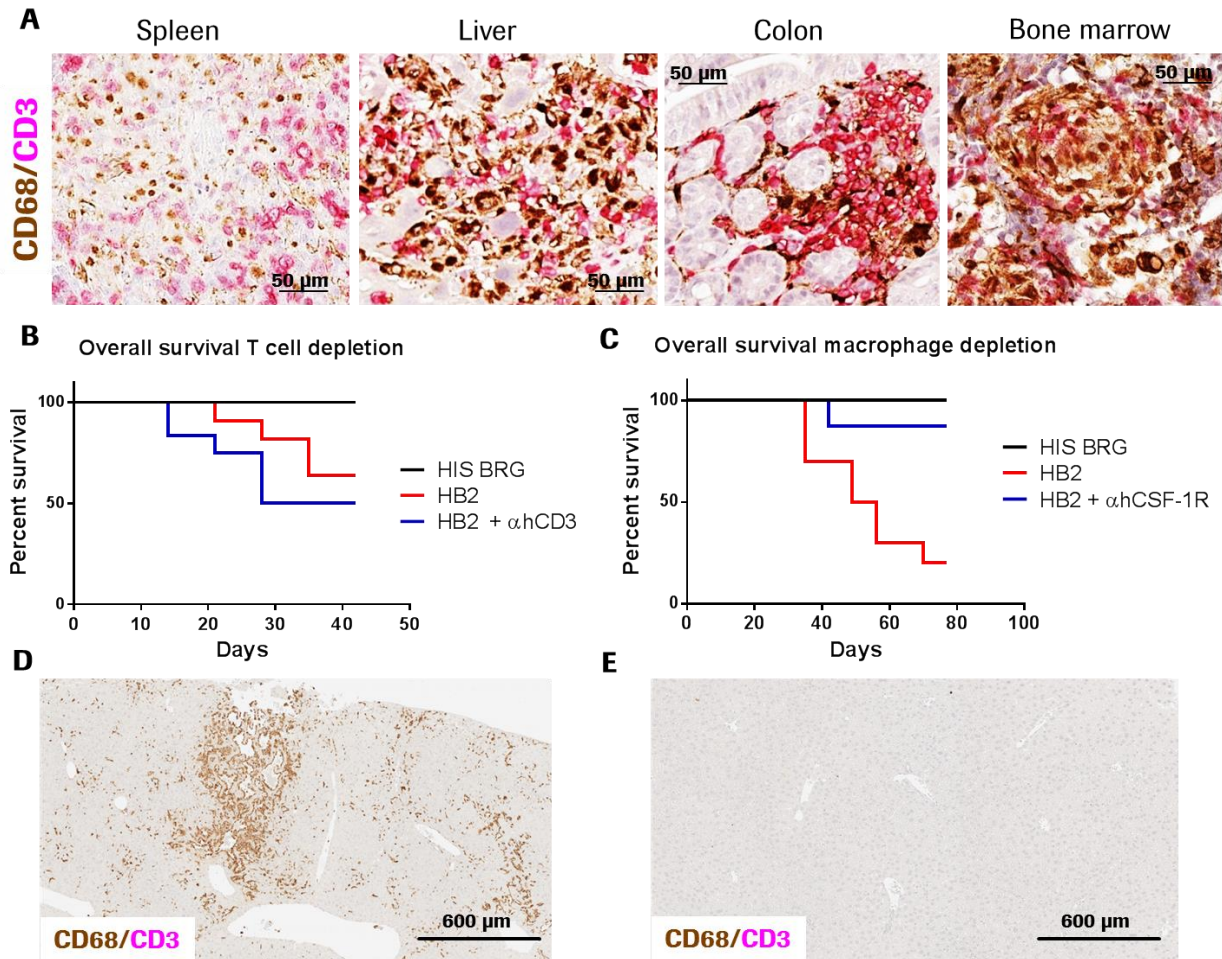


Figure 24: Prevention of graft versus host disease in HB2 mice by depletion of human macrophages

(A) Tissue sections of respective organs from HB2 mice containing granulomatous were co-stained by IHC for human CD3 (pink) and human CD68 (brown). (B+C) Overall survival of HIS BRG mice treated with four consecutive doses of control antibodies (HIS BRG mice), anti-mouse CSF-1R antibody (HB2 mice) or a combination of anti-mouse CSF-1R and anti-human CD3 (C: HB2 mice + α hCD3 CD3) or anti-human CSF-1R antibody (D: HB2 mice + hCSF-1R). (D) Representative liver sections of HB2 mice treated with anti-human CD3 antibody co-stained in IHC for human CD3 and human CD68 (E) Representative liver sections of HB2 mice treated with anti-human CSF-1R antibody co-stained in IHC for human CD3 and human CD68.

6. Discussion

6.1. Humanization of BRG mice

To date, several different protocols have been established for generation of human immune system mice. Human HSPCs capable of self-renewal and multi-lineage differentiation are prerequisite of all these HIS mouse models. In line with previous reports, CD34 enriched FLCs characterized in this study were confirmed to represent a very heterogeneous cell population (Figure 1). CD34 has been established as the surface marker of choice to isolate human HSPCs from cord blood, fetal liver, human bone marrow and human peripheral blood. However, high variations of humanization detected in HIS BRG mice indicate that CD34 is a non-reliable marker to determine the actual frequency of human HSPCs (Figure 1). Actually only fetal liver cells co-expressing CD34 and CD133 were reported to stably reconstitute immunodeficient mice⁹⁹. As a consequence, donor dependent variations of humanization levels most likely result from highly variable frequencies of multipotent CD34⁺CD133⁺ HSPCs within FLCs, which was observed in blood of HIS BRG mice at different time points after reconstitution (Figure 4 + Supplementary Figure 1). In their report, Notta and colleagues defined a panel of surface markers that allows distinction between human HSPCs capable of long term engraftment and multipotent progenitor cells in cord blood samples⁹⁸. In the present study, the declining average humanization levels in HIS BRG mice over time might be attributed to the low frequency of these LTRCs in analyzed fetal liver samples (Figure 1 + Figure 4). Humanization was reported to be consistent for up to 30 weeks in mice carrying SCID derived SIRP α isoforms such as NSG and NOG mice. Therefore, diminished humanization observed in HIS BRG mice might be a result from active phagocytosis of human HSPCs by xenoreactive mouse macrophages (Figure 4 + Supplementary Figure 2)⁹³. Colony formation *in vitro* and transient generation of multiple human hematopoietic lineages *in vivo* suggest that the majority of human FLCs injected into BRG mice represent multipotent progenitor cells devoid of self-renewal capability (Figure 2 + Figure 3). HSPCs injected into preconditioned BRG mice were found to efficiently home to the mouse bone marrow within the first two weeks after injection (Figure 3). This is remarkable because the process of switching hematopoiesis from the fetal liver to the bone marrow requires several cytokine dependent steps including extravasation of HSPCs into the blood stream and migration into the bone marrow¹⁶⁶. However, once engrafted in the mouse bone marrow niches, human HSPCs are exposed to a suboptimal environment as important cytokines required for maintenance and expansion of human HSPCs such as SCF and TPO were reported being not fully cross reactive^{146, 147}. As a consequence, the overall numbers of human leukocyte precursors are expected to be far lower in HIS BRG mice compared to intact human

or mouse bone marrow. This assumption is heavily supported by the comparably low overall numbers of human white blood cells in blood of HIS BRG mice (Supplementary Figure 2).

6.2. Multi-lineage differentiation of FLCs in HIS BRG mice

Although human HSPCs engrafted in HIS BRG mice were not able to quantitatively replace mouse HSPCs, they indeed exhibited multi-lineage differentiation potential. Human T and B cells were shown to repopulate peripheral blood as well as lymphoid organs in HIS BRG mice, so the presence of B and T cell precursors in the bone marrow was expected (Figure 3). Previous reports demonstrated that early steps of human B cell development are faithfully reflected in the bone marrow of HIS mice^{129,167}. The current study confirmed B cells differentiation through a series of sequential stages from pre-B cells to mature B cells in the bone marrow of HIS BRG mice (Figure 5). However, as reported before, low frequencies of mature B cells indicate suboptimal late stage maturation of human B lymphocytes in the bone marrow¹⁶⁸. The low frequency of pre-T cells and the absence of mature T cells in bone marrow indicate that similar to humans T cell development in HIS BRG mice is carried out in the thymus (Figure 5)¹²⁷. During human thymopoiesis, CD4 and CD8 double positive T cell progenitors are released from the bone marrow and migrate via bloodstream to the thymus to undergo positive and negative selection on peptide loaded human MHC molecules. Selected single positive T cells finally are released from the thymus to repopulate peripheral lymphoid organs¹⁵⁷. In general, human T cell development was found to be well reflected in HIS BRG mice (Figure 6 + Supplementary Figure 3). Functional human thymopoiesis has been reported in several HIS mouse models already, however detailed analysis of individual maturational stages has not been performed so far^{109, 122, 132, 157}. Human CD4⁺CD8⁺ double positive thymocytes detected in the thymus of HIS BRG mice are likely derived from CD3⁺CD7⁺ lymphoid progenitor cells detected in the bone marrow (Figure 6 + Supplementary Figure 3). Usually these progenitor cells are released in the blood stream and infiltrate the outer cortex of the thymus from where they pursue further differentiation stages in the cortical and medullary areas of the thymus¹⁶⁹. As reported for human thymocyte selection, CD4⁺CD8⁺ double positive thymocytes were shown to express high levels of CD1a and low levels of CD44, CD69, CD3 and TCR $\alpha\beta$ (Figure 6)¹⁶⁹. Upregulation of CD44, CD69, CD3 and TCR $\alpha\beta$ and downregulation of CD1a on CD4 or CD8 single positive cells has been reported to correlate with efficient positive and negative selection on MHC class molecules¹⁷⁰. Successful rearrangement of TCR alpha and beta chains during thymocyte selection has reported to result in a diverse TCR repertoire in HIS mice comparable to humans¹⁷¹. Antigen presentation was reported previously to be exclusively conducted by mouse epithelial cells and various mouse strains have been generated expressing human MHC class I (HLA-A2) and/or human MHC class II (HLA-DR) molecules^{134, 145}. However, the finding that

human thymocytes interact with other thymocytes as well as with human intrathymic dendritic cells in the thymus of NSG mice indicates, that human T cells are restricted to human MHC molecules in non-transgenic HIS mice as well¹²⁶. Strikingly, high frequencies of human antigen presenting cells were identified in thymi of HIS BRG mice and were shown to interact with human CD4⁺ thymocytes (Figure 7 + Figure 8). If human antigen presenting cells in thymi of HIS BRG mice resemble those found in humans still has to be further evaluated. In the present study, the majority of human MHC class II positive cells in the thymus were phenotypically immature B cells (Figure 6 + Supplementary Figure 3). B cell precursors have been reported to accumulate in the thymus of humans as well and to functionally contribute to T cell selection^{172, 173}. However, the role of B cells in thymi of HIS BRG is still not clear. Interestingly, most of human MHC class II positive cells rather exhibited an epithelial-like and not a lymphoid-like morphology (Figure 7). It remains to be further evaluated, if human B lymphocytes acquire different morphological features in the thymus compared to the periphery or if epithelial like human antigen presenting cells are lost during the FACS preparation procedure. In any case, human thymocytes were shown to undergo positive and negative selection and to interact with human antigen-presenting cells in the thymus of HIS BRG mice (Figure 6 + Figure 8). Efficient interaction of human antigen presenting cells with human thymocytes strongly suggests that human peripheral T cells are at least partially restricted to human MHC molecules (Figure 8). However, *ex vivo* experiments such as mixed lymphocytes reactions are required to confirm this assumption. Human B cells matured in the bone marrow as well as human T cells selected in the thymus were efficiently released into the periphery of HIS BRG mice as shown by the presence in all secondary lymphoid organs (Figure 9 + Figure 10). Limited development of lymph nodes structures in HIS BRG mice might be due to the absence of lymphoid tissue inducing cells and follicular dendritic cells which required for formation and organization of lymph nodes in mice and men (Supplementary Figure 4)^{174, 175}. Formation of lymphoid follicles is a tightly regulated process that requires participation of hematopoietic as well as non-hematopoietic cell types. The absence of key players such as follicular dendritic cells most likely explains the lack of lymphoid follicles in the spleen and lymph nodes of HIS BRG mice (Figure 9 + Figure 10 + Supplementary Figure 4)^{176, 177}. However, other aspects such as the low overall number of human leukocytes and the presence of phagocytic mouse cells might also contribute to improper development of humanized lymphoid follicles. Besides the chaotic structural organization of the human immune cells, also the frequency was shown to be not consistent among lymph nodes of individual mice analyzed (Figure 9). In normal BRG mice lymph node structures were undetectable, while human lymphocytes certainly induced their formation upon humanization (Figure 9).

6.3. Myelopoiesis in HIS BRG mice

Similar to other HIS mouse models described before^{122, 178}, HIS BRG mice generated in the present study largely reflect human lymphopoiesis while mature myeloid cell types were rarely detected. Detection of myeloid precursor cells in the bone marrow indicated, that underrepresentation of human monocytes and macrophages in these mice is either caused by retention of promonocytes in the bone marrow or by blockage of terminal differentiation of released cells in the periphery or both (Figure 3). The existence of a reservoir of human myeloid progenitor cells persisting in the bone marrow is supported by the observation, that human macrophages could even be generated in mice with normally insufficient humanization levels and also at very late time points after reconstitution (Figure 18). Human macrophages and dendritic cells are supposed to derive from monocytic and common dendritic cell precursors which are released from the bone marrow into the blood stream^{161, 179}. The retention of these precursors might be a possible explanation for low frequencies of both cell types reported in most HIS models. However, this fact does not explain why the generation of human monocytes in mice expressing human CSF-1 significantly improved reconstitution of human macrophages, but not of human dendritic cells^{100, 103}. These results rather suggest that even if myeloid precursor cells are released from the bone marrow, differentiation in the bone marrow and later terminal in the periphery is only achieved in presence of specific cytokines¹⁰³. In this context, several studies have confirmed that introduction of certain human cytokines significantly improves reconstitution of human innate immune cells in HIS mice^{100, 103, 139, 148}.

6.4. Mouse CSF-1 induces downstream signaling of the human CSF-1R

Human monocytes and macrophages were reported to be underrepresented in most HIS models and so far the only efficient approach to achieve systemic reconstitution of both cell types was by replacement of mouse by human CSF-1^{100, 103}. These results obviously provided *in vivo* evidence for the well-established assumption that mouse CSF-1 is not able to signal via the human CSF-1R¹⁴⁹. Using two different Biacore analyses, mouse CSF-1 was shown to indeed bind to human CSF-1R, but with a more than 12,000 fold lower affinity and a different binding kinetic compared to the cognate ligand (Figure 11). Despite the fact that mouse CSF-1 was found to rapidly dissociate from human CSF-1R upon binding, this interaction was found to be sufficient to activate CSF-1R signaling in human monocytes (Figure 12). Phosphorylation of human CSF-1R was found to require a certain threshold concentration of mouse CSF-1, but the downstream phosphorylation of AKT indicates that even lower doses can efficiently activate CSF-1R signaling. In monocytes stimulated with human CSF-1, activation of CSF-1R signaling correlated with reduced overall CSF-1R protein level as described before¹⁶⁰. Upon stimulation with mouse CSF-1 we

did not observe such a downregulation/degradation of the human CSF-1R. This might be caused by different binding behavior of both homologue cytokines to the human CSF-1R (Figure 11 + Figure 12). In this context high flexibility of CSF-1 within ternary CSF-1:CSF-1R complexes likely allows mouse CSF-1 to cooperatively bind to human CSF-1R in a different manner¹⁸⁰. The current data suggest that signaling via CSF-1R is indeed possible, however, internalization and degradation may only occur with high affinity association of the human CSF-1:CSF-1R complex.

6.5. Supraphysiological levels of mouse CSF-1 induce human myelopoiesis in HIS BRG mice

Finally, binding of human as well as mouse CSF-1 was shown to result in differentiation of peripheral blood as well as of bone marrow derived monocytes (Figure 13). The finding of mouse CSF-1 promoting survival and differentiation in a dose dependent manner suggests that a threshold concentration exists above which low affinity to the human CSF-1R can be compensated. Based on the phenotypic analysis performed in this study, the concentration level of mouse CSF-1 is not only a determining factor for survival but also for polarization of monocytes. In this context low and intermediate concentrations of mouse CSF-1 polarized human monocytes towards a M2-like macrophage subtype as seen by high expression human MHCII, CD11c and CD163 as well as low levels of CD80. All of these markers were found to be differently expressed upon differentiation of monocytes with super high mouse CSF-1 concentrations. Although increased expression of CD11c is characteristic for monocyte-derived dendritic cells, this assumption can only be addressed by a functional assay because most of the evaluated markers are redundant between macrophages and dendritic cells (Figure 13). In the present study, mouse CSF-1 was shown for the first time to not only bind to human CSF-1R but also to exhibit biological activity at high concentrations on human CSF-1R positive peripheral blood and bone marrow derived monocytes (Figure 11-13). Conversely, these results shed new light on the question why neither human monocytes nor macrophages are efficiently reconstituted in conventional HIS mouse models. So far only expression of human CSF-1 was reported to systemically improve human myelopoiesis in HIS mice^{100, 103}. These results underline the importance of active CSF-1R signaling for the generation of human monocytes and macrophages in these mice. The present study clearly shows that human myelopoiesis in conventional HIS BRG mice is indeed possible and rebuts the assumption of human CSF-1 being indispensably required for reconstitution of human monocytic cell types. Although a direct comparison is missing, the present study confirms that endogenous mouse CSF-1 can indeed be harnessed to achieve similar effects as seen in human CSF-1 knockin mice (Figure 16 + Figure 17)^{100, 103}. Underrepresentation of human monocytes and macrophages in HIS mice obviously results from insufficiently high mouse CSF-1 levels but not from preciously described lack of cytokine cross reactivity. Similar to what was described in

MISTRG mice, human macrophages generated in HB2 mice did respond to LPS by release of pro-inflammatory cytokines (Figure 20). However, additional *in vivo* as well as *ex vivo* experiments are required to finally validate of whether both macrophage populations exhibit comparable functional properties.

A major advantage of the HB2 mouse system compared to knock-in or transgenic mice constitutively expressing human cytokines such as CSF-1 is the inducibility of human myelopoiesis at different time points after reconstitution (Figure 18). In several studies HIS mice were allocated for experimental groups mainly based on the frequency of human CD45 positive cells in peripheral blood at a certain time point after reconstitution. In contrast, generation of human macrophages in HB2 was found to be independent of time and the level of humanization as determined in peripheral blood (Figure 18). In turn, this means that nearly 100% of all reconstituted HIS BRG mice could be used and showed improved reconstitution once injected with 2G2 antibody. In general, blockage of mouse CSF-1R more potently reduced tissue resident mouse macrophages rather than circulating monocytes (Figure 14). This indicates that mouse CSF-1 is a critical survival factor of terminal differentiated macrophages but not so crucial for circulating monocytes. This assumption is supported by significantly decreased numbers of mouse macrophages but not of monocytes in CSF-1 deficient *op/op* mice¹⁸¹. Remaining F4/80⁺ positive cells in spleen and bone marrow in both organs likely did not express CSF-1R or bypassed the blockage of one by activation of another survival pathway¹⁸¹. The observed increase of mouse CSF-1 in sera of HB2 mice confirms that CSF-1 is produced by cells of mesenchymal and epithelial origin which are not targeted by anti-mouse CSF-1R antibody treatment (Figure 15)¹⁸². Data from non-human primates treated with anti-CSF-1R antibody showed a rapid increase of CSF-1 in serum and the duration of this increase was dependent on the amount of antibody used⁴⁵. In the present study, continuously high levels of mouse CSF-1 were detected, indicating that the chosen amount of antibody of 30mg/kg body weight was sufficient to result in sustainably high CSF-1 levels (Figure 15). Whether continuously high or rather intermittently high levels of CSF-1 are needed for monocyte and macrophage reconstitution in HB2 mice, still needs to be evaluated.

However, the results presented here do not only provide *in vivo* evidence for mouse CSF-1 being capable of activating human CSF-1R signaling but also describes for the first time that an endogenous cytokine promotes human monocyte and macrophage reconstitution in HIS mice. Variability of human monocyte counts in blood of 2G2 treated mice likely reflects different initial humanization levels of individual animals (Figure 15). Compared to control mice human monocyte counts consistently increased upon

treatment with 2G2 in every mouse treated. The fact that monocytes finally accounted for approximately 50% of total human CD45 cells indicates that reconstitution of other human leukocytes was improved as well (Figure 15). Thus, further analysis is required to obtain a comprehensive picture of how the depletion of mouse macrophages and monocytes affects the white blood cell composition in HB2 mice. The final proof that mouse CSF-1 is instrumental for the improved human myelopoiesis in HB2 mice was achieved by blocking mouse CSF-1 resulting in significantly diminished human macrophages in various tissues (Figure 19). This result demonstrated that 2G2 effects observed in HB2 mice were driven by consecutive changes in the cytokine milieu rather than by the depletion of mouse monocytes and macrophages itself. So far antibodies blocking mouse CSF-1 have only been used to reduce physiological levels of mouse CSF-1 in immunocompetent mice. Here comparable dosage was used to neutralize the highly elevated levels mouse CSF-1 in HB2 mice. Strikingly, the blockage of mouse CSF-1 in HB2 mice was sufficient to diminish generation of human macrophages in HB2 mice. Compared to the tissue macrophages however, the number of human monocytes was not as profoundly reduced upon blockage of mouse CSF-1 (Figure 19). This observation indicates that differentiation but probably not survival of human monocytes is strictly dependent on CSF-1R signaling in humanized mice as well.

6.6. Characterization of human monocytes and macrophages in HB2 mice

Results obtained from any study in HB2 mice will only be of use if the human macrophages are functional. As implicated in their name phagocytosis is one of the unique features of macrophages. Although formation of granulomas *in vivo* implicates that human macrophages indeed exhibit phagocytic activity several head to head *ex vivo* assay have to be performed in addition to prove their phagocytic function (Figure 23). Another common readout for macrophage functionality is cytokine response to TLR stimulation. In the present study a TLR4 agonist was used to confirm that human macrophages generated in HB2 mice immediately release pro-inflammatory cytokine as TNF α and IL-6 upon engagement of this specific pattern recognition receptor (Figure 20). The unique cytokine response of different macrophage subsets to a specific stimulus will help to further characterize these in HB2 mice. The first phenotypical characterization showed that in contrast to human blood monocytes, the vast majority of monocytes in HB2 mice exhibited an inflammatory phenotype (Figure 16). In humans elevated levels of CD16 positive monocytes correlate with inflammatory diseases such as rheumatoid arthritis and cancer^{183, 184}. In HB2 mice this effect might be mediated by a CSF-1 biased cytokine milieu or an ongoing GvHD phenotype. An improved human myelopoiesis was already described in MISTRG mice, in which human monocyte and macrophage development is driven by human CSF-1 as well as GM-CSF. However, simultaneous expression of these both cytokines resulted in a similarly high proportion of

inflammatory monocytes and did not prevent development of anemia¹⁰⁰. Taken these results into account, increased frequencies of inflammatory monocytes in HB2 mice can also result from latent GvHD rather than from unilateral stimulation with mouse CSF-1. In line with this assumption human monocytes in HB2 mice exhibited a hyperactivated phenotype as seen by high expression of human MHC class II and CD86. In contrast to what has been reported in MISTRG mice, HB2 monocytes expressed human CSF-1R at much higher levels than those found in human blood (Figure 16). This might reflect that monocyte population from HB2 and MISTRG mice differ functionally but also might simply be a result of a unilaterally biased cytokine milieu. Whereas in MISTRG mice two cytokines, human GM-CSF as well as human CSF-1, promote survival, human monocytes from HB2 mice are exclusively exposed to mouse CSF-1 with low affinity binding to the human CSF-1R. In HB2 mice the presence of human monocytes correlated with infiltration of human macrophages in lymphoid as well as non-lymphoid organs (Figure 17). Induced supraphysiological mouse CSF-1 levels in HB2 mice thus not only enhance release of human monocytes from the bone marrow but obviously also promote terminal differentiation of these cells in the periphery. If human macrophages detected in non-lymphoid tissues such as the lung and the liver exhibit similar functions as in humans still needs validation. Professional antigen-presenting cells are necessarily required to induce adaptive immunity and humoral immune responses; an underrepresentation of dendritic cells and macrophages still limits the use of conventional HIS mouse models. Infiltration of human macrophages in secondary lymphoid organs of HB2 mice might partially overcome these limitations. Immunization with potentially immunogenic vaccines such as KLH might reveal whether HB2 mice represent an improved model to study humoral immune responses.

The high numbers of human macrophages detected in HB2 mice indicate that these cells not only efficiently differentiated in different mouse tissues but also actively proliferated at the site of infiltration likely in a mouse and/or human CSF-1 dependent manner. Given that α hCSF-1 injection slightly diminished human myelopoiesis indicates, that human myeloid cells at least partially trigger their own proliferation by endogenous production human CSF-1 (Figure 19). The enhanced myelopoiesis in HB2 mice was accompanied with an overall increase of total human cell counts (Figure 15). Previously an induced tolerance against human xenografted cells was reported to enhance humanization levels in HIS BRG mice expressing human SIRP α ¹¹², a result that is most likely explained by reduced number of phagocytic mouse immune cells. In the present study there is also the possibility that monocytes and/or macrophages support lymphopoiesis by providing cytokines, which would need further evaluation to prove.

6.7. Human TAMs in HB2 mice show M1- and M2-like features in tumor xenografts

In context of tumor biology macrophages have been reported to exhibit dual functionality. As professional antigen presenting cells they are capable of initiating T cell-mediated anti-tumoral immune responses, possibly leading to inhibition of tumor growth. Beside these M1-like TAMs, high frequencies of tumor promoting macrophages are regularly found in tumors of cancer patients. Polarization of monocytes and macrophages towards this M2-like phenotype was found to be mainly induced by specific cytokines such as CSF-1, IL-10 or TGF β but also by hypoxia in necrotic areas of the tumor¹⁸⁵. The ability of human macrophages to significantly influence human tumor growth was confirmed in the present study by inoculation of two cell lines, OVCAR5 and HT29, respectively. In line with previous reports, both human tumor cell lines grew equally fast in HIS BRG and non-humanized BRG mice (Figure 21)¹⁰⁰. Several reports have claimed that the human immune system established in conventional HIS mouse models are fully functional^{122, 178}, but the lack of anti-tumoral immunity raises doubts about these statements. However, in most of these models human macrophages were not efficiently reconstituted. In contrast to conventional HIS BRG mice growth of OVCAR5 as well as of HT29 tumors was significantly inhibited in HB2 mice (Figure 21). As 2G2 was reported previously to efficiently deplete mouse TAMs and to reduce tumor growth, diminished tumor growth in H2B mice could theoretically result from the absence of tumor promoting mouse TAMs⁴⁵. Surprisingly neither growth of OVCAR5 nor HT29 tumors was significantly inhibited in 2G2 injected animals (Figure 21). Reduced functionality of mouse macrophages reported in mice carrying knockout of the IL-2 receptor might be one explanation for this observation¹⁰⁸. Detailed analysis of HIS BRG and HB2 xenograft tumors finally revealed that diminished tumor growth was correlated with infiltration of human macrophages and T cells. Strikingly, human macrophages exhibited an M1-like phenotype at the tumor borders and an M2-like phenotype in the inside of the tumor. Human T cells were exclusively found at the tumor boundary and were co-located with CD68 positive CD204 negative M1-like macrophages (Figure 22). Taken together these results indicate that human macrophages efficiently induced anti-tumoral immune responses in HB2 mice by attracting and stimulating human tumor-infiltrating T cells. However, several additional experiments will be needed to finally validate this assumption and to decipher the role of M1- and M2-like macrophages as well as of human T cells in tumor growth inhibition. To determine whether these tumor models reflect the actual patient situation, growth of OVCAR5 and HT29 tumors should be monitored again in absence of M1- or M2-like macrophages.

Of particular interest is also the interaction of human T cells with human M1-like macrophages at the tumor boundaries, because just from the evident co-localization in tumor-bearing HB2 mice, additional

effector cells than macrophages are likely involved (Figure 22). In theory two different scenarios could be envisioned for T cell dependent rejection of xenografted tumors in HB2 mice: First, TAMs mediated the attraction of T cells into the tumor area. These T cells are not HLA matched, so tumor rejection might represent a classical alloreaction of HLA mismatched T cells. These T cells derived from the same HSC donors were also present in HIS BRG mice, therefore an alloreaction (and inhibition of tumor growth) should also have been initiated in these mice as well. An alloreaction is based on mismatched donors from the same species, but in HIS mice human T cells have been reported to be matched on mouse MHC molecules in the mouse thymus of HIS mice¹³⁴. An allo-reactivity towards tumor cells is therefore doubtful and might be caused by a classical xeno-reactivity of these cells. Second, the more likely theory of how human T cells could have contributed to tumor regression is by recognition of tumor-specific antigens presented by human M1-like macrophages. The lack of MHC-dependent T cell responses in most HIS mouse models was usually explained by lack of human restricted T cells¹³⁴. However, human antigen-presenting cells are highly underrepresented even in second generation HIS mouse models^{84,107}. The interaction of human T cells with human MHC molecules in the thymus and the presence of human antigen-presenting cells theoretically enable the induction of antigen-specific anti-tumoral immunity in HB2 mice (Figure 7 + Figure 8). To further evaluate this, human tumor infiltrating T cells should be isolated and stimulated with tumor-specific antigens in the absence of human antigen-presenting cells to finally clarify this hypothesis.

In summary, induction of human TAMs in HB2 mice correlated with significant reduction of human tumor growth and might provide a suitable model to investigate the interaction of human immune and tumor cells in a preclinical setting.

6.8. GvHD in HB2 mice is dependent on human macrophages

Theoretically humanized mice provide a powerful tool to investigate human immune responses in a small animal model; however expectations had to be lowered once it became clear that human innate immune cells do not efficiently develop in these models. In the last decade major efforts have been made by development of transgenic and knockin mouse strains to overcome these limitations. However, all of these attempts obviously did not taken into account that innate cell types such as macrophages and NK cells might not be tolerant against the mouse host tissue. Although other mechanisms might also contribute to macrophage dependent onset of GvHD, incompatibility of human SIRP α and mouse CD47 is the most reasonable explanation for granuloma formation in HB2 mice (Figure 23). Finally, only physiological expression of human instead of mouse CD47 will answer of whether the assumed

incompatibility is causative for development of GvHD. The observation that tissue integrity is most dramatically destroyed in the bone marrow of HB2 mice has certainly different reasons (Figure 23). The bone marrow is the source for all human monocytic precursor cells and therefore it is likely the first organ to be infiltrated with differentiated human macrophages. Granuloma formation was shown to correlate with impairment of the bone marrow function, but a reduction of mouse macrophages might also contribute to loss of tissue integrity (Figure 23). In this context, mouse macrophage depletion was reported to induce a trophic niche environment, finally leading to egress of mouse HSPCs from the bone marrow¹⁸⁶.

Nearly every organ analyzed was shown to be heavily infiltrated with human macrophages, but the observed anemia in animals with GvHD-like syndromes clearly indicate the destruction of bone marrow structures (Figure 17 + Figure 23). Finally, this was major cause responsible for increase mortality in HB2 mice. In men, an acute and chronic form of GvHD is described particularly in patients who underwent allogeneic stem cell transplantation. While acute GvHD is well characterized and mainly mediated by alloreactive T cells, the mechanisms underlying chronic GvHD are still poorly understood¹⁸⁷. However, recent work by Alexander and colleagues strongly indicates that macrophages play an important role in the onset of chronic GvHD¹⁸⁸. The depletion of macrophages in this setting markedly improved long term survival of mice by reducing cutaneous and pulmonary chronic GvHD¹⁸⁸. The onset of GvHD in HB2 mice was much faster than described for classical chronic GvHD models, but also here the depletion of macrophages rescued animals from GvHD-like syndromes and improved overall survival (Figure 24). Although GvHD was revealed at present to be a major issue in HB2 mice, there is still a time window of approximately 5 weeks in which human macrophages can be tested in different *in vivo* settings (Figure 24). Further experimental settings need to be tested aiming for controlling the frequency of monocyte and macrophages in HB2 mice in order to delay or event prevent the onset of GvHD symptoms. In this context the depletion of human macrophages by α hCSF-1R antibody provides a powerful tool to prevent occurrence of GvHD.

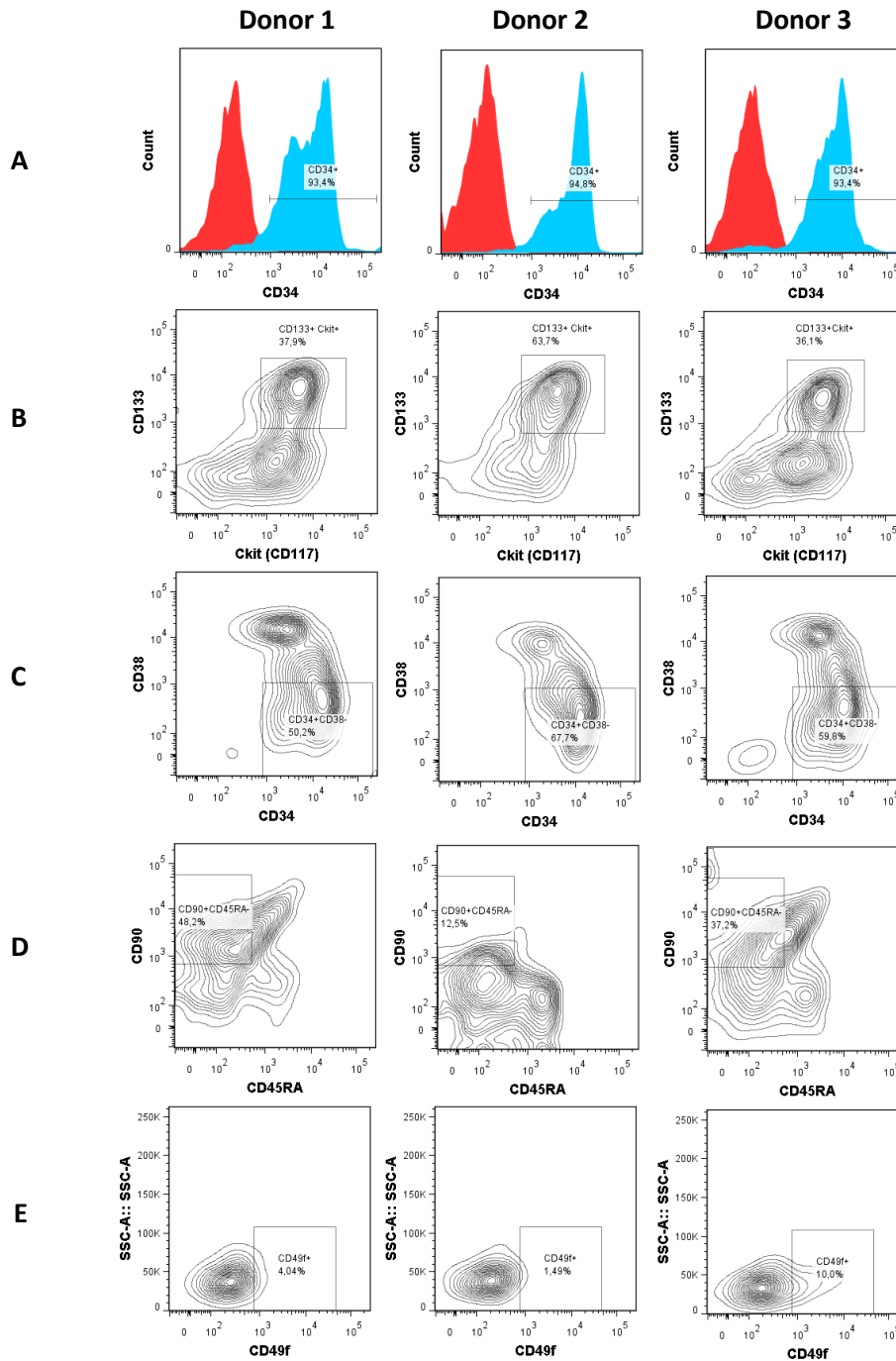
6.9. Future directions

HIS mice generally represent a valuable tool to study human immune responses in preclinical settings. However, functionality and integrity of the engrafted human immune system is necessarily required for reliable interpretation of results derived from studies performed in HIS mice. In HB2 mice a major limitation, the underrepresentation of human functional macrophages, could be overcome resulting in an improved HIS mouse model that more closely reflects human myelopoiesis. As presence of

professional antigen presenting cells is required for adaptive immunity reconstitution of human macrophages in HB2 mice might improve the quality of HLA-restricted as well as humoral immune responses. In this case, HB2 mice might serve as valuable model for immunization approaches. Moreover, HB2 mice offer the unique possibility to study the interaction of human tumor cells and human TAMs. These investigations might help to better understand basic principles of how TAMs attract other immune cells such as T cells to the tumor site and how anti-tumoral immune response are initiated. Moreover, manipulation of human TAMs in the tumor microenvironment could help to better understand the mechanisms underlying their dual role in tumor progression. Findings might finally result in novel therapeutic strategies of how to deplete or reprogram tumor-promoting TAMs and how to strengthen their anti-tumoral capabilities.

7. Supplementary figures

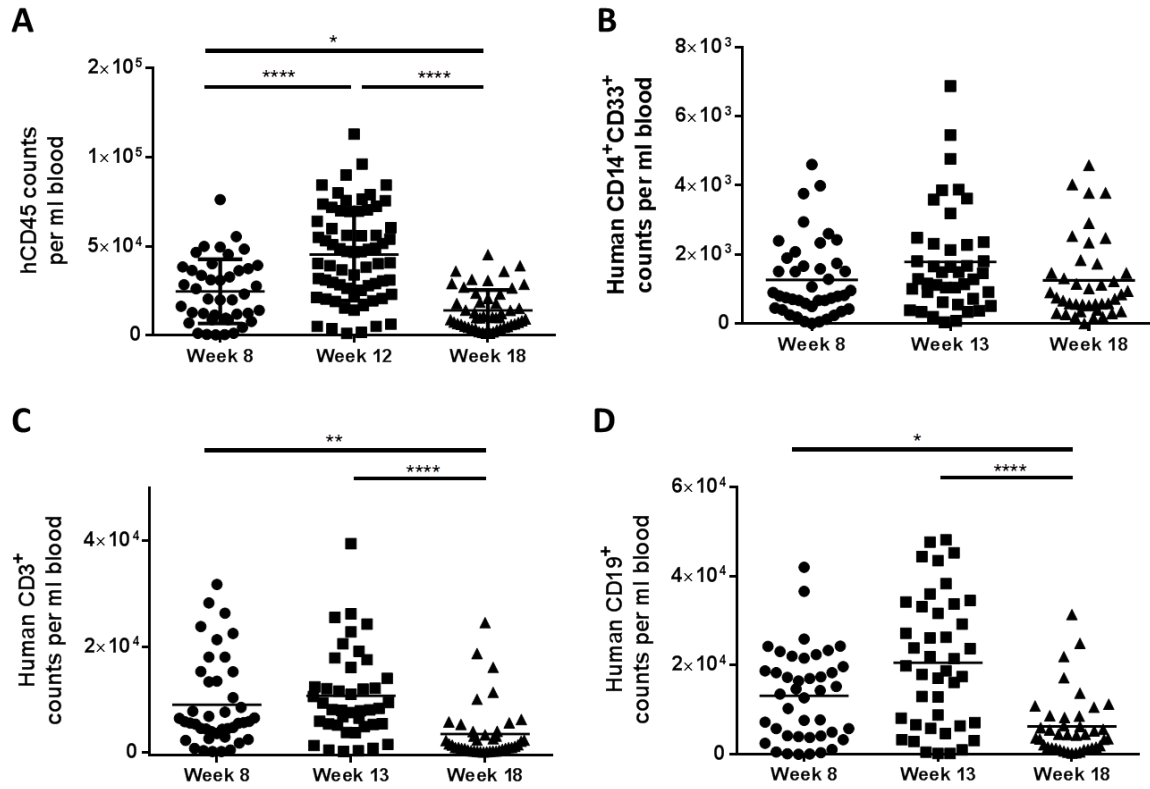
7.1. Phenotypic heterogeneity of isolated human FLCs



Supplementary Figure 1: Phenotypic heterogeneity of purchased human fetal liver cells

Representative flow cytometry analysis showing the frequency of human CD34⁺ (A), CD133⁺Ckit⁺ (B) CD34⁺CD38⁻ (C) and CD90⁺CD45RA⁻ (D) cells within CD34⁺CD38⁻ human fetal liver cells. (E) Frequency of human CD49f⁺ cells within CD34⁺CD38⁻CD90⁺CD45RA⁻ human fetal liver cells.

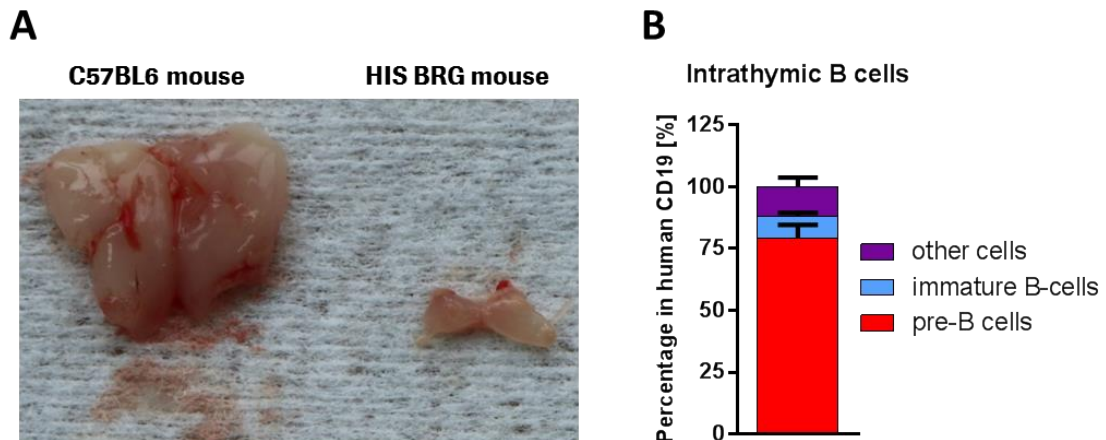
7.2. Human immune cell counts in peripheral blood of humanized mice



Supplementary Figure 2: Human leukocyte counts in peripheral blood of HIS BRG mice

Counts of total human hematopoietic cells (A), of human monocytes (B), of human T cells (C) and of human B cells (D) per milliliter of peripheral blood of HIS BRG mice at indicated time points after reconstitution. Each symbol represents an individual mouse and black bars indicate mean values (n= 42 mice; one-way analysis of variance (ANOVA) followed by Tukey test (*P < 0.05)).

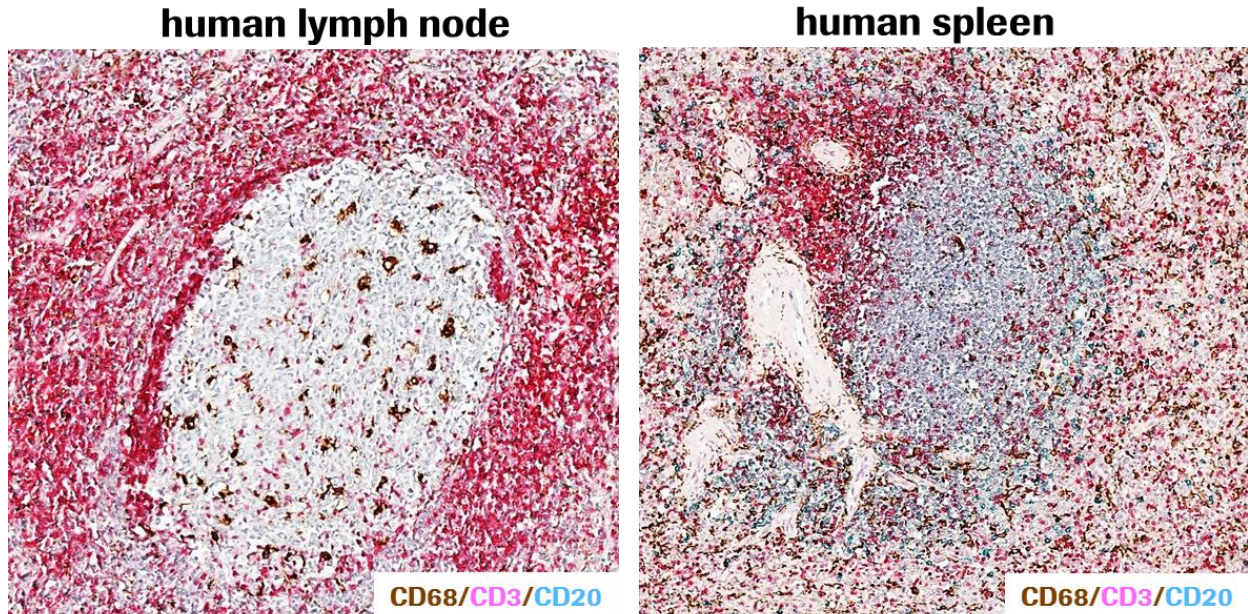
7.3. Thymus characterization in HIS BRG mice



Supplementary Figure 3: Structural and cellular characterization of thymic structures in HIS BRG mice

(A) Picture of thymic lobes removed from HIS BRG mice 12 weeks after reconstitution (right) and from 8 week old immunocompetent C57BL6 mice (left). (B) FACS analysis of CD19⁺ B cells isolated from thymi of HIS BRG mice co-stained for human IgM to identified CD19⁺IgM⁻ pre-B cells and CD19⁺IgM⁺ immature B cells.

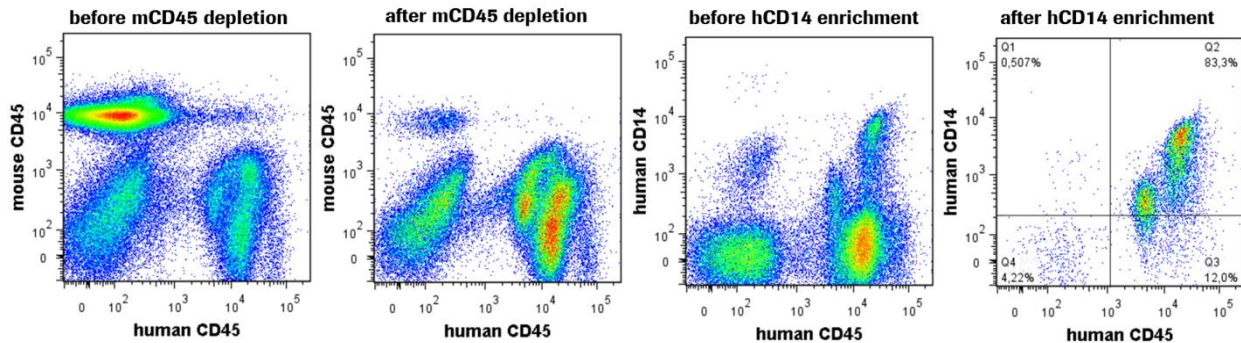
7.4. Characterization of follicular-like structures in human lymph nodes and human spleen



Supplementary Figure 4: IHC analysis of follicular-like structures in human lymph node and spleen

Human lymph node and spleen tissue sections were triple stained in IHC for human macrophages (CD68, brown), human T cells (CD3, pink) and human B cells (CD20, purple) to identify follicular like structures.

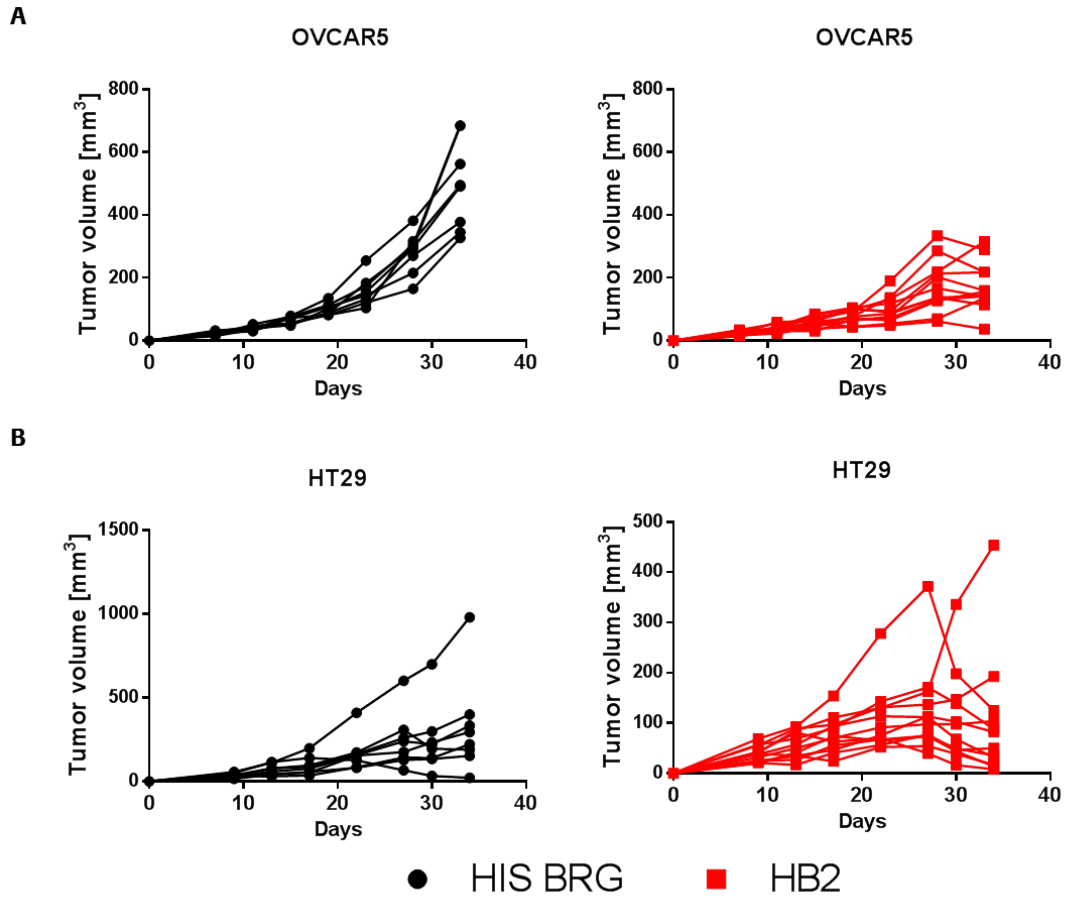
7.5. Isolation of human CD14 monocyte from bone marrow samples of HIS BRG mice



Supplementary Figure 5: Enrichment of human monocytes from bone marrow aspirates of HIS BRG mice

Bone marrow aspirates from HIS BRG mice reconstituted with a single HSC donor were pooled and stained for human and mouse CD45 (before mCD45 depletion); mouse immune cells were depleted by magnetic beads specific for mouse CD45⁺ (after mCD45 depletion); bone marrow cells depleted of mouse CD45 positive cells (before hCD14 enrichment) were finally enriched for human CD14⁺ cells by magnetic beads (after hCD14 enrichment).

7.6. Tumor growth kinetics of HT29 and OVCAR5 xenograft tumors in individual mice



Supplementary Figure 6: OVCAR5 and HT29 tumor growth in HB2 and HIS BRG mice

HT29 and OVCAR5 tumors were inoculated subcutaneously in the right flank of HIS BRG mice and either treated with a control antibody (HIS BRG mice) or with 2G2 (HB2 mice). (A) Volumes of OVCAR5 tumors grown in individual HIS BRG mice treated with control or 2G2 antibody. (B) Volumes of HT29 tumors grown in individual HIS BRG mice treated with control or 2G2 antibody.

8. Table of figures

Figure 1: Phenotyping of human CD34 enriched FLCs using FACS analysis	36
Figure 2: Colony types formed by FLCs in the colony formation cell (CFC) assay	37
Figure 3: Engraftment and differentiation of human FLCs in the bone marrow of newborn BRG mice.....	38
Figure 4: Analysis of human white blood cell composition in peripheral blood of HIS BRG mice	40
Figure 5: Morphological and cellular characterization of the bone marrow in HIS BRG mice.....	41
Figure 6: Thymus characterization in HIS BRG mice	43
Figure 7: Expression of human and mouse MHC class II molecules in the thymus of HIS BRG mice.....	44
Figure 8: Co-localization of human antigen presenting cells and human thymocytes in thymus of humanized mice	45
Figure 9: Morphological and cellular characterization of mesenteric lymph nodes in HIS BRG mice	47
Figure 10: Morphological and cellular characterization of the spleen in HIS BRG mice	48
Figure 11: Biacore analysis of mouse CSF-1 and human or mouse CSF-1R.....	50
Figure 12: Analysis of CSF-1R signaling in human monocytes stimulated with mouse and human CSF-1	51
Figure 13: Differentiation of human monocytes upon stimulation with mouse CSF-1 <i>in vitro</i>	52
Figure 14: Depletion of mouse monocytes and macrophages in HIS BRG mice	53
Figure 15: Blood analysis in HB2 mice.....	56
Figure 16: Phenotyping of human monocytes in HB2 mice	57
Figure 17: Infiltration of human macrophages in lymphoid and non-lymphoid tissues of HB2 mice.....	58
Figure 18: Time independent induction of human macrophages in HB2 mice.....	59
Figure 19: Diminished human myelopoiesis in HB2 mice upon blockage of mouse CSF-1.....	61
Figure 20: Cytokine response of human macrophages in HB2 mice upon stimulation with LPS <i>in vivo</i>	62
Figure 21: Growth of human tumor cell lines in HIS BRG and HB2 mice	63
Figure 22: Phenotyping of human tumor infiltrating immune cells.....	65
Figure 23: Characterization of graft versus host disease in HB2 mice	66
Figure 24: Prevention of graft versus host disease in HB2 mice by depletion of human macrophages.....	68

9. Abbreviation index

BRG mice. *BALB/c-RAG(2)^{-/-} Il2ry^{-/-} mice*
CSF-1. *Macrophage colony stimulating factor*
CSF-1R. *Colony stimulation factor 1 receptor*
FLCs. *Fetal liver cells*
GM-CSF. *Granulocyte-macrophage stimulating factor*
GvHD. *Graft versus host disease*
H&E. *Hematoxinilin and Eosin*
HB2 mice. *HIS BRG 2G2 treated mice*
HLA. *Human leukocyte antigen*
IHC. *Immunohistochemistry*
IL. *Interleukin*
LTRCs. *Long term repopulating cells*
MDSCs. *Myeloid derived suppressor cells*
NOG mice. *NOD.Cg-Prkdcscid Il2rgtm1Sug/JicTac mice*
NSG mice. *NOD.Cg-Prkdcscid Il2rgtm1Wjl/SzJ mice*
SIRP α . *Signal regulatory protein α*
TAMs. *Tumor-associated macrophages*

10. References

1. Siegel RL, Miller KD, Jemal A. Cancer statistics, 2015. *CA: a cancer journal for clinicians* 2015, **65**(1): 5-29.
2. Perou CM, Sorlie T, Eisen MB, van de Rijn M, Jeffrey SS, Rees CA, *et al.* Molecular portraits of human breast tumours. *Nature* 2000, **406**(6797): 747-752.
3. Sorlie T, Perou CM, Tibshirani R, Aas T, Geisler S, Johnsen H, *et al.* Gene expression patterns of breast carcinomas distinguish tumor subclasses with clinical implications. *Proceedings of the National Academy of Sciences of the United States of America* 2001, **98**(19): 10869-10874.
4. Moffitt RA, Marayati R, Flate EL, Volmar KE, Loeza SG, Hoadley KA, *et al.* Virtual microdissection identifies distinct tumor- and stroma-specific subtypes of pancreatic ductal adenocarcinoma. *Nature genetics* 2015, **47**(10): 1168-1178.
5. Collisson EA, Sadanandam A, Olson P, Gibb WJ, Truitt M, Gu S, *et al.* Subtypes of pancreatic ductal adenocarcinoma and their differing responses to therapy. *Nature medicine* 2011, **17**(4): 500-503.
6. Swartz MA, Iida N, Roberts EW, Sangaletti S, Wong MH, Yull FE, *et al.* Tumor Microenvironment Complexity: Emerging Roles in Cancer Therapy. *Cancer Res* 2012, **72**(10): 2473-2480.
7. Copier J, Dalglish AG, Britten CM, Finke LH, Gaudernack G, Gnjatic S, *et al.* Improving the efficacy of cancer immunotherapy. *European journal of cancer* 2009, **45**(8): 1424-1431.
8. Peggs KS, Quezada SA, Allison JP. Cancer immunotherapy: co-stimulatory agonists and co-inhibitory antagonists. *Clin Exp Immunol* 2009, **157**(1): 9-19.
9. Pardoll DM. The blockade of immune checkpoints in cancer immunotherapy. *Nat Rev Cancer* 2012, **12**(4): 252-264.
10. Yamazaki T, Akiba H, Iwai H, Matsuda H, Aoki M, Tanno Y, *et al.* Expression of programmed death 1 ligands by murine T cells and APC. *Journal of immunology* 2002, **169**(10): 5538-5545.
11. Freeman GJ, Long AJ, Iwai Y, Bourque K, Chernova T, Nishimura H, *et al.* Engagement of the PD-1 immunoinhibitory receptor by a novel B7 family member leads to negative regulation of lymphocyte activation. *The Journal of experimental medicine* 2000, **192**(7): 1027-1034.
12. Chen LP, Han X. Anti-PD-1/PD-L1 therapy of human cancer: past, present, and future. *Journal of Clinical Investigation* 2015, **125**(9): 3384-3391.
13. Nishimura H, Nose M, Hiai H, Minato N, Honjo T. Development of lupus-like autoimmune diseases by disruption of the PD-1 gene encoding an ITIM motif-carrying immunoreceptor. *Immunity* 1999, **11**(2): 141-151.
14. Dong H, Strome SE, Salomao DR, Tamura H, Hirano F, Flies DB, *et al.* Tumor-associated B7-H1 promotes T-cell apoptosis: a potential mechanism of immune evasion. *Nature medicine* 2002, **8**(8): 793-800.
15. Taube JM, Anders RA, Young GD, Xu H, Sharma R, McMiller TL, *et al.* Colocalization of inflammatory response with B7-h1 expression in human melanocytic lesions supports an adaptive resistance mechanism of immune escape. *Science translational medicine* 2012, **4**(127): 127ra137.
16. Leach DR, Krummel MF, Allison JP. Enhancement of antitumor immunity by CTLA-4 blockade. *Science* 1996, **271**(5256): 1734-1736.
17. Waterhouse P, Penninger JM, Timms E, Wakeham A, Shahinian A, Lee KP, *et al.* Lymphoproliferative disorders with early lethality in mice deficient in Ctl4-4. *Science* 1995, **270**(5238): 985-988.
18. Tivol EA, Borriello F, Schweitzer AN, Lynch WP, Bluestone JA, Sharpe AH. Loss of CTLA-4 leads to massive lymphoproliferation and fatal multiorgan tissue destruction, revealing a critical negative regulatory role of CTLA-4. *Immunity* 1995, **3**(5): 541-547.

19. Zhu C, Anderson AC, Schubart A, Xiong H, Imitola J, Khoury SJ, *et al.* The Tim-3 ligand galectin-9 negatively regulates T helper type 1 immunity. *Nature immunology* 2005, **6**(12): 1245-1252.
20. Huang CT, Workman CJ, Flies D, Pan X, Marson AL, Zhou G, *et al.* Role of LAG-3 in regulatory T cells. *Immunity* 2004, **21**(4): 503-513.
21. Munn DH, Mellor AL. Indoleamine 2,3-dioxygenase and tumor-induced tolerance. *The Journal of clinical investigation* 2007, **117**(5): 1147-1154.
22. Mellor AL, Keskin DB, Johnson T, Chandler P, Munn DH. Cells expressing indoleamine 2,3-dioxygenase inhibit T cell responses. *Journal of immunology* 2002, **168**(8): 3771-3776.
23. Brahmer JR, Drake CG, Wollner I, Powderly JD, Picus J, Sharfman WH, *et al.* Phase I study of single-agent anti-programmed death-1 (MDX-1106) in refractory solid tumors: safety, clinical activity, pharmacodynamics, and immunologic correlates. *Journal of clinical oncology : official journal of the American Society of Clinical Oncology* 2010, **28**(19): 3167-3175.
24. Hodi FS, Mihm MC, Soiffer RJ, Haluska FG, Butler M, Seiden MV, *et al.* Biologic activity of cytotoxic T lymphocyte-associated antigen 4 antibody blockade in previously vaccinated metastatic melanoma and ovarian carcinoma patients. *Proceedings of the National Academy of Sciences of the United States of America* 2003, **100**(8): 4712-4717.
25. Phan GQ, Yang JC, Sherry RM, Hwu P, Topalian SL, Schwartzentruber DJ, *et al.* Cancer regression and autoimmunity induced by cytotoxic T lymphocyte-associated antigen 4 blockade in patients with metastatic melanoma. *Proceedings of the National Academy of Sciences of the United States of America* 2003, **100**(14): 8372-8377.
26. Hodi FS, O'Day SJ, McDermott DF, Weber RW, Sosman JA, Haanen JB, *et al.* Improved survival with ipilimumab in patients with metastatic melanoma. *The New England journal of medicine* 2010, **363**(8): 711-723.
27. Powles T, Eder JP, Fine GD, Braiteh FS, Loriot Y, Cruz C, *et al.* MPDL3280A (anti-PD-L1) treatment leads to clinical activity in metastatic bladder cancer. *Nature* 2014, **515**(7528): 558-562.
28. Garon EB, Rizvi NA, Hui R, Leighl N, Balmanoukian AS, Eder JP, *et al.* Pembrolizumab for the treatment of non-small-cell lung cancer. *The New England journal of medicine* 2015, **372**(21): 2018-2028.
29. Herbst RS, Soria JC, Kowanetz M, Fine GD, Hamid O, Gordon MS, *et al.* Predictive correlates of response to the anti-PD-L1 antibody MPDL3280A in cancer patients. *Nature* 2014, **515**(7528): 563-567.
30. Rech AJ, Mick R, Martin S, Recio A, Aquino NA, Powell DJ, *et al.* CD25 Blockade Depletes and Selectively Reprograms Regulatory T Cells in Concert with Immunotherapy in Cancer Patients. *Science translational medicine* 2012, **4**(134).
31. Attia P, Maker AV, Haworth LR, Rogers-Freezer L, Rosenberg SA. Inability of a fusion protein of IL-2 and diphtheria toxin (Denileukin Diftitox, DAB(389)IL-2, ONTAK) to eliminate regulatory T lymphocytes in patients with melanoma. *J Immunother* 2005, **28**(6): 582-592.
32. Sznol M, Hodi FS, Margolin K, McDermott DF, Ernstoff MS, Kirkwood JM, *et al.* Phase I study of BMS-663513, a fully human anti-CD137 agonist monoclonal antibody, in patients (pts) with advanced cancer (CA). *Journal of Clinical Oncology* 2008, **26**(15).
33. Melero I, Gangadhar TC, Kohrt HE, Segal NH, Logan T, Urba WJ, *et al.* A phase I study of the safety, tolerability, pharmacokinetics, and immunoregulatory activity of urelumab (BMS-663513) in subjects with advanced and/or metastatic solid tumors and relapsed/refractory B-cell non-Hodgkin's lymphoma (B-NHL). *Journal of Clinical Oncology* 2013, **31**(15).
34. Curti BD, Kovacovics-Bankowski M, Morris N, Walker E, Chisholm L, Floyd K, *et al.* OX40 Is a Potent Immune-Stimulating Target in Late-Stage Cancer Patients. *Cancer Res* 2013, **73**(24): 7189-7198.
35. Guo ZQ, Wang X, Cheng DL, Xia ZJ, Luan M, Zhang SL. PD-1 Blockade and OX40 Triggering Synergistically Protects against Tumor Growth in a Murine Model of Ovarian Cancer. *PLoS one* 2014, **9**(2).

36. Chen SH, Lee LF, Fisher TS, Jessen B, Elliott M, Evering W, *et al.* Combination of 4-1BB Agonist and PD-1 Antagonist Promotes Antitumor Effector/Memory CD8 T Cells in a Poorly Immunogenic Tumor Model. *Cancer Immunol Res* 2015, **3**(2): 149-160.
37. Suntharalingam G, Perry MR, Ward S, Brett SJ, Castello-Cortes A, Brunner MD, *et al.* Cytokine storm in a phase 1 trial of the anti-CD28 monoclonal antibody TGN1412. *New Engl J Med* 2006, **355**(10): 1018-1028.
38. Herrmann I, Baeuerle PA, Friedrich M, Murr A, Filusch S, Ruttinger D, *et al.* Highly Efficient Elimination of Colorectal Tumor-Initiating Cells by an EpCAM/CD3-Bispecific Antibody Engaging Human T Cells. *PLoS one* 2010, **5**(10).
39. Brischwein K, Schlereth B, Guller B, Steiger C, Wolf A, Lutterbuese R, *et al.* MT110: A novel bispecific single-chain antibody construct with high efficacy in eradicating established tumors. *Mol Immunol* 2006, **43**(8): 1129-1143.
40. Bargou R, Leo E, Zugmaier G, Klinger M, Goebeler M, Knop S, *et al.* Tumor regression in cancer patients by very low doses of a T cell-engaging antibody. *Science* 2008, **321**(5891): 974-977.
41. Seimetz D, Lindhofer H, Bokemeyer C. Development and approval of the trifunctional antibody catumaxomab (anti-EpCAM x anti-CD3) as a targeted cancer immunotherapy. *Cancer Treat Rev* 2010, **36**(6): 458-467.
42. Sebastian M, Passlick B, Friccius-Quecke H, Jager M, Lindhofer H, Kanniss F, *et al.* Treatment of non-small cell lung cancer patients with the trifunctional monoclonal antibody catumaxomab (anti-EpCAM x anti-CD3): a phase I study. *Cancer Immunol Immun* 2007, **56**(10): 1637-1644.
43. Scarlett UK, Rutkowski MR, Rauwerdink AM, Fields J, Escovar-Fadul X, Baird J, *et al.* Ovarian cancer progression is controlled by phenotypic changes in dendritic cells. *Journal of Experimental Medicine* 2012, **209**(3): 495-506.
44. Carretero R, Sektioglu IM, Garbi N, Salgado OC, Beckhove P, Hammerling GJ. Eosinophils orchestrate cancer rejection by normalizing tumor vessels and enhancing infiltration of CD8(+) T cells. *Nature immunology* 2015, **16**(6): 609-+.
45. Ries CH, Cannarile MA, Hoves S, Benz J, Wartha K, Runza V, *et al.* Targeting tumor-associated macrophages with anti-CSF-1R antibody reveals a strategy for cancer therapy. *Cancer cell* 2014, **25**(6): 846-859.
46. Ugel S, De Sanctis F, Mandruzzato S, Bronte V. Tumor-induced myeloid deviation: when myeloid-derived suppressor cells meet tumor-associated macrophages. *Journal of Clinical Investigation* 2015, **125**(9): 3365-3376.
47. Murray PJ, Wynn TA. Protective and pathogenic functions of macrophage subsets. *Nature reviews Immunology* 2011, **11**(11): 723-737.
48. Goerdts S, Orfanos CE. Other functions, other genes: alternative activation of antigen-presenting cells. *Immunity* 1999, **10**(2): 137-142.
49. Hussein MR. Tumour-associated macrophages and melanoma tumourigenesis: integrating the complexity. *International journal of experimental pathology* 2006, **87**(3): 163-176.
50. DiPietro LA, Burdick M, Low QE, Kunkel SL, Strieter RM. MIP-1alpha as a critical macrophage chemoattractant in murine wound repair. *The Journal of clinical investigation* 1998, **101**(8): 1693-1698.
51. Murray HW. Interferon-gamma, the activated macrophage, and host defense against microbial challenge. *Annals of internal medicine* 1988, **108**(4): 595-608.
52. Gordon S, Martinez FO. Alternative Activation of Macrophages: Mechanism and Functions. *Immunity* 2010, **32**(5): 593-604.
53. Stout RD, Jiang C, Matta B, Tietzel I, Watkins SK, Suttles J. Macrophages sequentially change their functional phenotype in response to changes in microenvironmental influences. *Journal of immunology* 2005, **175**(1): 342-349.
54. Kawanishi N, Yano H, Yokogawa Y, Suzuki K. Exercise training inhibits inflammation in adipose tissue via both suppression of macrophage infiltration and acceleration of phenotypic switching from M1 to M2 macrophages in high-fat-diet-induced obese mice. *Exercise immunology review* 2010, **16**: 105-118.

55. Hagemann T, Lawrence T, McNeish I, Charles KA, Kulbe H, Thompson RG, *et al.* "Re-educating" tumor-associated macrophages by targeting NF-kappaB. *The Journal of experimental medicine* 2008, **205**(6): 1261-1268.
56. Noy R, Pollard JW. Tumor-Associated Macrophages: From Mechanisms to Therapy (vol 41, pg 49, 2014). *Immunity* 2014, **41**(5): 866-866.
57. Panni RZ, Linehan DC, DeNardo DG. Targeting tumor-infiltrating macrophages to combat cancer. *Immunotherapy* 2013, **5**(10): 1075-1087.
58. Zaynagetdinov R, Sherrill TP, Polosukhin VV, Han W, Ausborn JA, McLoed AG, *et al.* A Critical Role for Macrophages in Promotion of Urethane-Induced Lung Carcinogenesis. *Journal of immunology* 2011, **187**(11): 5703-5711.
59. Kuang DM, Zhao QY, Peng C, Xu J, Zhang JP, Wu CY, *et al.* Activated monocytes in peritumoral stroma of hepatocellular carcinoma foster immune privilege and disease progression through PD-L1. *Journal of Experimental Medicine* 2009, **206**(6): 1327-1337.
60. Kryczek I, Zou L, Rodriguez P, Zhu G, Wei S, Mottram P, *et al.* B7-H4 expression identifies a novel suppressive macrophage population in human ovarian carcinoma. *Journal of Experimental Medicine* 2006, **203**(4): 871-881.
61. Murdoch C, Muthana M, Coffelt SB, Lewis CE. The role of myeloid cells in the promotion of tumour angiogenesis. *Nat Rev Cancer* 2008, **8**(8): 618-631.
62. Gordon S, Mantovani A. Diversity and plasticity of mononuclear phagocytes Preface. *Eur J Immunol* 2011, **41**(9): 2470-2472.
63. Qian BZ, Pollard JW. Macrophage Diversity Enhances Tumor Progression and Metastasis. *Cell* 2010, **141**(1): 39-51.
64. Wang JM, Sherry B, Fivash MJ, Kelvin DJ, Oppenheim JJ. Human Recombinant Macrophage Inflammatory Protein-1-Alpha and Protein-1-Beta and Monocyte Chemotactic and Activating Factor Utilize Common and Unique Receptors on Human Monocytes. *Journal of immunology* 1993, **150**(7): 3022-3029.
65. Manthey CL, Johnson DL, Illig CR, Tuman RW, Zhou Z, Baker JF, *et al.* JNJ-28312141, a novel orally active colony-stimulating factor-1 receptor/FMS-related receptor tyrosine kinase-3 receptor tyrosine kinase inhibitor with potential utility in solid tumors, bone metastases, and acute myeloid leukemia. *Mol Cancer Ther* 2009, **8**(11): 3151-3161.
66. Garceau V, Smith J, Paton IR, Davey M, Fares MA, Sester DP, *et al.* Pivotal Advance: Avian colony-stimulating factor 1 (CSF-1), interleukin-34 (IL-34), and CSF-1 receptor genes and gene products. *Journal of leukocyte biology* 2010, **87**(5): 753-764.
67. Gow DJ, Sester DP, Hume DA. CSF-1, IGF-1, and the control of postnatal growth and development. *Journal of leukocyte biology* 2010, **88**(3): 475-481.
68. Pollard JW. Trophic macrophages in development and disease. *Nature Reviews Immunology* 2009, **9**(4): 259-270.
69. Chen XY, Liu HL, Focia PJ, Shim AHR, He XL. Structure of macrophage colony stimulating factor bound to FMS: Diverse signaling assemblies of class III receptor tyrosine kinases. *Proceedings of the National Academy of Sciences of the United States of America* 2008, **105**(47): 18267-18272.
70. Mitchem JB, Brennan DJ, Knolhoff BL, Belt BA, Zhu Y, Sanford DE, *et al.* Targeting Tumor-Infiltrating Macrophages Decreases Tumor-Initiating Cells, Relieves Immunosuppression, and Improves Chemotherapeutic Responses. *Cancer Res* 2013, **73**(3): 1128-1141.
71. Pyonteck SM, Gadea BB, Wang HW, Gocheva V, Hunter KE, Tang LH, *et al.* Deficiency of the macrophage growth factor CSF-1 disrupts pancreatic neuroendocrine tumor development. *Oncogene* 2012, **31**(11): 1459-1467.
72. Lin EY, Nguyen AV, Russell RG, Pollard JW. Colony-stimulating factor 1 promotes progression of mammary tumors to malignancy. *Journal of Experimental Medicine* 2001, **193**(6): 727-739.

73. Dorsch M, Hock H, Kunzendorf U, Diamantstein T, Blankenstein T. Macrophage Colony-Stimulating Factor Gene-Transfer into Tumor-Cells Induces Macrophage Infiltration but Not Tumor Suppression. *Eur J Immunol* 1993, **23**(1): 186-190.
74. Xu JY, Escamilla J, Mok S, David J, Priceman S, West B, *et al.* CSF1R Signaling Blockade Stanches Tumor-Infiltrating Myeloid Cells and Improves the Efficacy of Radiotherapy in Prostate Cancer. *Cancer Res* 2013, **73**(9): 2782-2794.
75. Priceman SJ, Sung JL, Shaposhnik Z, Burton JB, Torres-Collado AX, Moughon DL, *et al.* Targeting distinct tumor-infiltrating myeloid cells by inhibiting CSF-1 receptor: combating tumor evasion of antiangiogenic therapy. *Blood* 2010, **115**(7): 1461-1471.
76. DeNardo DG, Brennan DJ, Rexhepaj E, Ruffell B, Shiao SL, Madden SF, *et al.* Leukocyte Complexity Predicts Breast Cancer Survival and Functionally Regulates Response to Chemotherapy. *Cancer Discov* 2011, **1**(1): 54-67.
77. Lundholm M, Hagglof C, Wikberg ML, Stattin P, Egevad L, Bergh A, *et al.* Secreted Factors from Colorectal and Prostate Cancer Cells Skew the Immune Response in Opposite Directions. *Sci Rep-Uk* 2015, **5**.
78. Gabrilovich DI, Ostrand-Rosenberg S, Bronte V. Coordinated regulation of myeloid cells by tumours. *Nature Reviews Immunology* 2012, **12**(4): 253-268.
79. Fukuda K, Kobayashi A, Watabe K. The role of tumor-associated macrophage in tumor progression. *Front Biosci (Schol Ed)* 2012, **4**: 787-798.
80. Cassier PA, Italiano A, Gomez-Roca CA, Le Tourneau C, Toulmonde M, Cannarile MA, *et al.* CSF1R inhibition with emactuzumab in locally advanced diffuse-type tenosynovial giant cell tumours of the soft tissue: a dose-escalation and dose-expansion phase 1 study. *Lancet Oncol* 2015, **16**(8): 949-956.
81. Ries CH, Hoves S, Cannarile MA, Ruttinger D. CSF-1/CSF-1R targeting agents in clinical development for cancer therapy. *Curr Opin Pharmacol* 2015, **23**: 45-51.
82. Zhu Y, Knolhoff BL, Meyer MA, Nywening TM, West BL, Luo J, *et al.* CSF1/CSF1R blockade reprograms tumor-infiltrating macrophages and improves response to T-cell checkpoint immunotherapy in pancreatic cancer models. *Cancer Res* 2014, **74**(18): 5057-5069.
83. Richman LP, Vonderheide RH. Anti-human CD40 monoclonal antibody therapy is potent without FcR crosslinking. *Oncoimmunology* 2014, **3**(4).
84. Brehm MA, Shultz LD, Greiner DL. Humanized mouse models to study human diseases. *Curr Opin Endocrinol* 2010, **17**(2): 120-125.
85. Mosier DE, Gulizia RJ, Baird SM, Wilson DB. Transfer of a Functional Human Immune-System to Mice with Severe Combined Immunodeficiency. *Nature* 1988, **335**(6187): 256-259.
86. Pearson T, Greiner DL, Shultz LD. Creation of "humanized" mice to study human immunity. *Current protocols in immunology / edited by John E Coligan [et al]* 2008, **Chapter 15**: Unit 15 21.
87. King MA, Covassin L, Brehm MA, Racki W, Pearson T, Leif J, *et al.* Human peripheral blood leucocyte non-obese diabetic-severe combined immunodeficiency interleukin-2 receptor gamma chain gene mouse model of xenogeneic graft-versus-host-like disease and the role of host major histocompatibility complex. *Clin Exp Immunol* 2009, **157**(1): 104-118.
88. van Rijn RS, Simonetti ER, Hagenbeek A, Hogenes MCH, de Weger RA, Canninga-van Dijk MR, *et al.* A new xenograft model for graft-versus-host disease by intravenous transfer of human peripheral blood mononuclear cells in RAG2(-/-) gamma c(-/-) double-mutant mice. *Blood* 2003, **102**(7): 2522-2531.
89. Buchner SM, Sliva K, Bonig H, Volker I, Waibler Z, Kirberg J, *et al.* Delayed onset of graft-versus-host disease in immunodeficient human leucocyte antigen-DQ8 transgenic, murine major histocompatibility complex class II-deficient mice repopulated by human peripheral blood mononuclear cells. *Clin Exp Immunol* 2013, **173**(2): 355-364.

90. Mutis T, van Rijn RS, Simonetti ER, Aarts-Riemens T, Emmelot ME, van Bloois L, *et al.* Human regulatory T cells control xenogeneic graft-versus-host disease induced by autologous T cells in RAG2(-/-)gamma c(-/-) immunodeficient mice. *Clin Cancer Res* 2006, **12**(18): 5520-5525.
91. Hozumi N, Cole J, Lucien J, Terzioglu M, Gorczynski R, Sandhu J. A human model of xenogeneic graft-versus-host disease. *10th International Congress on Immunology, Vols 1 and 2* 1998: 255-260.
92. Ali N, Flutter B, Rodriguez RS, Sharif-Paghaleh E, Barber LD, Lombardi G, *et al.* Xenogeneic Graft-versus-Host-Disease in NOD-scid IL-2R gamma(null) Mice Display a T-Effector Memory Phenotype. *PloS one* 2012, **7**(8).
93. Shultz LD, Banuelos S, Lyons M, Samuels R, Burzenski L, Gott B, *et al.* NOD/LtSz-Rag1(null)Pfp(null) mice: A new model system with increased levels of human peripheral leukocyte and hematopoietic stem-cell engraftment. *Transplantation* 2003, **76**(7): 1036-1042.
94. Ito M, Hiramatsu H, Kobayashi K, Suzue K, Kawahata M, Hioki K, *et al.* NOD/SCID/gamma(null)(c) mouse: an excellent recipient mouse model for engraftment of human cells. *Blood* 2002, **100**(9): 3175-3182.
95. Mccune JM, Namikawa R, Kaneshima H, Shultz LD, Lieberman M, Weissman IL. The Scid-Hu Mouse - Murine Model for the Analysis of Human Hematolymphoid Differentiation and Function. *Science* 1988, **241**(4873): 1632-1639.
96. Lapidot T, Pflumio F, Doedens M, Murdoch B, Williams DE, Dick JE. Cytokine Stimulation of Multilineage Hematopoiesis from Immature Human-Cells Engrafted in Scid Mice. *Science* 1992, **255**(5048): 1137-1141.
97. Lepus CM, Gibson TF, Gerber SA, Kawikova I, Szczepanik M, Hossain J, *et al.* Comparison of human fetal liver, umbilical cord blood, and adult blood hematopoietic stem cell engraftment in NOD-scid/gamma c(-/-), Balb/c-Rag1(-/-)gamma c(-/-), and C.B-17-scid/bg immunodeficient mice. *Hum Immunol* 2009, **70**(10): 790-802.
98. Notta F, Doulatov S, Laurenti E, Poepl A, Jurisica I, Dick JE. Isolation of Single Human Hematopoietic Stem Cells Capable of Long-Term Multilineage Engraftment. *Science* 2011, **333**(6039): 218-221.
99. Chen QF, Khoury M, Limmon G, Choolani M, Chan JKY, Chen JZ. Human Fetal Hepatic Progenitor Cells are Distinct from, but Closely Related to, Hematopoietic Stem/Progenitor Cells. *Stem Cells* 2013, **31**(6): 1160-1169.
100. Rongvaux A, Willinger T, Martinek J, Strowig T, Gearty SV, Teichmann LL, *et al.* Development and function of human innate immune cells in a humanized mouse model. *Nature biotechnology* 2014, **32**(4): 364-372.
101. Czechowicz A, Kraft D, Weissman IL, Bhattacharya D. Efficient transplantation via antibody-based clearance of hematopoietic stem cell niches. *Science* 2007, **318**(5854): 1296-1299.
102. Manz MG. Human-hemato-lymphoid-system mice: opportunities and challenges. *Immunity* 2007, **26**(5): 537-541.
103. Rathinam C, Poueymirou WT, Rojas J, Murphy AJ, Valenzuela DM, Yancopoulos GD, *et al.* Efficient differentiation and function of human macrophages in humanized CSF-1 mice. *Blood* 2011, **118**(11): 3119-3128.
104. Singh M, Singh P, Gaudray G, Musumeci L, Thielen C, Vaira D, *et al.* An Improved Protocol for Efficient Engraftment in NOD/LTSZ-SCIDIL-2R gamma(NULL) Mice Allows HIV Replication and Development of Anti-HIV Immune Responses. *PloS one* 2012, **7**(6).
105. Lux A, Seeling M, Baerenwaldt A, Lehmann B, Schwab I, Repp R, *et al.* A Humanized Mouse Identifies the Bone Marrow as a Niche with Low Therapeutic IgG Activity. *Cell Rep* 2014, **7**(1): 236-248.
106. Groen RWJ, Noort WA, Raymakers RA, Prins HJ, Aalders L, Hofhuis FM, *et al.* e-Blood Reconstructing the human hematopoietic niche in immunodeficient mice: opportunities for studying primary multiple myeloma. *Blood* 2012, **120**(3): E9-E16.
107. Rongvaux A, Takizawa H, Strowig T, Willinger T, Eynon EE, Flavell RA, *et al.* Human Hemato-Lymphoid System Mice: Current Use and Future Potential for Medicine. *Annu Rev Immunol* 2013, **31**: 635-674.

108. Mazurier F, Fontanellas A, Salesse S, Taine L, Landriau S, Moreau-Gaudry F, *et al.* A novel immunodeficient mouse model - RAG2 x common cytokine receptor gamma chain double mutants - Requiring exogenous cytokine administration for human hematopoietic stem cell engraftment. *J Interf Cytok Res* 1999, **19**(5): 533-541.
109. Ishikawa F, Yasukawa M, Lyons B, Yoshida S, Miyamoto T, Yoshimoto G, *et al.* Development of functional human blood and immune systems in NOD/SCID/IL2 receptor gamma chain(null) mice. *Blood* 2005, **106**(5): 1565-1573.
110. Shultz LD, Schweitzer PA, Christianson SW, Gott B, Schweitzer IB, Tennent B, *et al.* Multiple Defects in Innate and Adaptive Immunological Function in Nod/Ltsz-Scid Mice. *Journal of immunology* 1995, **154**(1): 180-191.
111. Cao XQ, Shores EW, Huli J, Anver MR, Kelsall BL, Russell SM, *et al.* Defective Lymphoid Development in Mice Lacking Expression of the Common Cytokine Receptor-Gamma Chain. *Immunity* 1995, **2**(3): 223-238.
112. Strowig T, Rongvaux A, Rathinam C, Takizawa H, Borsotti C, Philbrick W, *et al.* Transgenic expression of human signal regulatory protein alpha in Rag2(-/-)gamma(-/-)(c) mice improves engraftment of human hematopoietic cells in humanized mice. *Proceedings of the National Academy of Sciences of the United States of America* 2011, **108**(32): 13218-13223.
113. Yamauchi T, Takenaka K, Urata S, Shima T, Kikushige Y, Iwamoto C, *et al.* Polymorphic Sirpa Is the Genetic Determinant for Nod-Based Mouse Lines to Achieve Efficient Human Cell Engraftment. *Exp Hematol* 2013, **41**(8): S34-S34.
114. Takenaka K, Prasolava TK, Wang JCY, Mortin-Toth SM, Khalouei S, Gan OI, *et al.* Polymorphism in Sirpa modulates engraftment of human hematopoietic stem cells. *Nature immunology* 2007, **8**(12): 1313-1323.
115. Barclay AN. Signal regulatory protein alpha (SIRP alpha)/CD47 interaction and function. *Curr Opin Immunol* 2009, **21**(1): 47-52.
116. Barclay AN, Brown MH. The SIRP family of receptors and immune regulation. *Nature Reviews Immunology* 2006, **6**(6): 457-464.
117. Ide K, Wang H, Tahara H, Liu JX, Wang XY, Asahara T, *et al.* Role for CD47-SIRP alpha signaling in xenograft rejection by macrophages. *Proceedings of the National Academy of Sciences of the United States of America* 2007, **104**(12): 5062-5066.
118. Iwamoto C, Takenaka K, Urata S, Yamauchi T, Shima T, Kuriyama T, *et al.* The BALB/c-specific polymorphic SIRPA enhances its affinity for human CD47, inhibiting phagocytosis against human cells to promote xenogeneic engraftment. *Exp Hematol* 2014, **42**(3): 163-171.
119. Subramanian S, Boder ET, Discher DE. Phylogenetic divergence of CD47 interactions with human signal regulatory protein alpha reveals locus of species specificity - Implications for the binding site. *J Biol Chem* 2007, **282**(3): 1805-1818.
120. Subramanian S, Parthasarathy R, Sen S, Boder ET, Discher DE. Species- and cell type-specific interactions between CD47 and human SIRP alpha. *Blood* 2006, **107**(6): 2548-2556.
121. Legrand N, Huntington ND, Nagasawa M, Bakker AQ, Schotte R, Strick-Marchand H, *et al.* Functional CD47/signal regulatory protein alpha (SIRP alpha) interaction is required for optimal human T- and natural killer- (NK) cell homeostasis in vivo. *Proceedings of the National Academy of Sciences of the United States of America* 2011, **108**(32): 13224-13229.
122. Traggiai E, Chicha L, Mazzucchelli L, Bronz L, Piffaretti JC, Lanzavecchia A, *et al.* Development of a human adaptive immune system in cord blood cell-transplanted mice. *Science* 2004, **304**(5667): 104-107.
123. McDermott SP, Eppert K, Lechman ER, Doedens M, Dick JE. Comparison of human cord blood engraftment between immunocompromised mouse strains. *Blood* 2010, **116**(2): 193-200.
124. Hiramatsu H, Nishikomori R, Heike T, Ito M, Kobayashi K, Katamura K, *et al.* Complete reconstitution of human lymphocytes from cord blood CD34(+) cells using the NOD/SCID/gamma c(null) mice model. *Blood* 2003, **102**(3): 873-880.

125. Tanner A, Hallam SJ, Nielsen SJ, Cuadra GI, Berges BK. Development of human B cells and antibodies following human hematopoietic stem cell transplantation to Rag2(-/-)gamma c(-/-) mice. *Transpl Immunol* 2015, **32**(3): 144-150.
126. Halkias J, Yen BN, Taylor KT, Reinhartz O, Winoto A, Robey EA, *et al.* Conserved and divergent aspects of human T-cell development and migration in humanized mice. *Immunol Cell Biol* 2015, **93**(8): 716-726.
127. Lang JL, Kelly M, Freed BM, McCarter MD, Kedl RM, Torres RM, *et al.* Studies of Lymphocyte Reconstitution in a Humanized Mouse Model Reveal a Requirement of T Cells for Human B Cell Maturation. *Journal of immunology* 2013, **190**(5): 2090-2101.
128. Choi B, Chun E, Kim M, Kim ST, Yoon K, Lee KY, *et al.* Human B Cell Development and Antibody Production in Humanized NOD/SCID/IL-2R gamma(null) (NSG) Mice Conditioned by Busulfan. *J Clin Immunol* 2011, **31**(2): 253-264.
129. Becker PD, Legrand N, van Geelen CMM, Noerder M, Huntington ND, Lim A, *et al.* Generation of Human Antigen-Specific Monoclonal IgM Antibodies Using Vaccinated "Human Immune System" Mice. *PLoS one* 2010, **5**(10).
130. Manz MG. Human-hemato-lymphoid-system mice: Opportunities and challenges. *Immunity* 2007, **26**(5): 537-541.
131. Li LP, Lampert JC, Chen XJ, Leitao C, Popovic J, Muller W, *et al.* Transgenic mice with a diverse human T cell antigen receptor repertoire. *Nature medicine* 2010, **16**(9): 1029-U1127.
132. Yahata T, Ando K, Nakamura Y, Ueyama Y, Shimamura K, Tamaoki N, *et al.* Functional human T lymphocyte development from cord blood CD34(+) cells in nonobese diabetic/Shi-scid, IL-2 receptor gamma null mice. *Journal of immunology* 2002, **169**(1): 204-209.
133. Stavnezer J, Amemiya CT. Evolution of isotype switching. *Semin Immunol* 2004, **16**(4): 257-275.
134. Shultz LD, Saito Y, Najima Y, Tanaka S, Ochi T, Tomizawa M, *et al.* Generation of functional human T-cell subsets with HLA-restricted immune responses in HLA class I expressing NOD/SCID/IL2r gamma(null) humanized mice. *Proceedings of the National Academy of Sciences of the United States of America* 2010, **107**(29): 13022-13027.
135. Hu Z, Van Rooijen N, Yang YG. Macrophages prevent human red blood cell reconstitution in immunodeficient mice. *Blood* 2011, **118**(22): 5938-5946.
136. Hu Z, Yang YG. Full reconstitution of human platelets in humanized mice after macrophage depletion. *Blood* 2012, **120**(8): 1713-1716.
137. Conlon KC, Lugli E, Welles HC, Rosenberg SA, Fojo AT, Morris JC, *et al.* Redistribution, Hyperproliferation, Activation of Natural Killer Cells and CD8 T Cells, and Cytokine Production During First-in-Human Clinical Trial of Recombinant Human Interleukin-15 in Patients With Cancer. *Journal of Clinical Oncology* 2015, **33**(1): 74-U123.
138. Chen QF, He F, Kwang J, Chan JKY, Chen JZ. GM-CSF and IL-4 Stimulate Antibody Responses in Humanized Mice by Promoting T, B, and Dendritic Cell Maturation. *Journal of immunology* 2012, **189**(11): 5223-5229.
139. Willinger T, Rongvaux A, Takizawa H, Yancopoulos GD, Valenzuela DM, Murphy AJ, *et al.* Human IL-3/GM-CSF knock-in mice support human alveolar macrophage development and human immune responses in the lung. *Proceedings of the National Academy of Sciences of the United States of America* 2011, **108**(6): 2390-2395.
140. Ito R, Takahashi T, Katano I, Kawai K, Kamisako T, Ogura T, *et al.* Establishment of a human allergy model using human IL-3/GM-CSF-transgenic NOG mice. *Journal of immunology* 2013, **191**(6): 2890-2899.
141. Li Y, Chen Q, Zheng D, Yin L, Chionh YH, Wong LH, *et al.* Induction of functional human macrophages from bone marrow promonocytes by M-CSF in humanized mice. *Journal of immunology* 2013, **191**(6): 3192-3199.
142. Wege AK, Melkus MW, Denton PW, Estes JD, Garcia JV. Functional and phenotypic characterization of the humanized BLT mouse model. *Curr Top Microbiol* 2008, **324**: 149-165.

143. Melkus MW, Estes JD, Padgett-Thomas A, Gatlin J, Denton PW, Othieno FA, *et al.* Humanized mice mount specific adaptive and innate immune responses to EBV and TSST-1. *Nature medicine* 2006, **12**(11): 1316-1322.
144. Lan P, Tonomura N, Shimizu A, Wang SM, Yang YG. Reconstitution of a functional human immune system in immunodeficient mice through combined human fetal thymus/liver and CD34(+) cell transplantation. *Blood* 2006, **108**(2): 487-492.
145. Danner R, Chaudhari SN, Rosenberger J, Surls J, Richie TL, Brumeanu TD, *et al.* Expression of HLA Class II Molecules in Humanized NOD.Rag1KO.IL2RgcKO Mice Is Critical for Development and Function of Human T and B Cells. *PLoS one* 2011, **6**(5).
146. Takagi S, Saito Y, Hijikata A, Tanaka S, Watanabe T, Hasegawa T, *et al.* Membrane-bound human SCF/KL promotes in vivo human hematopoietic engraftment and myeloid differentiation. *Blood* 2012, **119**(12): 2768-2777.
147. Rongvaux A, Willinger T, Takizawa H, Rathinam C, Auerbach W, Murphy AJ, *et al.* Human thrombopoietin knockin mice efficiently support human hematopoiesis in vivo. *Proceedings of the National Academy of Sciences of the United States of America* 2011, **108**(6): 2378-2383.
148. Katano I, Takahashi T, Ito R, Kamisako T, Mizusawa T, Ka Y, *et al.* Predominant development of mature and functional human NK cells in a novel human IL-2-producing transgenic NOG mouse. *Journal of immunology* 2015, **194**(7): 3513-3525.
149. Koths K. Structure-function studies on human macrophage colony-stimulating factor (M-CSF). *Molecular reproduction and development* 1997, **46**(1): 31-37; discussion 37-38.
150. Cosgun KN, Rahmig S, Mende N, Reinke S, Hauber I, Schafer C, *et al.* Kit Regulates HSC Engraftment across the Human-Mouse Species Barrier. *Cell Stem Cell* 2014, **15**(2): 227-238.
151. Huntington ND, Alves NL, Legrand N, Lim A, Strick-Marchand H, Mention JJ, *et al.* IL-15 transpresentation promotes both human T-cell reconstitution and T-cell-dependent antibody responses in vivo. *Proceedings of the National Academy of Sciences of the United States of America* 2011, **108**(15): 6217-6222.
152. Elegheert J, Desfosses A, Shkumatov AV, Wu X, Bracke N, Verstraete K, *et al.* Extracellular complexes of the hematopoietic human and mouse CSF-1 receptor are driven by common assembly principles. *Structure* 2011, **19**(12): 1762-1772.
153. Coughlan AM, Harmon C, Whelan S, O'Brien E, O'Reilly V, Crotty P, *et al.* Myeloid engraftment in humanized mice: impact of G-CSF treatment and transgenic mouse strain. *Stem cells and development* 2016.
154. Brasel KA, Foster S, Cerretti DP, Sun J, Smothers JF, Mehlin C. Human c-fms antigen binding proteins. Google Patents; 2009.
155. Kavanaugh WM. Use of antibody to m-csf. Google Patents; 2007.
156. Cooke KR, Kobzik L, Martin TR, Brewer J, Delmonte J, Jr., Crawford JM, *et al.* An experimental model of idiopathic pneumonia syndrome after bone marrow transplantation: I. The roles of minor H antigens and endotoxin. *Blood* 1996, **88**(8): 3230-3239.
157. Parietti V, Nelson E, Telliarn G, Le Noir S, Pla M, Delord M, *et al.* Dynamics of human prothymocytes and xenogeneic thymopoiesis in hematopoietic stem cell-engrafted nonobese diabetic-SCID/IL-2rgammanull mice. *Journal of immunology* 2012, **189**(4): 1648-1660.
158. Petrie HT. Cell migration and the control of post-natal T-cell lymphopoiesis in the thymus. *Nature reviews Immunology* 2003, **3**(11): 859-866.
159. Takahama Y. Journey through the thymus: stromal guides for T-cell development and selection. *Nature reviews Immunology* 2006, **6**(2): 127-135.

160. Jacquel A, Benikhlef N, Paggetti J, Lalaoui N, Guery L, Dufour EK, *et al.* Colony-stimulating factor-1-induced oscillations in phosphatidylinositol-3 kinase/AKT are required for caspase activation in monocytes undergoing differentiation into macrophages. *Blood* 2009, **114**(17): 3633-3641.
161. Gordon S, Taylor PR. Monocyte and macrophage heterogeneity. *Nature Reviews Immunology* 2005, **5**(12): 953-964.
162. Bartocci A, Mastrogiannis DS, Migliorati G, Stockert RJ, Wolkoff AW, Stanley ER. Macrophages Specifically Regulate the Concentration of Their Own Growth-Factor in the Circulation. *Proceedings of the National Academy of Sciences of the United States of America* 1987, **84**(17): 6179-6183.
163. Lokeshwar BL, Lin HS. Development and Characterization of Monoclonal-Antibodies to Murine Macrophage Colony-Stimulating Factor. *Journal of immunology* 1988, **141**(2): 483-488.
164. Cenci S, Weitzmann MN, Gentile MA, Aisa MC, Pacifici R. M-CSF neutralization and egr-1 deficiency prevent ovariectomy-induced bone loss. *The Journal of clinical investigation* 2000, **105**(9): 1279-1287.
165. Dessureault S, Shpitz B, Alloo J, Rotstein O, Sandhu J, Hozumi N, *et al.* Physiologic human T-cell responses to OKT3 in the human peripheral blood lymphocyte-severe combined immunodeficiency mouse model. *Transplantation* 1997, **64**(6): 811-816.
166. Ciriza J, Thompson H, Petrosian R, Manilay JO, Garcia-Ojeda ME. The migration of hematopoietic progenitors from the fetal liver to the fetal bone marrow: Lessons learned and possible clinical applications. *Exp Hematol* 2013, **41**(5): 411-423.
167. Chang H, Biswas S, Tallarico AS, Sarkis PT, Geng S, Panditrao MM, *et al.* Human B-cell ontogeny in humanized NOD/SCID gamma(c>null) mice generates a diverse yet auto/poly- and HIV-1-reactive antibody repertoire. *Genes and immunity* 2012, **13**(5): 399-410.
168. Rossi MID, Medina KL, Garrett K, Kolar G, Comp PC, Shultz LD, *et al.* Relatively normal human lymphopoiesis but rapid turnover of newly formed B cells in transplanted nonobese diabetic/SCID mice. *Journal of immunology* 2001, **167**(6): 3033-3042.
169. Germain RN. T-cell development and the CD4-CD8 lineage decision. *Nature Reviews Immunology* 2002, **2**(5): 309-322.
170. Zuniga-Pflucker JC. Innovation - T-cell development made simple. *Nature Reviews Immunology* 2004, **4**(1): 67-72.
171. Marodon G, Desjardins D, Mercey L, Baillou C, Parent P, Manuel M, *et al.* High diversity of the immune repertoire in humanized NOD.SCID.gamma c(-/-) mice. *Eur J Immunol* 2009, **39**(8): 2136-2145.
172. Yamano T, Nedjic J, Hinterberger M, Steinert M, Koser S, Pinto S, *et al.* Thymic B Cells Are Licensed to Present Self Antigens for Central T Cell Tolerance Induction. *Immunity* 2015, **42**(6): 1048-1061.
173. Hashimoto Y, Montecino-Rodriguez E, Leathers H, Stephan RP, Dorshkind K. B-cell development in the thymus is limited by inhibitory signals from the thymic microenvironment. *Blood* 2002, **100**(10): 3504-3511.
174. Coles MC, Veiga-Fernandes H, Foster KE, Norton T, Pagakis SN, Seddon B, *et al.* Role of T and NK cells and IL7/IL7r interactions during neonatal maturation of lymph nodes. *Proceedings of the National Academy of Sciences of the United States of America* 2006, **103**(36): 13457-13462.
175. Randall TD, Carragher DM, Rangel-Moreno J. Development of secondary lymphoid organs. *Annu Rev Immunol* 2008, **26**: 627-650.
176. Roozendaal R, Mebius RE. Stromal Cell-Immune Cell Interactions. *Annual Review of Immunology, Vol 29* 2011, **29**: 23-43.
177. Fu YX, Huang GM, Wang Y, Chaplin DD. B lymphocytes induce the formation of follicular dendritic cell clusters in a lymphotoxin alpha-dependent fashion. *Journal of Experimental Medicine* 1998, **187**(7): 1009-1018.

178. Ishikawa F, Yasukawa M, Lyons B, Yoshida S, Miyamoto T, Yoshimoto G, *et al.* Development of functional human blood and immune systems in NOD/SCID/IL2 receptor $\{\gamma\}$ chain(null) mice. *Blood* 2005, **106**(5): 1565-1573.
179. Breton G, Lee J, Liu K, Nussenzweig MC. Defining human dendritic cell progenitors by multiparametric flow cytometry. *Nat Protoc* 2015, **10**(9): 1407-1422.
180. Felix J, De Munck S, Verstraete K, Meuris L, Callewaert N, Elegheert J, *et al.* Structure and Assembly Mechanism of the Signaling Complex Mediated by Human CSF-1. *Structure* 2015, **23**(9): 1621-1631.
181. Wiktorjdrzejczak W, Bartocci A, Ferrante AW, Ahmedansari A, Sell KW, Pollard JW, *et al.* Total Absence of Colony-Stimulating Factor 1 in the Macrophage-Deficient Osteopetrotic (Op Op) Mouse. *Proceedings of the National Academy of Sciences of the United States of America* 1990, **87**(12): 4828-4832.
182. Chitu V, Stanley ER. Colony-stimulating factor-1 in immunity and inflammation. *Curr Opin Immunol* 2006, **18**(1): 39-48.
183. Sanford DE, Belt BA, Panni RZ, Mayer A, Deshpande AD, Carpenter D, *et al.* Inflammatory Monocyte Mobilization Decreases Patient Survival in Pancreatic Cancer: A Role for Targeting the CCL2/CCR2 Axis. *Clin Cancer Res* 2013, **19**(13): 3404-3415.
184. Kawanaka N, Yamamura M, Aita T, Morita Y, Okamoto A, Kawashima M, *et al.* CD14⁺,CD16⁺ blood monocytes and joint inflammation in rheumatoid arthritis. *Arthritis Rheum* 2002, **46**(10): 2578-2586.
185. Van Overmeire E, Laoui D, Keirsse J, Van Ginderachter JA. Hypoxia and tumor-associated macrophages A deadly alliance in support of tumor progression. *Oncoimmunology* 2014, **3**(1).
186. Winkler IG, Sims NA, Pettit AR, Barbier V, Nowlan B, Helwani F, *et al.* Bone marrow macrophages maintain hematopoietic stem cell (HSC) niches and their depletion mobilizes HSCs. *Blood* 2010, **116**(23): 4815-4828.
187. Socie G, Blazar BR. Acute graft-versus-host disease: from the bench to the bedside. *Blood* 2009, **114**(20): 4327-4336.
188. Alexander KA, Flynn R, Lineburg KE, Kuns RD, Teal BE, Olver SD, *et al.* CSF-1-dependant donor-derived macrophages mediate chronic graft-versus-host disease. *Journal of Clinical Investigation* 2014, **124**(10): 4266-4280.